Highly loaded HPT blading in KTH test turbine

An attempt to reduce the number of blades in the first stage in a high pressure turbine

Thesis for the degree of Master of Science in Engineering
by
Magnus Persson

June 2015
Division of Thermal Power Engineering
Department of Energy Sciences
Lund University, Sweden

This degree project for the degree of Master of Science in Engineering has been conducted at the Division of Thermal Power Sciences, Department of Energy Sciences, Faculty of Engineering, Lund University, and at Siemens Industrial Turbomachinery AB.

Supervisor at the Division of Thermal Power Sciences was Dr. Magnus Genrup.
Supervisors at Siemens Industrial Turbomachinery AB were Lars Hedlund, Ken Flydalen and Navid Mikaillian.
Examiner at Lund University was Dr. Marcus Thern.

Division of Thermal Power Engineering
Department of Energy Sciences
Faculty of Engineering
Lund University
P.O. Box 118
SE-221 00 Lund
Sweden

ISRN LUTMDN/TMHP-15/5348-SE
ISSN 0282-1990

Lund 2015

To Ellinor

Abstract

The main goal with this thesis was to investigate the possibility to reduce the number of blades in a high pressure gas turbine row. The reason for this study was the interest to reduce the amount of cooling air needed within the blade row by reducing the wetted area, hopefully without losing efficiency. Another reason for reducing the number of blades was to reduce the costs.

A new design of an uncooled scaled model blade for a first stage blade row in a modern industrial gas turbine was developed. The design process mixed a combination of new ideas and more proven design principles of Siemens Industrial Turbomachinery AB. The new blade row was designed so it would fit in the existing test turbine at the Royal Institute of Technology in Stockholm.

This new blade row containing 50 blades was then compared to the existing BC7M blade row which has 60 blades. By the use of Siemens in-house codes beta2, MAC1, Multall and Cato such parameters as efficiency, Zweifel coefficient, degree of reaction and losses were studied.

The final design of the new blade resulted in a reduction of the blades combined wetted area by 9320 mm^2 or 9.7 %, this without losing more than 0.12 percentage efficiency from 92.02 % to 91.90 % according to the Multall results. According to the beta2 results the efficiency increased with 0.16 percentage from 92.03 % to 92.19 %. The profile hub-section area has though decreased by 1276 mm^2 or 20.4 % which means that this extra uncovered platform wetted area on the rotor may need cooling.

Even though these numbers appear to be good, some problem has to be solved before being able to manufacture this new blade row, e.g. the stagnation point at the leading edge, especially at the tip-section occurs on the pressure side. This will not be a problem for this uncooled model. However in case of a cooled full scale design, the shower head cooling at the leading edge will end up on the suction side, which may result in an overheated pressure side. Of course a structural analysis should be done as well.

Keywords: Highly loaded blading, High pressure turbine, Industrial gas turbine, Zweifel coefficient, Cooling, Reduce the number of blades

Acknowledgements

Without many helpful people this thesis would not have been possible to accomplish. I would like to thank all people at the RTA department for helping me during the project.

Especially I would like to thank my main supervisor Lars Hedlund and my two supervisors Ken Flydalen and Navid Mikaillian for giving me support throughout the project.

I would also like to thank Mats Annerfeldt for giving me the great opportunity to do my master thesis at Siemens Industrial Turbomachinery AB in Finspång and also Magnus Genrup for helping me get in contact with Siemens in the beginning.

Finally I would like to thank all the employees at Siemens for making this time enjoyable and my family and girlfriend for all their love and support.

Magnus Persson

Magnus Persson
Finspång 2015-06-01

Table of Contents

List of Figures

List of Tables

Nomenclature

Latin Symbols

A	[m^2]	Area
a	[m/s]	Local sonic velocity
B	[m]	Axial chord
b	[m]	Chord
c	[m/s]	Absolute velocity
c_p	[kJ/(kgK)]	Specific heat capacity at constant pressure
c_v	[kJ/(kgK)]	Specific heat capacity at constant volume
D	[-]	Diffusion factor
H	[-], [m]	Shape parameter, blade height
h	[kJ/kg]	Enthalpy
i	[°]	Incidence
M	[-]	Mach number
$\dot{m}$	[kg/s]	Mass flow
n	[pcs], [rpm]	Number of blades, rotational speed
P	[W], [Pa]	Power, Pressure
R	[kJ/kgK]	Specific gas constant
Re	[-]	Reynolds number
r	[m]	Radius
s	[J/K], [m]	Entropy, surface distance
T	[K]	Temperature
TI	[%]	Turbulence intensity
t, s	[m]	Pitch, spacing
U	[m/s]	Blade speed
v	[m/s]	Velocity
w	[m/s]	Relative velocity or work
x	[m]	Axial distance
ZW	[-]	Zweifel coefficient

Abbreviations

Cato	Common Airfoil Tool
KTH	Royal Institute of Technology
LE	Leading edge
PS	Pressure side
SIT	Siemens Industrial Turbomachinery AB
SS	Suction side
TE	Trailing edge

Greek letters

α	[°]	Absolute flow angle
β	[°]	Relative flow angle
γ	[-]	Ratio of specific heats
Δ	[-]	Difference
δ	[°]	Uncovered turning angle
δ^*	[m]	Displacement thickness
η	[-]	Efficiency
θ	[m]	Momentum thickness
Λ	[-]	Degree of reaction
λ	[-]	Laval number
μ	[Ns/m^2]	Dynamic viscosity
Π	[-]	Pressure ratio (total-to-static)
ρ	[kg/m^3]	Density
τ	[Nm]	Torque
Φ	[-]	Flow coefficient
ψ	[-]	Stage loading coefficient
ω	[°], [rad/s]	Wedge angle, angular velocity

Subscripts

0	Turbine inlet, vane inlet
1	Vane outlet, blade inlet
2	Blade outlet, turbine outlet
a, ax or x	Axial
h	Enthalpy
is or s	Isentropic
m	Metal, blade, meridional
max	Maximum
opt	Optimum
p	Pressure
r	Radial
rel	Relative property
s	Specific
T	Temperature
ts	Total-to-static
tt	Total-to-total
θ	Tangential

Superscripts

*	Stagnation, total, critical

1 Introduction

1.1 Background

During the last decades, international expertise in larger companies has driven gas turbine development towards reducing the number of blades on the rotor disc. This in order to decrease the cooling air needed and also reduce costs.

It is of high interest for a world leading company as Siemens to continue to be in the forefront of gas turbine development, this since the customers make huge investments when buying a gas turbine worth millions of Euros. A small improvement in efficiency might be crucial to whether a contract is concluded or not. The main reason to have fewer blades is that the amount of cooling air needed can be significantly reduced, since the wetted area decrease. Fewer blades will also lead to savings opportunities in material costs, which will give opportunities for SIT to reduce the price of a gas turbine to be more competitive.

Together with the Royal Institute of Technology (KTH), SIT wishes to get some test data for a rotor disc with fewer blades. However before it is even possible to manufacture a blisc containing fewer blades, SIT has to do a theoretical analysis and then design an aerofoil that can be used.

1.2 Objective

The objective will be to find out how the efficiency will vary when reducing the number of blades. Another objective will be to develop a new aero-design of a blade that can be tested later in the KTH test turbine.

1.3 Method

To investigate how the losses will be affected by a rotor with fewer blades, a profile loss study will be carried out to determine how losses vary with the pitch for the same profile geometry. A number of calculations will be made on a turbine cascade containing a blade row with 60 blades (BC7M). The BC7M is an uncooled model of a blade in the first stage of a high pressure turbine. Then the main work will be to design a new blade (B50) that is optimized at a higher loading, which will be the case when the blade row consists of fewer blades (50pcs). Many parameters will then be analysed both as 1D-results and as radial distributions. The main focus will be to study some loss parameters to find out how these affects the efficiency. To be sure that the parameters that will be analysed are comparable for BC7M and the new profile, some stage parameters will be analysed to make sure that they are unchanged.

1.4 Limitations

This report will have its main focus on the aerodynamic part of designing blades. In other words, no greater efforts will be put on the strength of materials and hence no structural analysis will be performed. However there will be some smaller explanations about it where the author thought that it is of importance for the understanding. The designing process is limited by the existing test turbine, which means that the blade profile must fit in that turbine. No economic analysis will be performed. No improvements of the in-house codes used at Siemens will be made by the author. The analysis will be for stationary cases, no transient consideration will be taken into account due to that the programs that will be used do not offer the opportunity to run transient cases.

2 Theory

2.1 Basic gas turbine principles

Today gas turbines exist in many different applications worldwide. There are two main applications for gas turbines, as engine for aircrafts or in electrical power generation. An aircraft engine creates net thrust either by using a high velocity out from the gas turbine or using a high mass flow rate. The other alternative is the power generation applications where power is generated by a generator, making use of the rotational speed of the turbine shaft. This thesis is about the latter alternative.

The terms simple cycle and combined cycle is often used in the gas turbine industry to explain which application the gas turbine will be used in. The combined cycle is when a steam cycle is connected to the gas cycle. This application is useful when both power and heat are required. When there is no steam cycle connected to the exhaust gas from the gas cycle, the cycle is called a simple cycle. From a simple cycle only power is extracted. This one is illustrated in Figure 1.

To explain the thermodynamics in a gas turbine, the ideal open gas cycle will be used. This one is illustrated in Figure 2 where the numbers are related to the numbers in Figure 1. First air enters the compressor at point one and is isentropic compressed from one constant pressure to another constant pressure, and also to a higher temperature level at point two. Then the compressed air enters the combustion chamber where fuel is injected. Under constant pressure the gas composition is now heated up to a higher temperature level to point three. Under isentropic relation the gas composition is expanded through the turbine to point four which has an atmospheric pressure if the cycle is open, which is the case in Figure 1. If the turbine cycle were closed the gas would be cooled down under constant pressure. This closed cycle is called the Brayton cycle and is mainly used in steam cycles and is not so common in gas turbine applications. (Cengel & Boles, 2011, pp. 503-504)

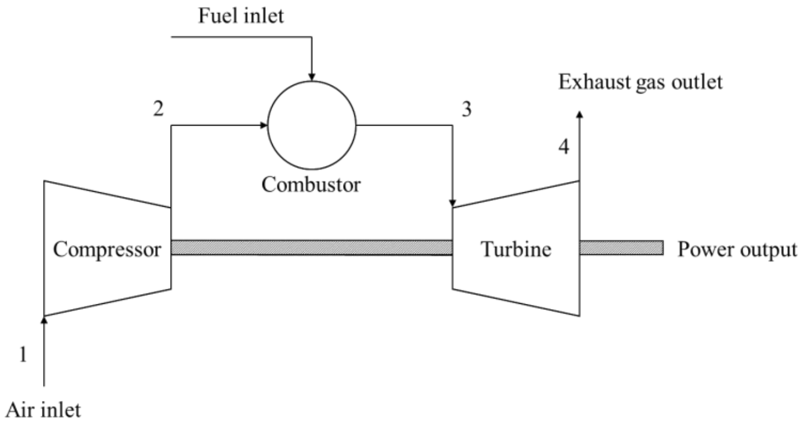

Figure 1: Simple gas turbine cycle

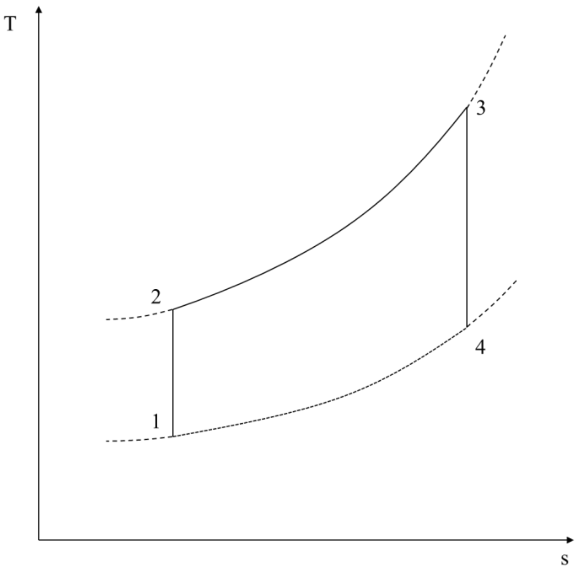

Figure 2: T-s diagram for the closed ideal cycle (Brayton cycle) and the open ideal cycle.

2.2 Turbine parameters

2.2.1 Turbine efficiency

The turbine efficiency can be defined in many different ways, isentropic total-to-static and isentropic total-to-total efficiency. The isentropic efficiency is defined as the actual work done compared to the isentropic (ideal) work done.

The first efficiency mentioned above is commonly used when the stage exit kinetic energy can be used in the next stage or as a propulsive jet in an aircraft engine. The second one is used when the kinetic energy cannot be used as mentioned above. It can be said that since the total-to-total efficiency in addition to the internal losses in terms of increasing entropy also counts the remaining kinetic energy as a loss, the total-to-total efficiency will always be greater than the total-to-static efficiency. (Denton, 2012, p. 18)

For a turbine the isentropic total-to-total- and total-to-static efficiency can be written as:

$$\eta_{tt} = \frac{h_0^* - h_2^*}{h_0^* - h_{2,is}^*} \tag{1}$$

$$\eta_{ts} = \frac{h_0^* - h_2^*}{h_0^* - h_{2,is}} \tag{2}$$

2.2.2 Euler work equation

In a turbine, the work is done by a fluid on the rotor blade. This work can be determined by the equation called the Euler work equation and the derivation will be presented in this section. The Euler work equation has been derived numerous of times in different literature. The following approach is according to (Denton, 2012, p. 7), (Mikaillian, 2012, pp. 4-5) and (Anton & Wiberg, 2013, pp. 22-23).

The work done in a turbine can be expressed as the tangential velocity change over the blade row. According to Newton’s second law of motion, the torque done by the rotor on the fluid can be written as the change of angular momentum in a row of blades as follows:

$$\tau = \dot{m} \cdot (r_2 \cdot c_{\theta 2} - r_1 \cdot c_{\theta 1}) \tag{3}$$

The power output can be expressed as the product of the torque and the angular velocity:

$$P = \tau \cdot \omega \tag{4}$$

The angular velocity can be expressed as $\omega = U/r$, where U is the blade speed. By combining Equation (3) and (4) the following expression can be stated:

$$P = \dot{m} \cdot (U_2 \cdot c_{\theta 2} - U_1 \cdot c_{\theta 1}) \tag{5}$$

By dividing with the mass flow, the specific work is obtained in Equation (6). This equation is the equation that normally is called the Euler's turbomachinery equation.

$$w_s = U_2 \cdot c_{\theta 2} - U_1 \cdot c_{\theta 1} \tag{6}$$

This equation shows the specific work done by the rotor on the fluid, which gives a positive work in a compressor, and a negative work in a turbine. To get a positive specific work in a turbine the sign is just changed:

$$w_{s,turbine} = U_1 \cdot c_{\theta 1} - U_2 \cdot c_{\theta 2} \tag{7}$$

2.2.3 Mollier diagram

In the Mollier diagram (enthalpy-entropy diagram), see Figure 3, the stagnation enthalpy drop can be seen. The specific work done by the stage, assuming that the stage is adiabatic can be written as the stagnation enthalpy drop over the stage.

$$w_s = \Delta h^* = \mathrm{h}_0^* - h_2^* \tag{8}$$

Since no work is done in the stator (assuming no cooling air):

$$h_1^* = h_0^* \tag{9}$$

Thus

$$w_s = h_1^* - h_2^* \tag{10}$$

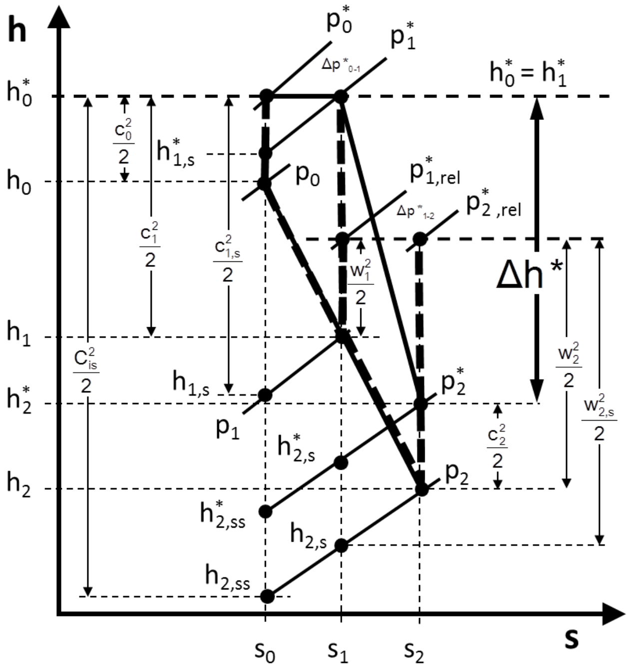

Figure 3: Mollier diagram describing a turbine expansion. Based on (Korpela, 2011)

2.2.4 Total-to-total isentropic efficiency

Often stagnation temperatures and stagnation pressures are known from various calculation programs. Hence it might be a good idea to develop a more useful expression of the efficiency. The total-to-total isentropic efficiency can be written as mentioned in Equation (1). By assuming a perfect gas the stagnation enthalpy can be written as:

$$h^* = c_p \cdot T^* \tag{11}$$

Thus the total-to-total isentropic efficiency can be written as:

$$\eta_{tt}^* = \frac{h_0^* - h_2^*}{h_0^* - h_{2,is}^*} = \frac{c_p(T_0^* - T_2^*)}{c_p(T_0^* - T_{2,is}^*)} \tag{12}$$

Assuming constant c_p gives:

$$\eta_{tt}^* = \frac{T_0^* - T_2^*}{T_0^* - T_{2,is}^*} \tag{13}$$

The isentropic relation (Saravanamuttoo, Rogers, Cohen, & Straznicky, 2009, p. 56):

$$\frac{p_2^*}{p_0^*} = \left(\frac{T_2^*}{T_0^*}\right)^{\frac{\gamma}{\gamma-1}} \tag{14}$$

The total-to-total isentropic efficiency can finally be written as:

$$\eta_{tt}^* = \frac{T_0^* - T_2^*}{T_0^* \cdot \left(1 - \left(\frac{p_2^*}{p_0^*}\right)^{\frac{\gamma-1}{\gamma}}\right)} \tag{15}$$

2.2.5 Relative stagnation pressure for compressible flows

The relative total pressure is of interest for a blade. In the following section an expression of the (relative) stagnation pressure as a function of (relative) Mach number and the specific heat for a compressible flow will be derived.

To start with, the stagnation temperature can be written as:

$$T^* = T + \frac{c^2}{2 \cdot c_p} \tag{16}$$

By assuming a perfect gas (Saravanamuttoo, Rogers, Cohen, & Straznicky, 2009, p. 231), the local sonic velocity can be written as:

$$a = \frac{c}{M} = \sqrt{\gamma \cdot R \cdot T} \tag{17}$$

By inserting Equation (17) into Equation (16) the following expression is obtained:

$$T^{*} = T + \frac{M^{2} \cdot \gamma \cdot R \cdot T}{2 \cdot c_{p}} \tag{18}$$

The definition of the specific gas constant R and the ratio of specific heats γ are:

$$R = c_{p} - c_{v} \tag{19}$$

$$\gamma = \frac{c_{p}}{c_{v}} \tag{20}$$

Combining Equation (19) and (20) yields:

$$R = c_{p} - \frac{c_{p}}{\gamma} = c_{p} \cdot \left(1 - \frac{1}{\gamma}\right) \tag{21}$$

Equation (21) can then be simplified to:

$$\frac{R}{c_{p}} = 1 - \frac{1}{\gamma} = \frac{\gamma - 1}{\gamma} \tag{22}$$

Input of Equation (22) into Equation (18) gives:

$$T^{*} = T \cdot \left(1 + \frac{\gamma - 1}{2} \cdot M^{2}\right) \tag{23}$$

Or

$$\frac{T^{*}}{T} = 1 + \frac{\gamma - 1}{2} \cdot M^{2} \tag{24}$$

Then by using the isentropic relation in Equation (14), the following equation can be written. The relative properties can be chosen if of interest.

$$\frac{p^{*}_{(rel)}}{p} = \left(\frac{T^{*}}{T}\right)^{\frac{\gamma}{\gamma-1}} = \left[1 + \frac{\gamma - 1}{2} \cdot M^{2}_{(rel)}\right]^{\frac{\gamma}{\gamma-1}} \tag{25}$$

2.2.6 Flow coefficient

By assuming a fully axial turbine, the flow coefficient is defined as the axial velocity over blade speed as follows:

$$\phi = \frac{c_a}{U} \tag{26}$$

For a non-axial turbine the flow coefficient will be written as the meridional velocity over blade speed instead. The meridional velocity can be written as in Equation (27). Note that for a fully axial flow the meridional velocity will be equal to the axial velocity since the radial velocity is equal to zero.

$$c_m = \sqrt{c_a^2 + c_r^2} \tag{27}$$

By studying the velocity triangles in Figure 5, it can be understood that if the flow coefficient is low, the relative angle becomes closer to tangential reference plane, giving a blade with higher stagger angle, and vice versa for a high flow coefficient. With the assumption that the rotational speed of the blade is constant, the rate of mass flow is proportional to the flow coefficient. This gives a relation where an increased flow coefficient increases the mass flow as well. (Denton, 2012, pp. 100-101)

2.2.7 Stage loading

The stage loading is defined as in Equation (28) and it is an approach to measure the work output from the stage.

$$\psi = \frac{\Delta h_0}{U^2} \tag{28}$$

By assuming an adiabatic and fully axial turbine with constant radius, the Euler work equation can be used to rewrite the stage loading as follows:

$$\psi = \frac{\Delta h_0}{U^2} = \frac{\Delta c_\theta}{U} \tag{29}$$

Where $\Delta h_0 = U \cdot \Delta c_\theta$, where Δc_θ represents the turning of the flow through the stage. It is clear that for a high loaded stage, the turning of the flow has to be large. A high stage loading coefficient will affect the efficiency negatively since these high loaded blades will give low reaction and also an increased swirl between the stages (Denton, 2012, p. 101).

2.2.8 Degree of reaction

The difficulties with the degree of reaction are that there is more than one definition used in industry. The degree of reaction is the ratio between the static enthalpy, temperature or pressure drop in the rotor and the drop in the whole stage. These three definitions are presented in Equation (30) to (32), where Λ_p, Λ_h and Λ_T are respectively based on pressure, enthalpy and temperature.

$$\Lambda_p = \frac{p_2 - p_3}{p_1 - p_3} \tag{30}$$

$$\Lambda_h = \frac{h_2 - h_3}{h_1 - h_3} \tag{31}$$

$$\Lambda_T = \frac{T_2 - T_3}{T_1 - T_3} \tag{32}$$

It is of high importance to be aware of which definition that is used when comparing different degree of reactions, since the difference between these may vary by the amount of 5-10 % (Moustapha, Zelesky, Baines, & Japikse, 2003, p. 17). The degree of reaction will vary at different radii. A higher stagger and less turning of the flow in the rotor compared to the stator will give a higher degree of reaction (Denton, 2012, p. 12).

2.2.9 Reynolds number

Reynolds number is normally defined as the density times the velocity times a characteristic length divided by the dynamic viscosity. In turbines the most common way according to (Denton, 2012, p. 13) is to define the density and the velocity at the blade row exit and using the chord as the characteristic length as follows:

$$Re = \frac{\rho_2 \cdot c_2 \cdot b}{\mu} \tag{33}$$

At lower Reynolds number the boundary layer will become more and more laminar. Laminar boundary layers will be discussed later on. However the main problem with them are that they will tend to separate much easier, however in return they will give less losses.

2.3 Blade profile design

2.3.1 Blade notation

In order to be able to understand the continuation of the report, a turbine blade angle and distance notation is shown in Figure 4.

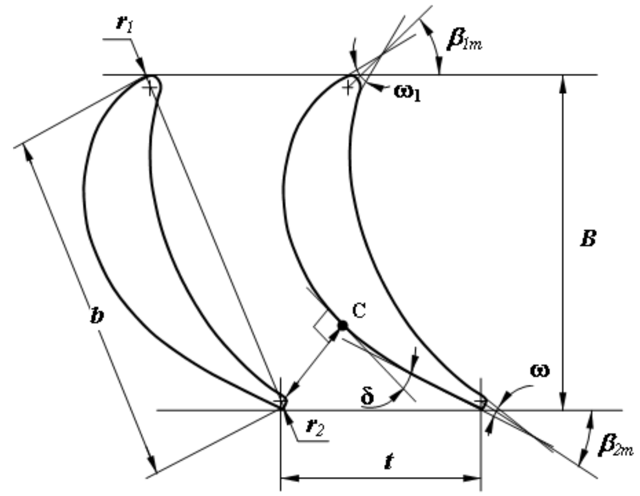

Figure 4: Turbine blade angle and distance notation

2.3.2 Velocity triangles

At SIT the designers prefer to define the angles from the tangential plane, unlike many textbooks that defines angles from the axial plane instead. In Figure 5 the velocity triangles of a turbine cascade are presented with both angle notations. As for the degree of reaction it is of high importance to make sure which angle notation that is used to avoid confusion.

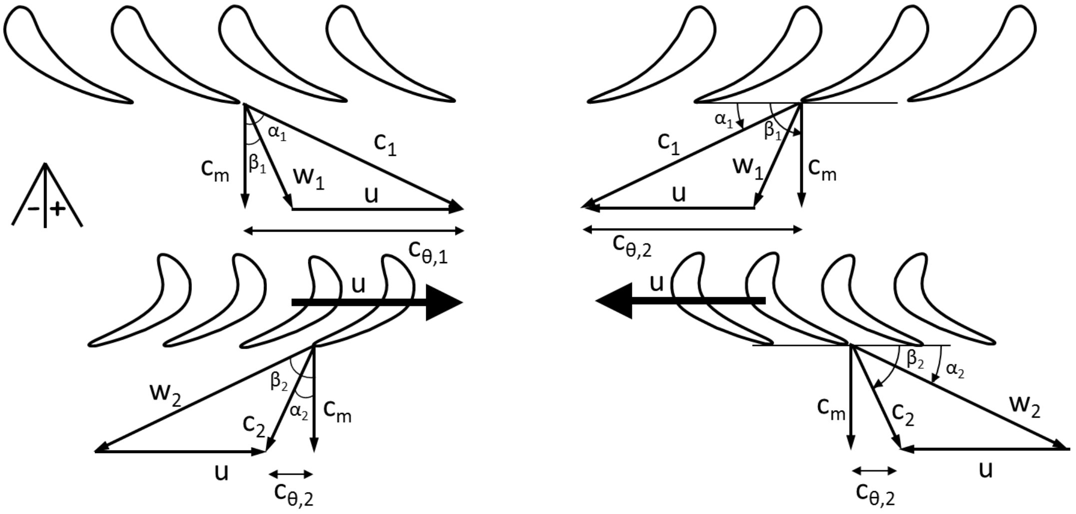

(a) *(b)*

Figure 5: Velocity triangles describing a turbine cascade. Angles defined from (a) axial reference plane, (b) tangential reference plane. Based on (Genrup, 2014, p. 14)

2.3.3 Blade spacing

The distance between the blades on the rotor disc depends primarily on how many blades that are attached to the rotor disc. The spacing or pitch does also depend on the radial position. For example close to the hub, the pitch is small and with increased radius the pitch is increased. The equation for the pitch is shown in Equation (34).

$$t = \frac{2 \cdot \pi \cdot r}{n} \tag{34}$$

Where *r* is the radius and *n* is the number of blades.

The optimum pitch has to be carefully taken under investigation. Assuming a certain number of blades, decreasing the number of blades will then result in a decreased viscous loss due to the fact that the friction loss is reduced with decreased wetted area. The negative aspect by doing this is that turning of the flow field will be less as a result of a decreased guidance from the fewer number of blades. This may also result in a higher velocity on the blade suction side surface resulting in a larger diffusion on the suction side surface, giving an increased risk of boundary layer separation. The suction side diffusion describes the deceleration on the suction side close to the blade. If instead the number of blades is increased the guidance will be better resulting in less separation loss, however the wetted area is increased which gives higher friction loss. In Figure 6 it is illustrated how the losses are affected by the axial solidity which is the inverse of the pitch-to-axial chord ratio.

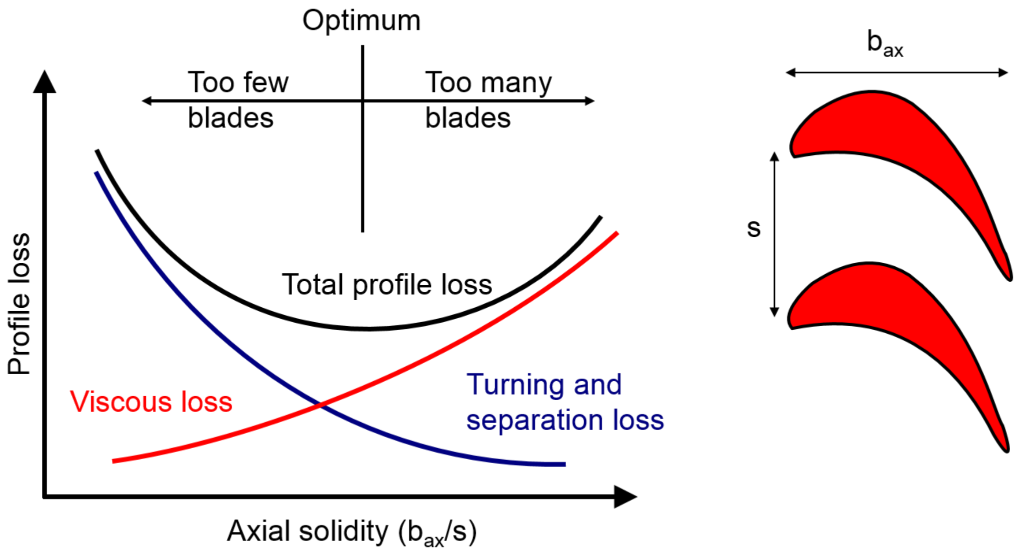

Figure 6: Profile loss as a function of axial solidity. Based on (General Electric)

2.3.4 Zweifel coefficient

The empirical Zweifel coefficient is a designing parameter which main purpose is to find the optimum pitch-to-axial chord ratio and hence the optimum number of blades with the lowest losses according the previous discussion in blade spacing section. The Zweifel coefficient describes the ratio between the actual and the ideal tangential force on a blade.

The tangential load on the blade is actually the area between the pressure distribution on the suction side surface and the pressure side surface, which is shown in Figure 7. The ideal case assumes that the pressure on the suction side surface is constant with no diffusion which means that the stagnation pressure line is constant. On the pressure side the velocity is assumed to be zero giving that the stagnation pressure is equal to the static pressure and constant. (Hodson, 2012, p. 72), (Mikaillian, 2012, pp. 13-14) and (Dixon & Hall, 2010, pp. 85-87)

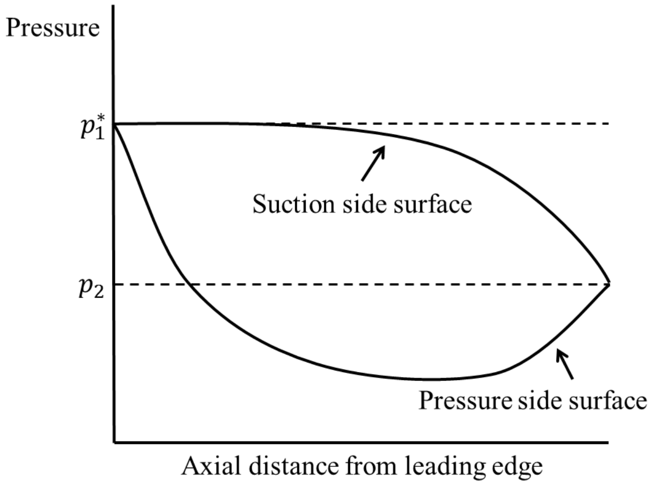

Figure 7: Actual and ideal pressure distribution. Redesign of Figure 27 in (Hodson, 2012, p. 72)

With this in mind, the Zweifel coefficient can be written as:

$$ZW = \frac{\dot{m} \cdot (c_{\theta 2} - c_{\theta 1})}{(p_{01} - p_2) \cdot B \cdot H} \tag{35}$$

Where ṁ is the mass flow, B is the axial chord and H is the blade height.

By assuming incompressible and loss free flow the following relation can be written:

$$p_{01} - p_2 = \frac{1}{2} \cdot \rho \cdot c_2^2 \tag{36}$$

And the assumption that the axial velocity is constant gives:

$$\dot{m} = \rho \cdot H \cdot t \cdot c_a \tag{37}$$

Then Equation (35) can be simplified as:

$$ZW = \frac{\rho \cdot H \cdot t \cdot c_a \cdot (c_{\theta 2} - c_{\theta 1})}{\frac{1}{2} \cdot \rho \cdot c_2^2 \cdot B \cdot H} \tag{38}$$

By looking in the velocity triangles in Figure 5a, it can be seen that:

$$c_\theta = c_a \cdot \tan\alpha \tag{39}$$

And

$$c_2 = c_a \cdot \sec\alpha = c_a \cdot 1/\cos\alpha \tag{40}$$

This gives that:

$$ZW = \frac{2 \cdot t \cdot c_a^2 \cdot (\tan\alpha_2 - \tan\alpha_1)}{c_a^2 \cdot 1/\cos^2\alpha_2 \cdot B} \tag{41}$$

More simplified:

$$ZW = 2 \cdot \frac{t}{B} \cdot \cos^2\alpha_2 \cdot (\tan\alpha_2 - \tan\alpha_1) \tag{42}$$

In an empirical way, Zweifel decided that the Zweifel coefficient giving the lowest profile loss was approximately 0.8. This is true for turbines with a flow outlet angle of 60-70 degrees (Dixon & Hall, 2010, p. 86). In modern low pressure turbines, the development has gone towards an increased value for the Zweifel coefficient, especially in the aviation industry where the weight of the engine is of great importance. An increased Zweifel coefficient gives the opportunity to reduce the number of blades and hence the weight.

Equation (42) is according (Moustapha, Zelesky, Baines, & Japikse, 2003, p. 20) defined from the axial plane. As mentioned before Siemens prefer to define all angles from the tangential plane instead. In Figure 8 the angles are presented using both Moustaphas definition from the axial plane and from the tangential plane according to Siemens in Finspång. Some geometrical relations that can be seen in Figure 8 are stated below:

$$\tan\beta_{1,x} = \frac{w_{\theta 1}}{c_x} = \cot\beta_{1,\theta} \tag{43}$$

$$\tan\beta_{2,x} = \frac{w_{\theta 1}}{c_x} = \cot\beta_{2,\theta} \tag{44}$$

$$\cos\beta_{2,x} = \frac{c_x}{w_2} = \sin\beta_{2,\theta} \tag{45}$$

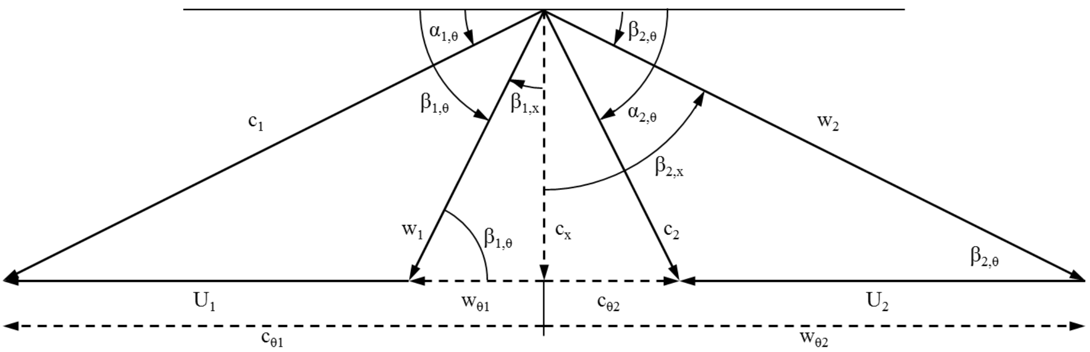

Figure 8: Velocity triangles with angle notation from both axial and tangential plane.

This gives the Zweifel coefficient with angles defined from the tangential plane.

$$ZW_I = 2 \cdot \frac{t}{B} \cdot (\cot\beta_1 + \cot\beta_2) \cdot \sin^2\beta_2 \tag{46}$$

Another equation that will be used to determine the Zweifel coefficent is shown below in Equation (47).

$$ZW_{II} = \frac{\rho_2 s_2 c_{m2}\left(w_{\theta,1} - w_{\theta,2}\right)}{C_{ax}\,(p_1^* - p_2)} \tag{47}$$

2.3.5 Velocity distribution

The pressure distribution was discussed in the previous chapter. It is now appropriate to study one of the most important parameter that is used when profiling blade geometry, the velocity distribution. This since the velocity at the blade surface describes how the boundary layers are built up and hence how large the losses will be (Hodson, 2012, p. 49). There are normally two approaches that the velocity distribution can be shown graphically, either by having axial position or s/s_{max} on the x-axis, where s/s_{max} is the non-dimensional surface length. Both ways of describing the velocity distribution is shown in Figure 9. Note that both pictures are schematic ones however they are representing the same case.

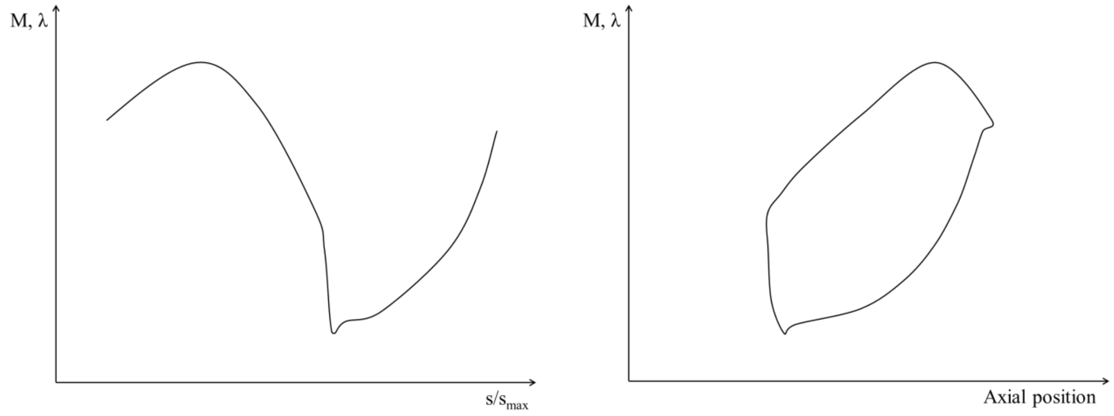

(a) (b)

Figure 9: Velocity distribution with (a) s/s$_{max}$ and (b) axial position on the x-axis.

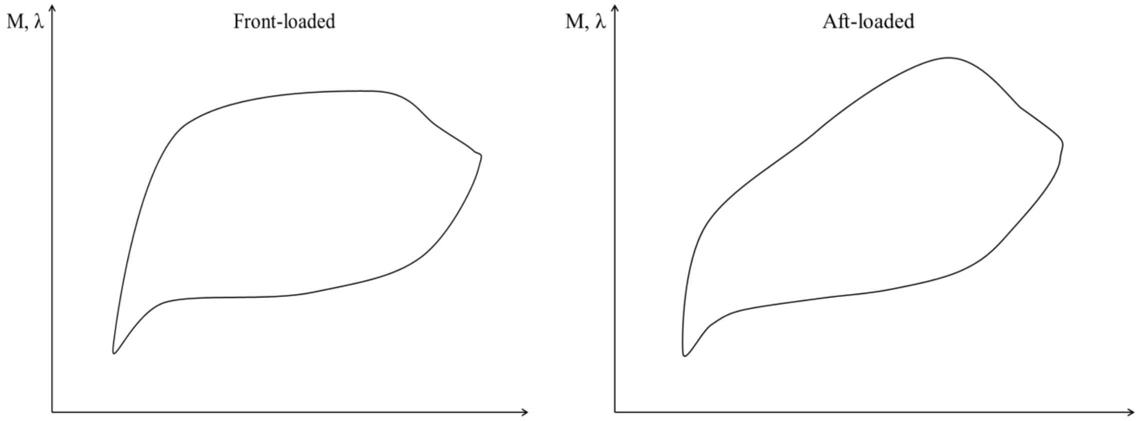

(a) (b)

Figure 10: Velocity distribution for (a) front-loaded and (b) aft-loaded blade. Based on (Denton, 2012)

The upper side (the convex side) of a turbine blade is called the suction side since the pressure is lower on this side compared to the other side and will be denoted with SS in the following part of the report. The other side is called the pressure side since the pressure is higher on this side compared to the SS and will be denoted PS. Two more abbreviations will be used in this chapter, the leading edge and trailing edge will be denoted LE and TE respectively.

The profile loss varies with the velocity to the power of two for laminar boundary layers and the velocity to the power of three for turbulent boundary layers. Hence on the SS, approximately 80 % of the profile losses occur since the velocity is higher on the SS compared to the PS. Therefore the main focus for an engineer is to aerodynamically design this one correct. The most crucial part on the SS is the deceleration from the velocity peak to the TE, since a too large diffusion can give rise to a boundary layer separation. If this boundary layer separation occurs not too close to the trailing edge, the laminar boundary layer will be able to reattach as turbulent boundary layer before the TE, creating a separation bubble. However if boundary layer separation occurs close to the TE, there might be a risk of having a boundary layer separation that will not be able to reattach. This will cause the losses to increase rapidly.

The PS of the velocity distribution will be of less importance from an aerodynamic point of view. Hence the aerodynamicist chooses to optimize the SS surface, and then let other aspects affect the PS design e.g. in a cooled blade there has to enough space in the aerofoil for the cooling air. The blade cannot be too thin due to the risk of having too high material stress levels.

A blade can be said to be front-, mid-, or aft-loaded. The front- and aft-loaded profiles will be discussed below. The mid-loaded profile is then somewhere in between the front- and aft-loaded profiles.

The turning of the flow creates the pressure gradient on both the SS surface and the PS surface.

2.3.5.1. Front-loaded

The area between the SS and PS velocity distribution is simply the blade loading. Higher blade loading will be needed when having fewer blades. By having a fast and early acceleration on the SS surface it is possible to obtain this. The velocity profile for a front-loaded blade is shown in Figure 10a.

2.3.5.2. Aft-loaded

For an uncooled aft-loaded profile the surface distance with laminar boundary layer is longer than for a front-loaded profile due to the longer acceleration which gives thinner boundary layer. A thin boundary layer give less losses since the area with shear stresses becomes smaller. Another reason for having an aft-loaded profile is that the secondary losses becomes smaller since the pressure gradient is lower close to the leading edge where most of the secondary losses is created by this pressure gradient. If the profile is film cooled the film cooling at the leading edge will trigger transition to turbulent boundary layer. Then it is more important to keep the velocity peak low since the profile loss depends on the velocity to the power of three for turbulent boundary layers. For laminar boundary layers the loss depends on the velocity to the power of two instead. The velocity profile for an aft-loaded blade is shown in Figure 10b.

2.3.5.3 Laval and Mach number

In the report both Mach and Laval distributions will be presented. Hence the two definitions will be described.

The Mach number is defined as the local speed over the local speed of sound.

$$M = \frac{c}{a} \tag{48}$$

Where

$$a = \sqrt{\gamma \cdot R \cdot T} \tag{49}$$

The Laval number is defined as the local speed over the critical speed of sound.

$$\lambda = \frac{c}{a^*} \tag{50}$$

Where the critical speed of sound is:

$$a^* = \sqrt{\gamma \cdot R \cdot T^*} \tag{51}$$

The main difference is that the Laval number will refer to the same velocity under all circumstances. (Dahlquist, 2008)

An equation that can be used to go from Mach number to Laval number has been derived by (Dahlquist, 2008). Note that for Mach number equal to one, the Laval number is also one.

$$\lambda = \sqrt{\frac{\gamma + 1}{\frac{2}{M^2} + \gamma - 1}} \tag{52}$$

2.3.6 Diffusion coefficient

If the diffusion is too large, the flow will separate. One rule that is used to get an acceptable diffusion is to use diffusion coefficients. As for many other parameters there is more than one definition. The one that will be used in this report is according to (Mamaev & Sandymirova, 1995, p. 37):

$$D = \frac{\lambda_{max}}{\lambda_2} - 1 \tag{53}$$

Where λ_{max} and λ_2 are the maximum isentropic Laval number on the SS and the average of the isentropic Laval number after the blade trailing edge. The blade velocity distribution should be designed to give a diffusion coefficient lower than a D_{opt} according to (Mamaev & Sandymirova, 1995, p. 38).

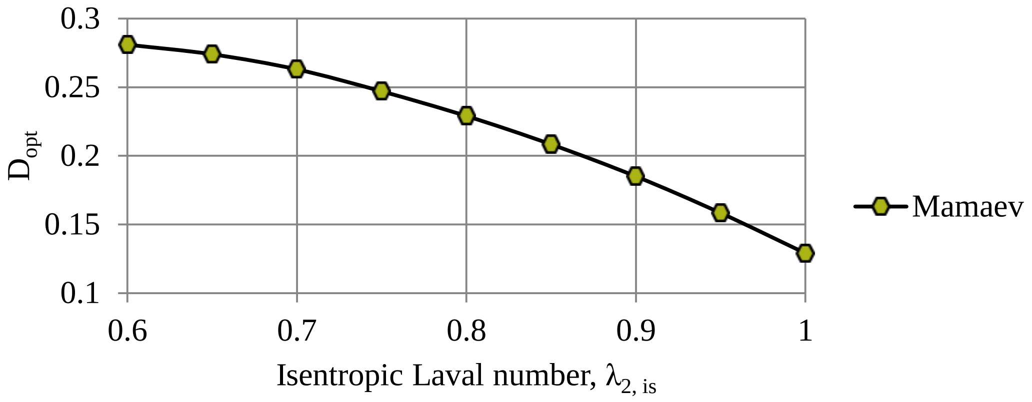

Figure 11: Optimum diffusion coefficient according to Mamaev. Redesign of Figure 2 in (Mamaev & Sandymirova, 1995, p. 38)

2.3.7 Incidence

The induced or design incidence is the angle between the inlet flow and the blade metal leading edge angle and is defined as follows:

$$i = \beta_{1,m} - \beta_1 \tag{54}$$

If the blade metal angle is larger than the flow inlet angle, the turning of the flow becomes greater and the incidence is said to be positive. Hence a negative incidence means less turning of the flow. The definition above may vary depending if the angles are taken from the axial or tangential direction. Equation (54) is defined from the tangential plane. With more positive incidence the stagnation point will move towards the pressure side and if the incidence is negative the stagnation point will move towards the suction side. In Figure 12 the blade surface velocity effects of positive and negative incidence are shown. If the blade is too front-loaded there might be a risk of getting velocities above Mach one at high incidence and hence a risk of having a shock wave.

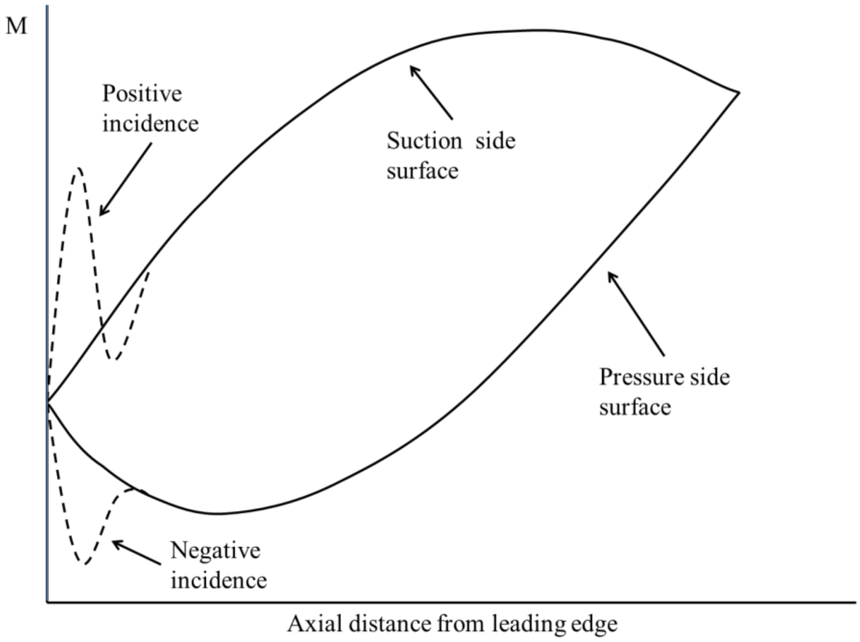

Figure 12: Effects of incidence. Redesign of Figure 4.3 in (Moustapha, Zelesky, Baines, & Japikse, 2003, p. 99)

2.3.8 Shape parameter and skin friction coefficient.

Where the transition point appears will have large effects of the total flow and the losses. This effect is hard to scale down. Hence in experiments the user often forces the transition to appear at a certain position where it is expected to appear for a full-scale airfoil by modifying the surface at this position (Cebeci & Bradshaw, 1977, p. 16).

The shape parameter and the skin friction coefficient can be used to decide if the boundary layer is laminar or turbulent. These factors can then be used to find the transition point.

The shape parameter H is defined as the displacement thickness δ^* over the momentum thickness θ (Cebeci & Bradshaw, 1977, pp. 17-18):

$$H = \frac{\delta^*}{\theta} \tag{55}$$

The shape parameter is equal to one when boundary layer is absent. For constant pressure flows, normally the boundary layer is turbulent at a shape parameter equal to 1.2-1.5 and laminar at 2.6 (Cebeci & Bradshaw, 1977, p. 18). At a shape parameter equal to 2-3 according to (Cebeci & Bradshaw, 1977, p. 18) there is a risk of having turbulent boundary layer separation and at a value of 4 there is a risk of getting laminar boundary layer separation. The skin friction coefficient can also be used to decide whether the boundary layer is turbulent or laminar and to decide where separation might occur. There might be a risk of separation for a skin friction coefficient value less than 0.0015 for both turbulent and laminar boundary layers.

2.4 Losses

Throughout a turbine many interesting phenomena are happening with the working fluid where some of them are creating losses. Four kinds of losses will be presented in this section namely the profile, secondary, trailing edge and tip clearance losses. There are many correlations describing these losses and a few of them is described by (Dahlquist, 2008). In Figure 13, these losses are shown schematically.

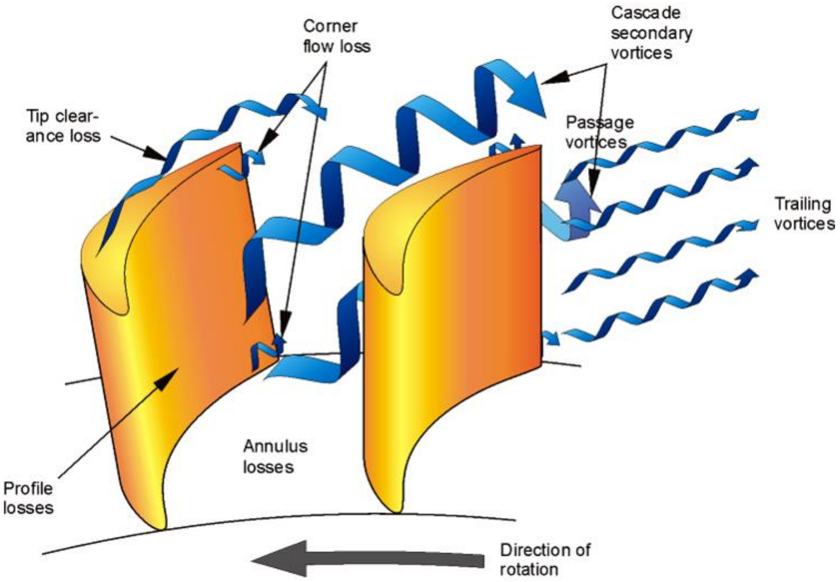

Figure 13: Turbine losses. (Moustapha, Zelesky, Baines, & Japikse, 2003, p. 32)

2.4.1 Profile losses

The profile losses are the losses that occur due to the blade surface skin friction. The surface friction is depending on a few parameters such as the roughness, Reynolds number, the flow velocity and the size of the wetted area which is the area that is in contact with the working fluid (Moustapha, Zelesky, Baines, & Japikse, 2003). The annulus losses can be described in the same manner as the profile loss, but instead on the endwalls. These losses will depend on the aspect ratio. A lower aspect ratio will lead to higher endwall losses (Denton, 2012, p. 17). The velocity on the surface has a big impact on the losses due to the fact that the entropy generation is proportional to the velocity squared for laminar boundary layer (Miller & Denton, 2012, p. 150). Since the velocity is higher on the suction side compared to the pressure side the losses are much higher on the suction side. According to (Miller & Denton, 2012, p. 150) the difference between the suction side and pressure side may be a factor five.

The profile loss can normally be mentioned as the energy loss (enthalpy) or the Traupel loss (enthalpy). The Traupel loss includes a correction factor for the trailing edge loss. For a turbine, the pressure loss is defined as the stagnation pressure drop over the reference dynamic pressure based on turbine exit values. The energy definition is loss of kinetic energy over reference kinetic energy where the loss of kinetic energy is the turbine exit enthalpy difference between isentropic and actual expansion. The denominator is based on turbine exit values. (Hodson, 2012, pp. 47-48)

2.4.2 Secondary losses

All of the flows that do not follow the main direction are called secondary flows. These secondary flows are vortices created by boundary layers and the curvature of the flow passage. Multiple vortices that appear at the trailing edge when the flow separates create a wake. The two passage vortices that are shown in Figure 14 are created due to the boundary layers of the two endwalls and the pressure gradient that exist between the two blades. On all rotors there is a gap between the blade and the casing. Due to the pressure difference between the pressure and suction side some fluid will take this way instead of performing work on the blade. This will of course act as a loss. Depending if the blade is shrouded or unshrouded the tip clearance losses will vary. The tip clearance can affect the flow far down on the blade. The tip clearance leakage will form a vortex sheet, which is shown in Figure 15. The secondary losses can in worst case stand for 2/3 of the total loss through a blade row (Moustapha, Zelesky, Baines, & Japikse, 2003, p. 33).

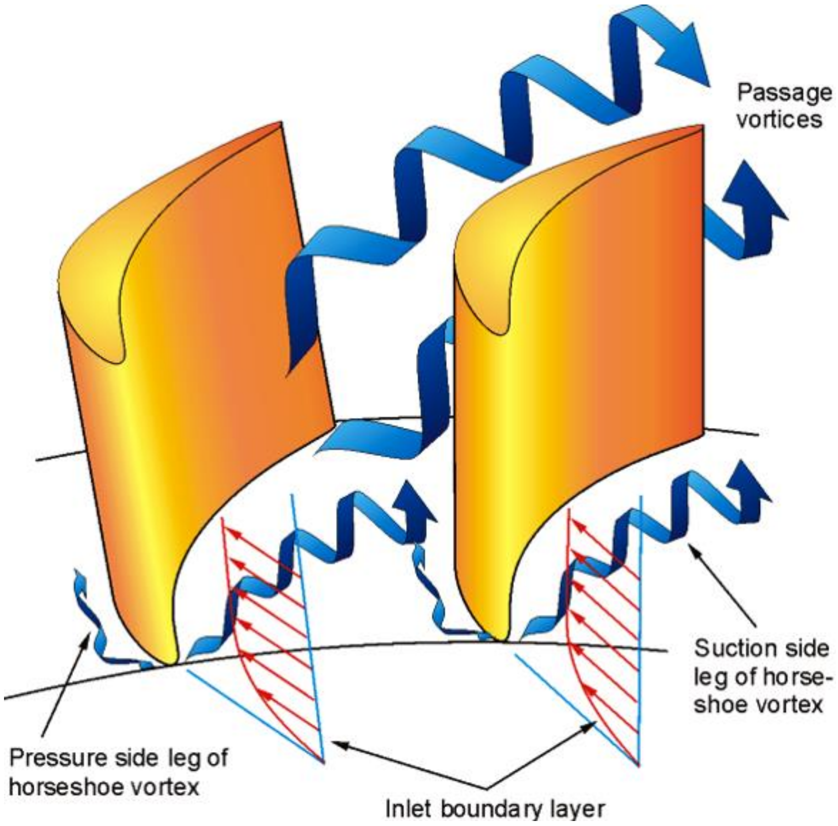

Figure 14: Secondary losses. (Moustapha, Zelesky, Baines, & Japikse, 2003, p. 41)

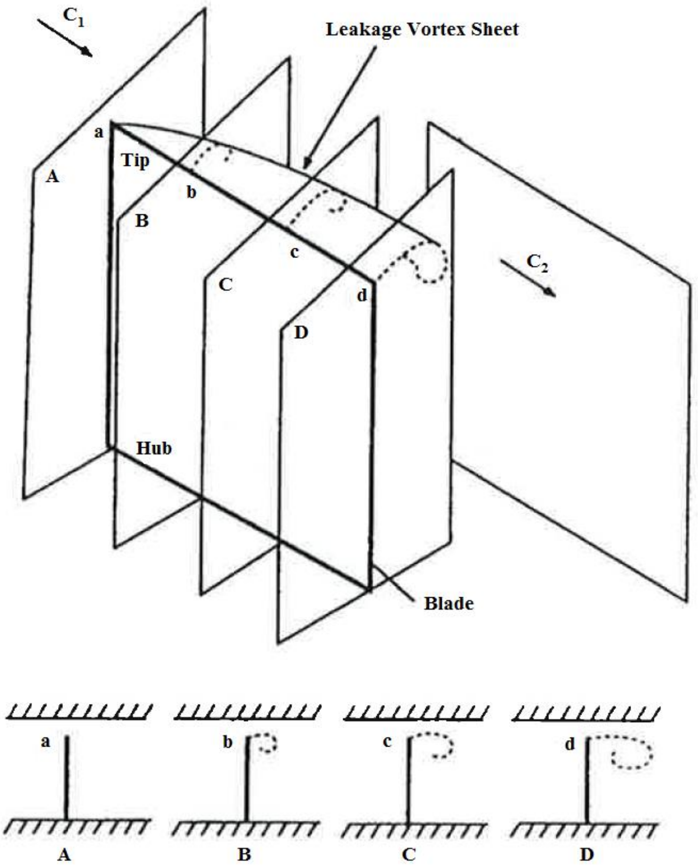

Figure 15: Tip clearance leakage vortex sheet. Redesign of Figure 15 in (Longley, 2012, p. 96)

The horseshoe vortex is built up at the stagnation point close to the blade leading edge. Initially the static pressure in the boundary layer is assumed to be constant at an arbitrarily distance from the leading edge. In the boundary layer the velocity gradient is high, giving a larger stagnation pressure far from the wall and a lower stagnation pressure close to the wall. When the flow is approaching the stagnation point the dynamic pressure gradually is converted to static pressure until it reaches the wall where the flow velocity is zero. The static pressure will then be larger further from the wall creating a pressure gradient. The flow will be guided by this pressure field creating a vortex (Hedlund, Horseshoe vortex, 2015). This part of building up the horseshoe vortex is shown in Figure 16. This vortex will then be split between the pressure and suction side of the blade. There are different philosophies of what happens to these “legs” of the horseshoe vortex. According to (Sieverding, 1985) Langston says that the suction side leg of the horseshoe vortex merges with the passage vortex that is created by the boundary layer in the passage due to the pressure gradient. The pressure side of the horseshoe leg will act as a counter vortex in the corner of the blade and the endwall. This is shown in Figure 17. In the same part of the journal, Sieverding proclaims that Klein instead thinks that the suction side of the horseshoe leg will be dissipated close to the passage vortex.

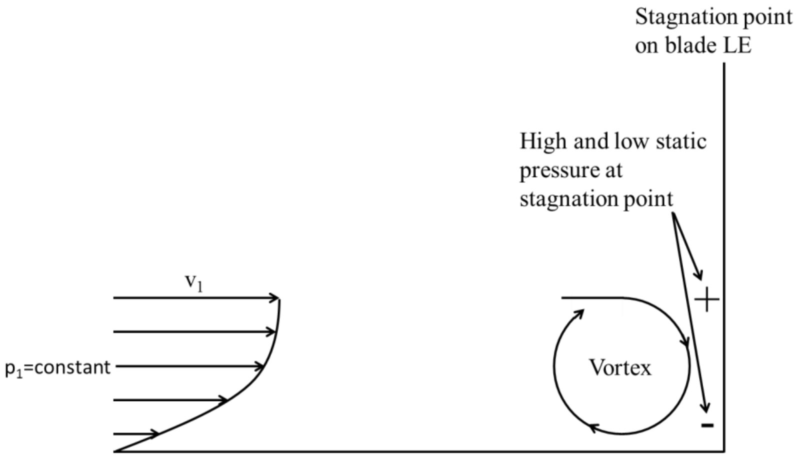

Figure 16: Horseshoe vortex initialisation

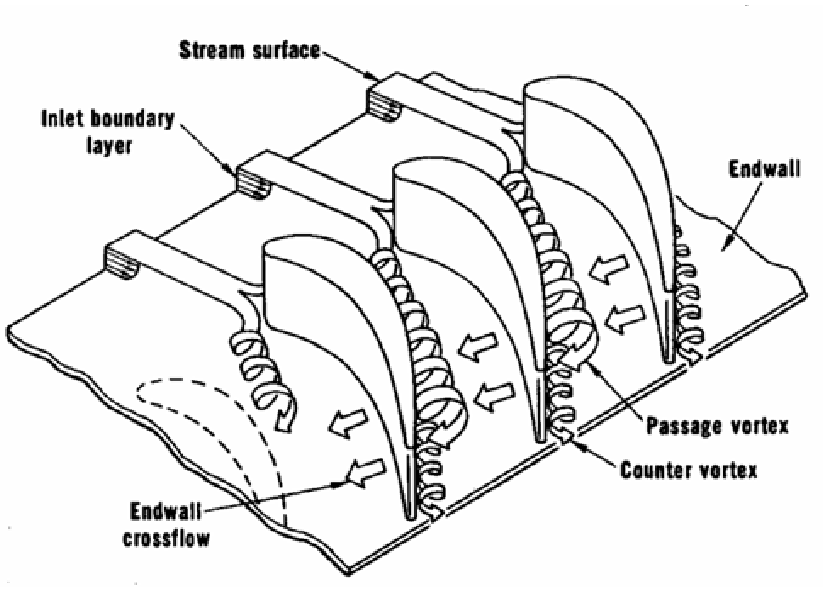

Figure 17: Schematically description of a horseshoe, passage and counter vortex according to Langston. (Lampart, 2009, p. 323)

3 Computational programs

During this thesis a few in-house codes have been used, Cato, beta2, Multall, MAC1 and GasTable. All program handles geometry and boundary conditions in different ways, which of course will affect the comparison of the results.

3.1 Common Airfoil Tool (CATO)

For 2-D profiling of both compressor and turbine blades, the Common Airfoil Tool (CATO) is used at Siemens in Finspång. This program uses Bezier polynomials to describe the geometry of the profile at each section. This program also includes the possibility to use a 2-D Mises and Navier Stokes solver, both which runs fast. This program comes with the opportunity to create sections from scratch or by importing coordinates. It also features the great possibility to see the whole turbine including vanes, blades and channel geometry in a 3-D view. It also produces output files that can be used in other in-house codes.

3.2 Beta2 - 2D through flow solver

The beta2 is a two dimensional through flow solver that has correlations for some 3D effects. The code is based on prof. Mamaev's correlations. There are many built-in loss models that the user can choose between. It also gives the user the opportunity to choose if cooling air should be injected or not. Fillets, roughness, clearance are also some basic parameters that can be set by the user. It also offers the opportunity to decide where the transition point appears or if it should be left to the code to decide. The code is as fast as CATO and is therefore very good at an early state of the design process. During this thesis only version 2.07.04 is used.

3.3 Multall - 3D solver

The Multall solver is developed by Professor John Denton. This code offers the opportunity to analyse the 3D effects of the flow in a turbine or compressor. Since this is a 3D solver, the calculations take way longer time to complete compared to e.g. beta2. The user has to decide what kind of accuracy that is needed to speed up the calculation as much as possible. In Multall it is only possible to run with the assumption of a perfect gas. Only steady state conditions can be analysed in Multall i.e. a transient analysis cannot be done in Multall. Actually Multall by itself does not give any visualisation of the results. To visualize the results, the MayaVi Data Visualizer is used.

3.4 MAC1

The MAC1 program is a mean line code. When a beta2 run is done a MAC1 input file is created. This very simple program will only be used to analyse the losses.

3.5 GasTable

The GasTable v1.9 program will be used to decide the mass fractions of the molecules that exist in the air. This program uses the NASA-SP 273 gas table. The molecules that are included are sulphur dioxide, water, carbon dioxide, nitrogen, oxygen, argon and helium. All other substances in the air are neglected in this program. There is an add-in for excel which can be used to get some gas properties e.g. enthalpy if the gas composition and some other properties e.g. pressure and temperature are known.

4 Method

This thesis has been carried out in several small steps. The approach for each step depends on the previous stage results. Therefore the method will be described in chronological order with intermediate results during the method. To be able to understand which main steps that is included, a short description is presented below.

First of all the boundary conditions for the KTH test turbine will be stated.

Then the former profile BC7M is presented involving the blade geometry, some solver parameters and then a run with the Mises solver in Cato followed up with its result. This part is of interest since this provides the case that the new profile later will be compared to. Another reason for doing this calculation of BC7M is that this has not been fully done before. Also beta2 and Multall setups followed by calculations will be done for the BC7M at this part.

The next section will analyse how the profile losses will depend on the number of blades i.e. its dependence of the pitch-to-chord ratio. This will be done in two main sections, the simplest where the turning of the flow is not kept constant and one where the profile is closed or opened to keep the same flow outlet angle and thereby the turning of the flow.

The next important step will be when the newer profile B50_v01_03 is designed. This profile will have fewer blades than the existing BC7M. How many will be decided in the profile loss study. The profiling is a multistep process that will be discussed as precisely that is needed to follow the process fairly well.

The new profile will be analysed by running some calculations in beta2, Cato and Multall. This will be done with many different approaches. The steps that are going to be presented are the following:

- In beta2, B50_v01_03 and BC7M will studied with tip recess.
- For Multall the above two profiles will be studied with a channel with tip recess.

All these calculations will then be compared to each other to see the differences between the profiles. More precise explanation will be presented later on.

4.1 Stage boundary conditions

The boundary conditions for the test turbine were decided by (Anton & Wiberg, 2013) during their thesis, and these conditions are still valid and will be used since comparable results would be preferable. Since the total-to-static pressure ratio was decided, the total inlet pressure and static outlet pressure was set as boundary conditions. Adjustments will though be done. In (Anton & Wiberg, 2013) they had some problems with some CFX calculations that prevented them to use an inlet total pressure radial distribution that has been derived from experiments. They used a constant total pressure radial distribution instead. Since CFX will not be used during this project this experimental developed radial total pressure distribution will be used. This total pressure radial distribution is shown in Figure 18. A 1D value for the inlet total pressure is shown in Table 1. The rotational speed was set to be 10300 rpm instead of 10270 rpm that was stated in (Anton & Wiberg, 2013). This due to that they mentioned in their Appendix A that it was changed to 10300 for the BC6M. At the inlet the total temperature was set to be constant at all radii. Also the turbulence intensity was stated since the KTH test turbine has a perforated grid that produces approximately 6 % turbulence intensity at the turbine inlet. All these boundary conditions are presented in Table 1.

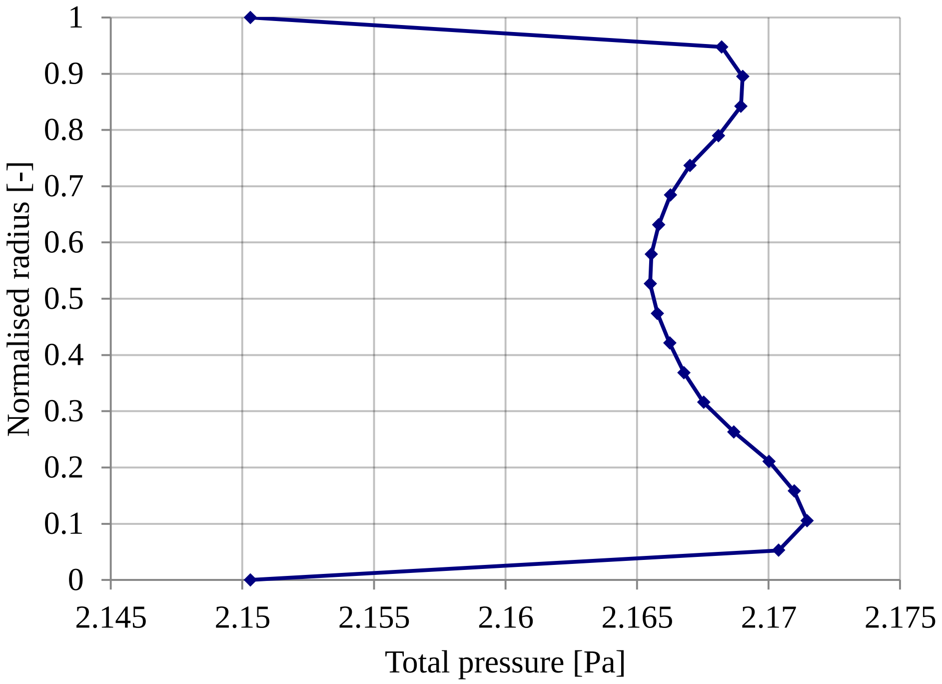

Figure 18: Turbine inlet total pressure radial distribution

Table 1: Boundary conditions for the test turbine stage

p^*_0 [bar]	2.167
T^*_0 [K]	345
p_2 [bar]	1.013
Π [-]	2.139
TI_0 [%]	6
n [rpm]	10300

4.2 Existing profile BC7M.

The BC7M is a manufactured blade profile which will be tested at the KTH test turbine in the fall 2015. That profile is very close to the BC6M that was developed during a previous master thesis by (Anton & Wiberg, 2013). The BC6M is an uncooled scaled model of a cooled modern industrial gas turbine blade. During the upgrade from the BC6M to the BC7M done in (Flydalen, 2013), a small velocity peak close to the leading edge was removed without any large geometry adjustments.

4.2.1 BC7M - Geometry

The BC7M has been designed in three radial sections named hub, mid and tip, where the hub-section is at the smallest radius and the tip-section at the largest radius. These sections have been designed as cylindrical sections. This means that the sections are not plain at one radius or in other words the leading edge has one radius and the trailing edge has another radius. A three dimensional view of the Cato model is shown in Figure 19 and the whole blisc containing 60 blades in Figure 20. From the three dimensional view it can be worth mentioning that the blade is quite simple. In Figure 21 the geometry for each section is shown. Some section parameters are also presented in Table 2. These sections will be compared to the newer profile further on. The optimum pitch-to-chord ratio was decided to be 0.827 in (Anton & Wiberg, 2013) by using the following correlation described in (Klebanov & Mamaev, 1969).

$$\bar{t}_{0nm} = \bar{t}_{0nm_O} \cdot K_{KP} \cdot (1 + \Delta\bar{t}_{0nm}) \tag{56}$$

Where K_{KP} is a correction for that the trailing edge diameter is finite. $\bar{t}_{0nm_O}$ is the preferable pitch-to-chord ratio if the exit Laval number is 0.8 and $\Delta\bar{t}_{0nm}$ is a correction to that the Laval number is not 0.8. For more information of this the reader is referred to (Klebanov & Mamaev, 1969). Note that the final pitch-to-chord value did not become the same as the optimum value since the chord could not be set directly in Cato.

Figure 19: 3D-view of the BC7M.

Figure 20: BC7M manufactured blisc.

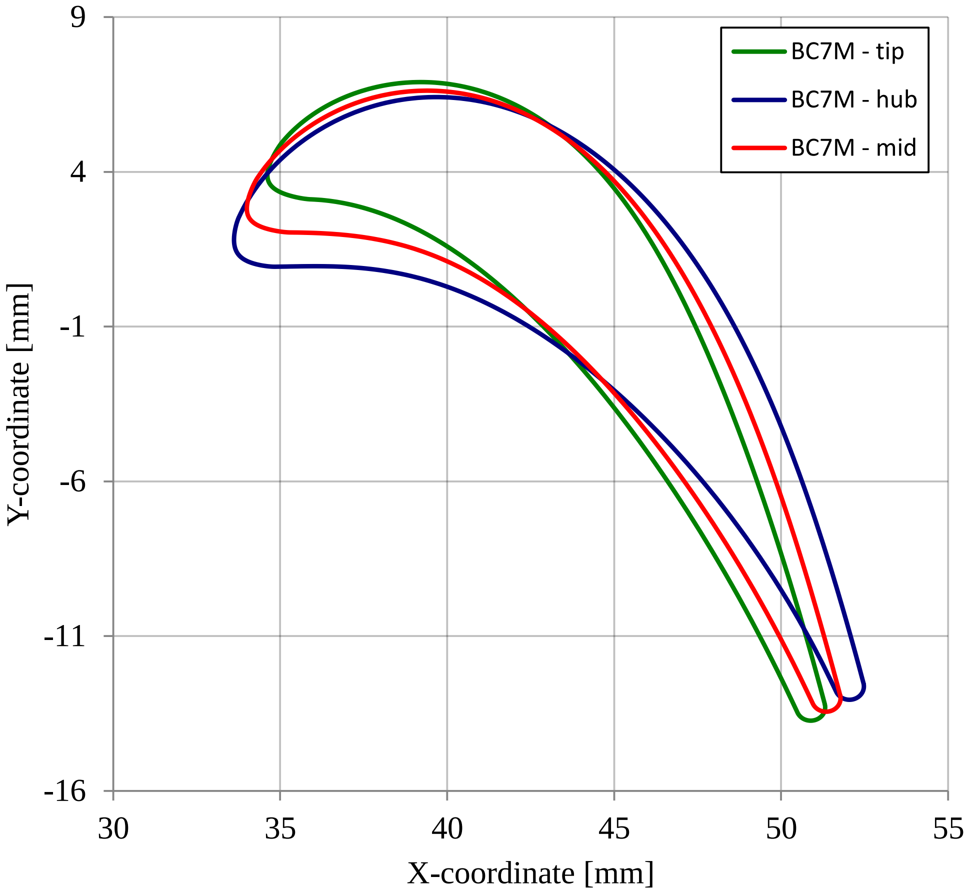

Figure 21: BC7M sections geometry. (Cato)

Table 2: Geometry parameters for the BC7M. (Cato)

	BC7M - hub	**BC7M - mid**	**BC7M - tip**
Section area [mm^2]	104.08	91.44	84.74
Area 2D/Chord $2D^2$	0.19	0.16	0.15
Axial width [mm]	18.86	17.78	16.70
CG X-coordinate [mm]	43.39	43.41	43.55
CG Y-coordinate [mm]	-0.00	0.00	-0.08
Chord 2D [mm]	23.38	23.60	23.86
Chord 3D [mm]	23.39	23.61	23.87
Effective exit angle [°]	19.22	19.21	19.27
Exit angle [°]	18.64	18.61	18.57
Flexural resistance w3	102.94	82.45	65.83
Flexural resistance w4	385.83	356.91	321.02
Flexural resistance w5	77.70	59.30	47.23
Flexural resistance w6	252.09	228.51	215.07
Inlet angle [°]	56.00	61.00	65.00
Inlet wedge [°]	66.41	59.12	54.32
Lean [°]	-2.49	-2.48	-2.47
LE diameter [mm]	2.32	2.32	2.31
LE row distance [mm]	9.65	9.34	8.89
Main axis angle [°]	0.84	0.75	0.67
Maximum thickness [mm]	6.04	5.31	4.97
Max. thick. pos./Chord 2D	0.19	0.18	0.19
Max. thick. / Chord 2D	0.26	0.23	0.21
Moment of inertia u	3856.80	3509.90	3300.80
Moment of inertia v	423.20	304.38	220.21
Pitch / Chord 2D	0.79	0.85	0.90
Pitch / Chord 3D	0.79	0.85	0.90
Radius TE [mm]	176.91	190.97	204.54
Stagger angle [°]	52.07	47.54	43.29
TE diameter [mm]	0.86	0.87	0.87
Throat distance [mm]	6.09	6.57	7.06
Uncovered turning angle [°]	22.36	22.63	23.31
Blade wetted area [mm^2][1]	1598.43		

---

[1] Value is taken from the program Siemens NX

4.2.2 BC7M - Cato, Mises results

To get results for reference, a Mises run was done for the BC7M. In the Mises solver only the rotor is analysed, hence the rotor boundary conditions had to be stated. The relative stagnation pressure at inlet, outlet Mach number and the relative flow inlet angle was set as boundary conditions for the rotor. The values for these at hub-, mid- and tip-section are shown in Table 3, where the pressure and Mach number are taken from new beta2 calculations, while the inlet flow angle is taken from (Anton & Wiberg, 2013, p. 105).

Also some other conditions had to be stated. These input parameters to the Mises solver will be mentioned as the solver parameters. The solver parameters can be found in Appendix A. All three sections, hub, mid and tip had their own solver parameters. After all the solver parameters have been chosen, the next step was to run the Mises solver. The result is shown in Table 4. In Figure 22 to Figure 25 the Mach number, static pressure, shape parameter and skin friction coefficient are presented. These results will not be discussed any more in this section, but will be used to compare with later on.

Table 3: Boundary conditions for the rotor

	hub	mid	tip
$p^*_{1,rel}$ [bar]	149580	152575	155410
$M_{2,rel}$ [-]	0.782	0.785	0.785
β_1 [°]	49.14	56.59	60.24

Table 4: Mises results for the BC7M in Cato.

Aerodynamic results	**BC7M_hub**	**BC7M_mid**	**BC7M_tip**
Section name	hub	mid	tip
Mises solver parameters	BC7M_v07_hub	BC7M_v07_mid	BC7M_v08_tip
$M_{1,real}$ [-]	0.24	0.2158	0.2087
$M_{2,real}$ [-]	0.78	0.78	0.78
$M_{1,is}$ [-]	0.24	0.22	0.21
$M_{2,is}$ [-]	0.80	0.80	0.80
β_1 [°]	49.15	56.59	60.24
β_2 [°]	18.85	18.82	18.93
p_1 [Pa]	143700	147700	150800
p_2 [Pa]	97790	99620	101700
p^*_1 [Pa]	149600	152600	155400
p^*_2 [Pa]	146500	149600	152700
T^*_1 [K]	312.5	313.6	315.0
T^*_2 [K]	312.5	313.6	315.0
w_1 [m/s]	84.52	76.36	74.03
w_2 [m/s]	262.00	263.20	263.80
Re_1 (chord) [-]	149200	134700	125600
Re_2 (chord) [-]	366000	366000	353100
Forces and moments			
Force in x-direction/(mass V1)	5.02	5.70	5.87
Torque about y/(mass r1 V1)	3.60	3.82	3.88
Torque about z/(mass r1 V1)	-0.079	-0.071	-0.072
Losses			
Outlet ref. viscous [%]	5.99	5.67	5.11
Outlet ref, inviscid [%]	0.00	0.00	0.00
Outlet ref. total [%]	5.99	5.67	5.11
Energy viscous, [%]	4.65	4.39	3.96
Energy inviscid [%]	0.00	0.00	0.00
Energy total [%]	4.65	4.39	3.96
Traupel, TE [%]	4.89	4.58	4.31
Hart TE (unrealiable yet) [%]	4.50	4.18	3.87

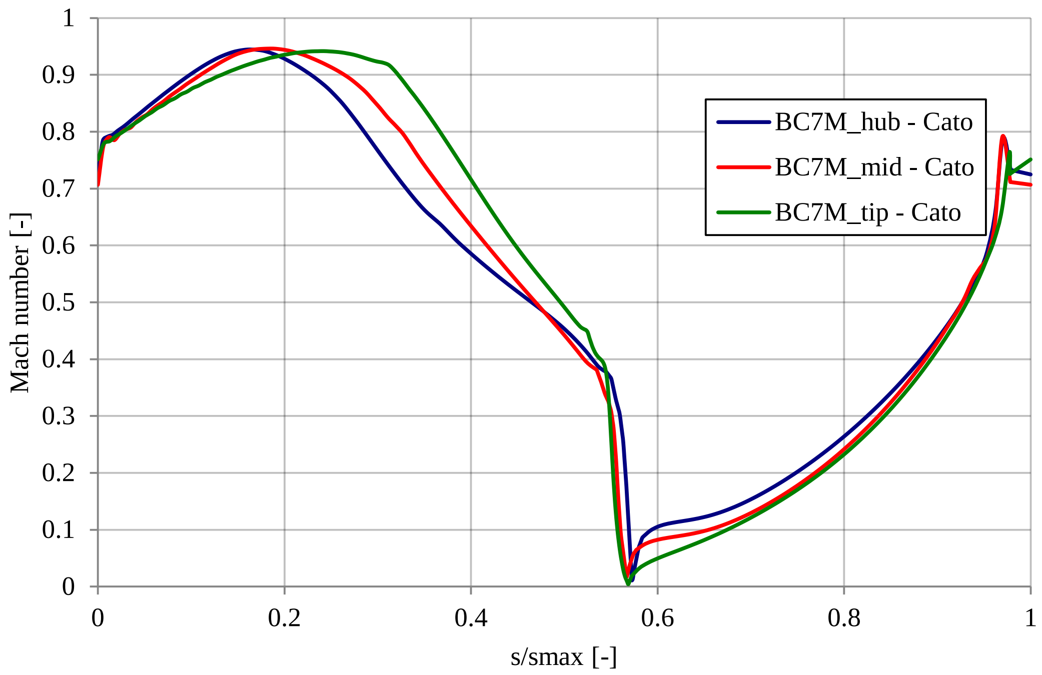

Figure 22: Mach number as a function of s/s_{max} for BC7M (Mises, Cato).

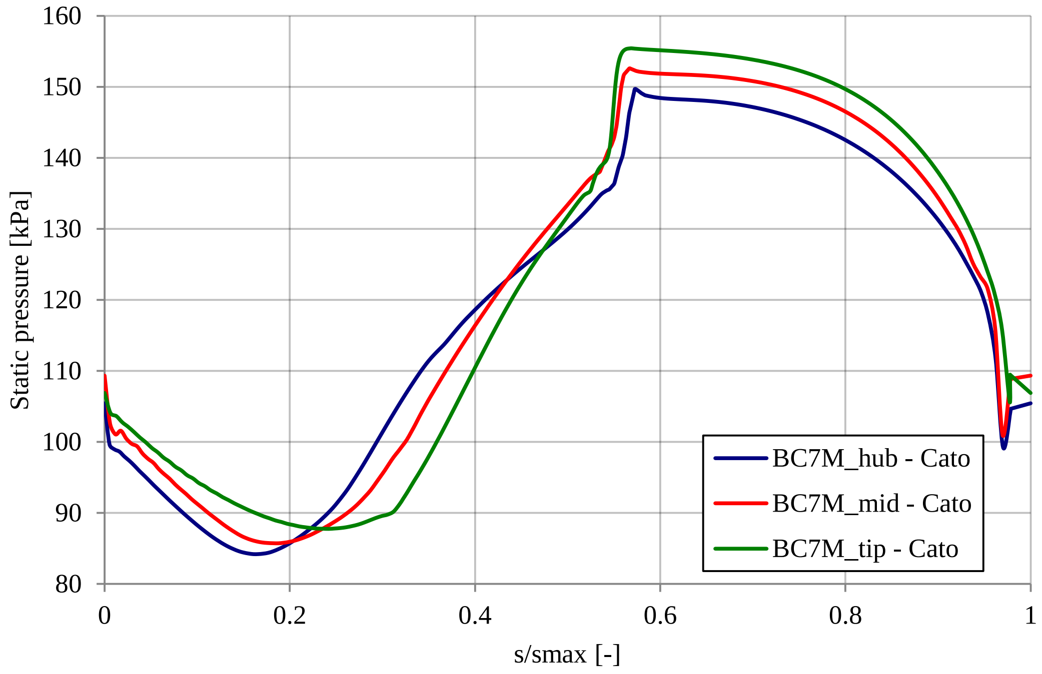

Figure 23: Static pressure as a function of s/s_{max} for BC7M (Mises, Cato).

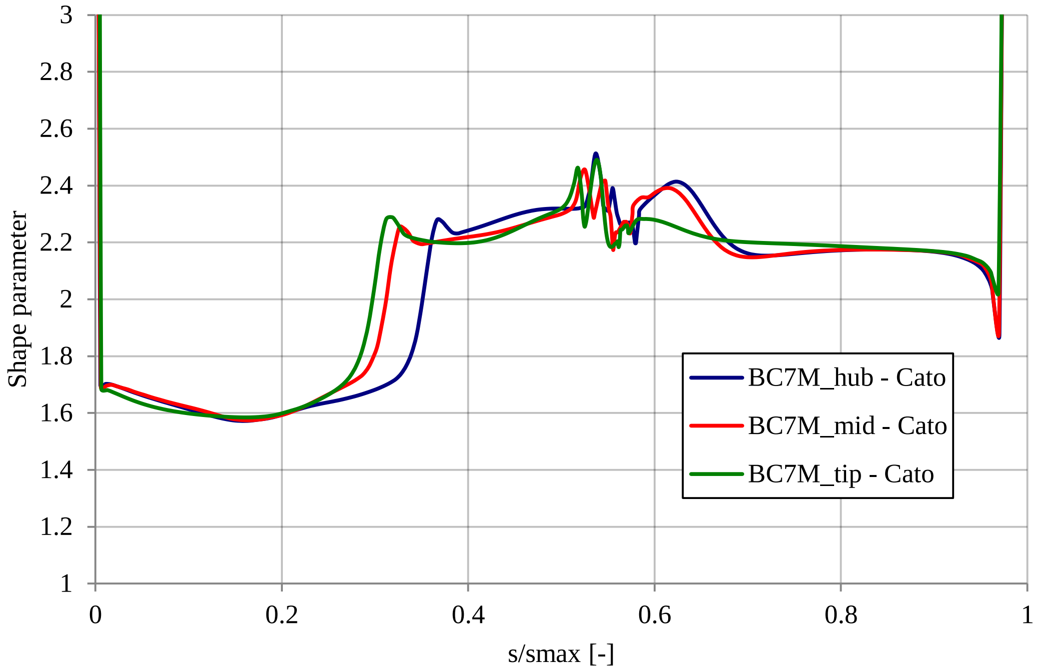

Figure 24: Shape parameter as a function of s/s$_{max}$ for BC7M (Mises, Cato).

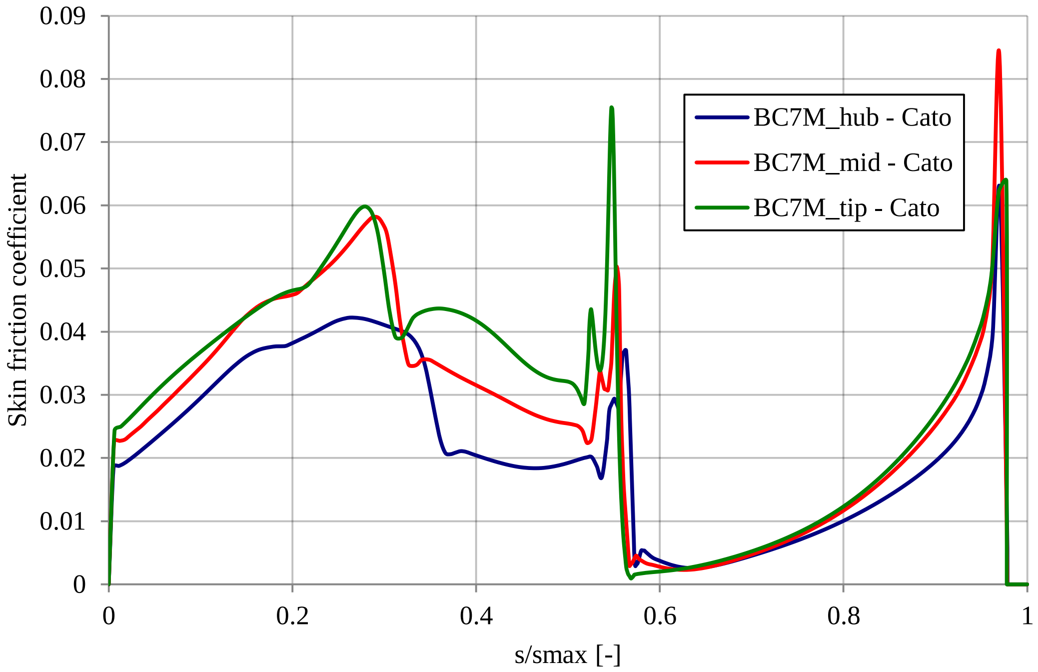

Figure 25: Skin friction coefficient as a function of s/s$_{max}$ for BC7M (Mises, Cato).

4.2.3 BC7M - Setup in beta2.

When the Cato reference cases were set, it was appropriate to run the in-house code *beta2 v.2.07.04aa* to get a beta2 reference case as well.

A geometry file was exported from Cato v.4.5.3.0. Then the easiest way to establish a beta2 input file is to use an old one and replace the old profile in this case the BC6M with the new one (BC7M).

It cannot be concluded which version of Cato that has been used creating the BC6M Cato output files, however in older versions of Cato the sections which are exported are always plain no matter how they are designed. In newer version the user can choose how to export the sections. The BC6M was designed at cylindrical sections (mentioned as conical in Cato) in a time where it only could have been exported at plain sections.

The amount of sections that was exported could easily be chosen by the user in older versions of Cato. In newer versions it is more difficult. Therefore only three sections were exported from Cato for the BC7M compared to the ten sections for the BC6M.

When using the beta2 software, the whole stage is analyzed. The stator row is the B4M row, which is an old profile that was used in the previous analysis by (Anton & Wiberg, 2013). The channel geometry is also needed, and for this, the same geometry will be used as in previous calculations by (Anton & Wiberg, 2013). The channel geometry, the B4M vane and the BC7M blade are shown in Figure 26. As can be seen, there is a tip recess at the casing. The reason for using tip recess is to reduce the tip clearance losses.

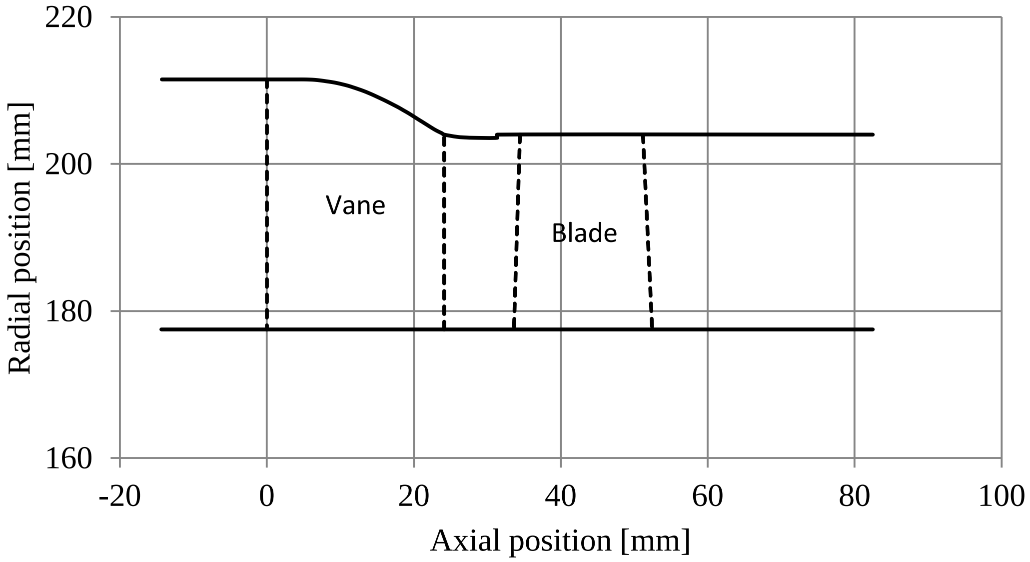

Figure 26: Channel geometry with the B4M vane and BC7M blade.

Since the whole stage is studied in this case, the whole turbine boundary condition should be set. The same properties that (Anton & Wiberg, 2013) used will be used again since this will give comparable results. These values are shown in Table 1. Note that the inlet total pressure which is set in the input file is the inlet total pressure radial distribution shown in Figure 18.

In addition to these boundary conditions, other input parameters had to be set, e.g. gas composition, more geometrical description, which loss model that is used, if cooling air is used and numerical parameters. These parameters will be further described in Appendix B.

The results of these calculations will not be presented separately here, however they will be presented in comparisons with a different profile later on in this report.

4.2.4 BC7M - Multall setup

To be able to improve the Cato model of the blade profile later on, Multall 3D calculations were performed. This gives the opportunity to analyse vortices, tip leakage and other parameters. As for beta2, the easiest way to create Multall input files is to use old files.

As a start, the blade BC7M was exported to a Multall (vda) file. The mesh was then created including 1.24 millions of nodal points. This mesh is in need of a careful analysis to ensure that the result will not be affected by a poor mesh. Since the inlet flow is axial the mesh upstream of the vane leading edge will be axial and thereby following the flow direction. No finer or coarser mesh will be studied since the mesh used is a standard mesh used at SIT.

Worth mentioning is that the Multall solver does not model the trailing edge of a profile well. Actually the flow will accelerate when it turns around the trailing edge creating some velocity peaks due to the high curvature and unnecessary unrealistic data will be presented. To avoid this, a cusp is made at the trailing edge giving a sharp edge to the mesh to force the flow to separate. There will also be a cusp at the leading edge to avoid getting too skewed mesh. A stretching of the mesh is done to make sure that the mesh is fine enough at the boundary layers and close to leading and trailing edges.

The boundary conditions that were set were the total pressure at the turbine inlet which is presented in Figure 18. At the turbine exit the static pressure is assumed to be atmospheric pressure as presented in Table 1. Axial flow is assumed into the turbine. In the control file that will be presented soon, there is an option to choose how the static pressure at the outlet will be determined. The decision was taken to set the static pressure at the hub and then let the program use radial equilibrium to decide the radial distribution. The value set at the hub was set in an iterative approach so that the 1D Dzung average result will be equal to the boundary condition presented in Table 1. The total temperature at the inlet was set as constant across the radius and the rotational speed was set to 10300 rpm according to Table 1. The gas constant and the specific heat were set to be 287.9 J/kgK and 1009.5 J/kgK according to previous beta2 results. There will be more values in the boundary condition file, however these will only be a guess for the first iteration. Later on Multall will create a restart file that will be used instead of these guesses.

The control file is also needed before it is possible to run Multall. Multiple parameters were set in the control file and only the one of interest will be described. The tip clearance modelling is set in this control file. Analysis of the input data used by Anton & Wiberg showed that they had done a tip clearance modelling with much smaller gap than it was meant to be. According to (Flydalen, 2015) this gap should be decided using the following equation:

$$Multall\ input\ clearance\ data = \frac{gap}{blade\ span} \cdot factor \qquad (57)$$

The factor that is used is 2/3, obtained from (Flydalen, 2015), which is not the same which is mentioned in the Multall manual where they say that a factor of 0.6 should be used. The gap should be 0.3 mm and the blade height is 26.5 mm. Making use of Equation (57) the Multall input data for the clearance will be 0.0075. The mesh stretching and the Reynolds number were also set in the control file. The Reynolds number was adjusted so that the result Reynolds number was consistent with the beta2 results.

Not exactly the same channel geometry will be used for Multall and beta2 that (Anton & Wiberg, 2013) did use. There will be two differences. First of all (Anton & Wiberg, 2013) did not use the tip recess channel in Multall, however for this study a channel with tip recess will be used. It will not look exactly the same due to the fact that Multall cannot create a mesh if it is like in the beta2 chapter. Hence the tip recess will be modelled differently and this is shown in Figure 28 where the black line shows the beta2 tip recess and the red one represents the Multall tip recess. Another thing that occurred after the first Multall calculation was that the pressure contours from the stagnation point did affect the boundary conditions at the inlet. Therefore the inlet was made longer for the Multall calculations compared to the geometry used in beta2 and the geometry used by (Anton & Wiberg, 2013), as can be seen in Figure 27.

As for the beta2 results, the results of these calculations will not be presented separately here. Instead these results will be presented in comparisons with a different profile later on in this report.

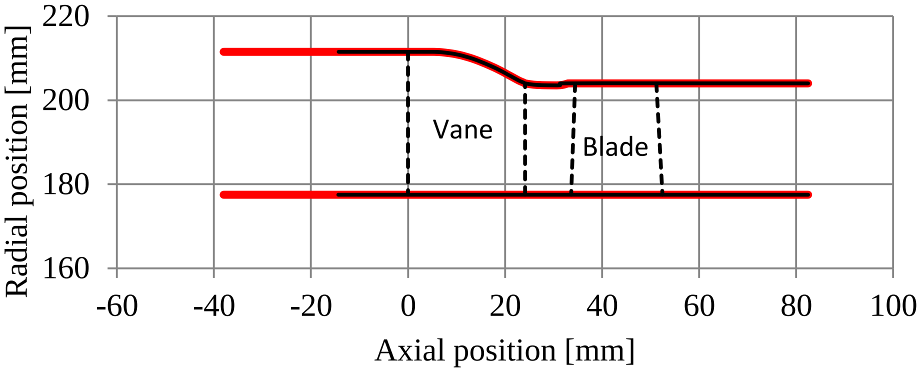

Figure 27: Multall (red) and beta2 (black) channel

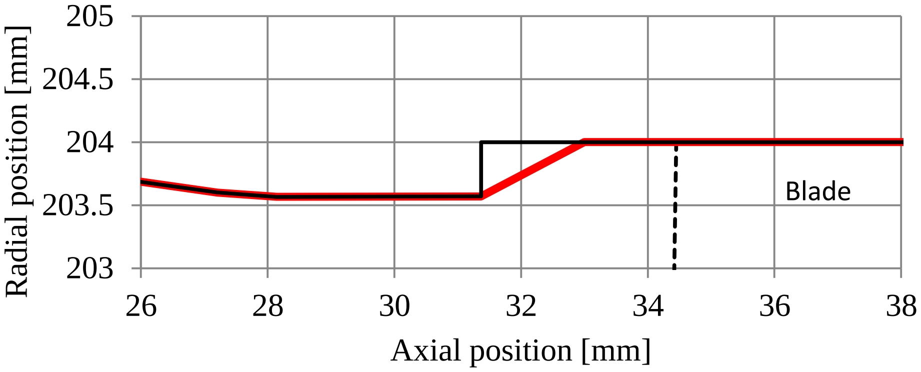

Figure 28: Tip recess for Multall (red) and beta2 (black) channel.

4.3 *Profile loss study for variation of the pitch-to-chord ratio, BC7M*

When the reference case was set, the first real analysis started. The aim of the first analysis was to see how the profile loss varies with different pitch-to-chord ratio. This was done in the mid-section of the existing profile geometry of BC7M.

This profile loss study with different pitch-to-chord ratio had two different main approaches. The first and the simplest one was just to remove or add some blades, which according to the previous theory will give more or less turning of the flow and hence a smaller or larger flow outlet angle. The second approach also closes or opens the passage to get the same flow outlet angle as the reference case with 60 blades. Both approaches used the Mises solver in Cato version 3.5.

4.3.1 BC7M - Different flow outlet angle

As mentioned before the first approach was to just adjust the number of blades without closing or opening the passage. Cato does not offer the opportunity to just change the number of blades in the geometry interface without changing the whole geometry. Instead this had to be solved in another way. There are at least two different approaches that will work. The first is to calculate the pitch-to-chord ratio for different number of blades, using constant chord since the profile geometry is fixed. The pitch was given in Equation (34). Hence the pitch-to-chord ratio can be written as:

$$\frac{t}{c} = \frac{\frac{2 \cdot r \cdot \pi}{n}}{c} = \frac{2 \cdot r \cdot \pi}{n \cdot c} \tag{58}$$

In the Mises solver in Cato, the pitch-to-chord ratio can then be used as a solver parameter. Then the calculation can be done using the solver parameters described in Appendix A and of course using the calculated value of the pitch-to-chord ratio instead of the default value for 60 blades that is mentioned in Appendix A. Then the Traupel and Energy profile losses were plotted as functions of pitch-to-chord ratio.

The other approach to do the same calculation was more complicated than the first one. This method used the export and import features in Cato. By exporting the geometry for the BC7M mid-section as coordinates and then import it again, the opportunity to change the number of blades without changing the whole geometry appears. It is of importance to note the pitch-to-chord ratio that then is given, since this will disappear when running the Mises solver. This import and export coordinates method will have a slight impact of the chord since the chord is calculated in a different way when just using coordinates compared to when Bezier functions is used. The same solver parameters as in the previous method was used and is described in Appendix A.

4.3.2 BC7M - Same flow outlet angle

The second approach keeps the turning of the flow at a constant value compared to the reference case with 60 blades, when changing the number of blades. For this case it is not possible to just rotate the blades in the Mises solver input parameters. The only possibility is to use the import and export feature again since this also offers an option to rotate the coordinates. This becomes an iterative method, were the rotation needed to get the right flow outlet angle has to be guessed. Then the import and export procedure has to be done until the right flow outlet angle is achieved. This has to be repeated for all of the number of blades studied. The solver parameters were the same as in previous methods and are described in Appendix A. Of course by rotating the blade the metal inlet angle will be changed, and since the flow inlet angle is fixed, the incidence will be changed. The profile loss were then plotted and compared to the export and import method with different flow outlet angle.

4.3.3 Comparing profile losses for the BC7M mid-section.

The comparison between the two different methods of changing the pitch-to-chord ratio without opening and closing the passage is shown in Figure 29. It can be seen that the methods that should be doing the same thing actually gives a result that is not equal. The main reason for this is assumed to be that the chord is actually not calculated in the same way in both methods since the first method uses Bezier functions describing the curve and the other one uses coordinates. Nevertheless, the Traupel loss tends to be higher in almost the whole area studied.

By taking into account that the turning of the flow should be the same as before removing or adding blades the results looks different as can be seen in Figure 30. For pitch-to-chord ratios higher than approximately 1.05 the whole solution does not converge any more due to strong separation.

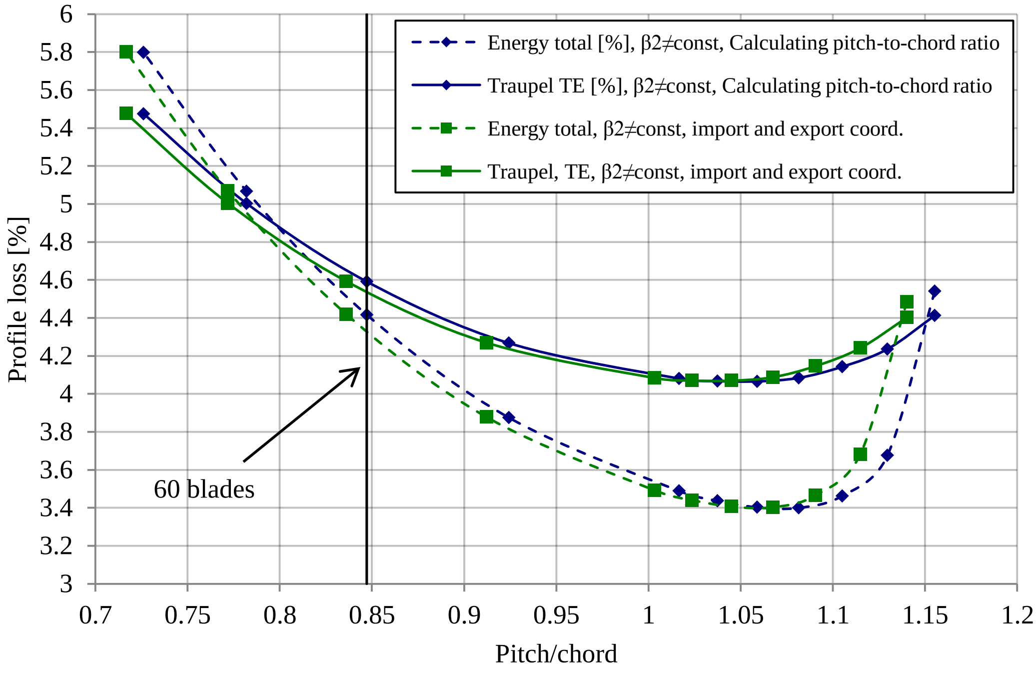

Figure 29: Profile loss comparison between the two different methods, import and export coordinates method and calculating the pitch-to-chord ratio method, both with changed flow outlet angle β_2. (Mises, Cato)

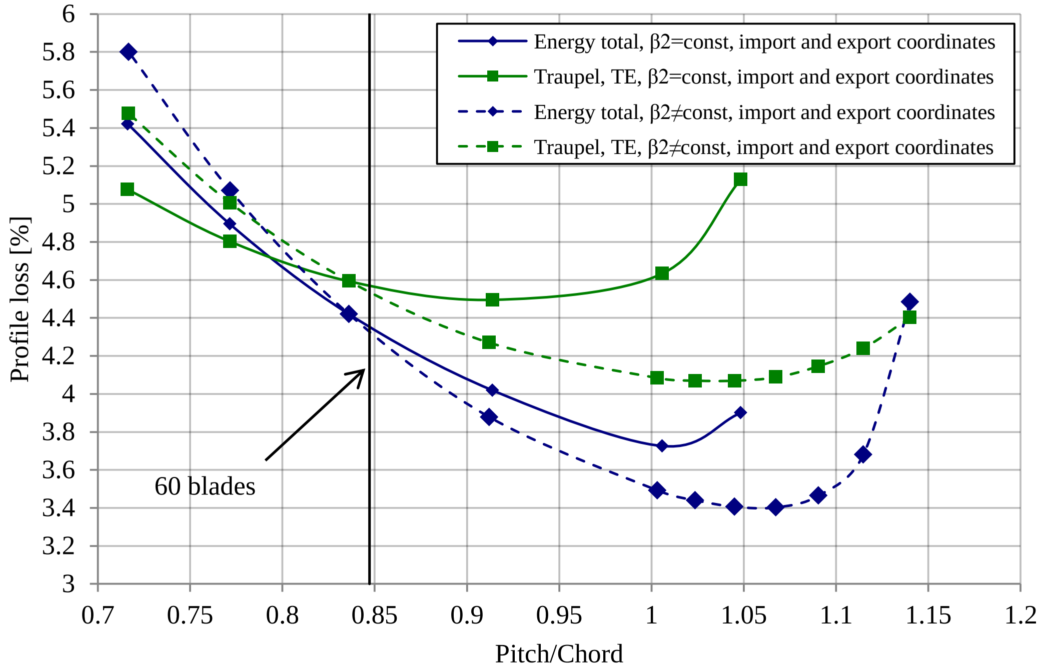

Figure 30: Profile loss comparison between two different cases, one where the flow outlet angle β_2 is kept constant and one where it is changed.

4.4 *Profiling of B50_v01*

As a result of the previous profile loss study, the decision was made to try to design a row with 50 blades with a pitch-to-chord ratio at approximately one at the mid-section. This since at this pitch-to-chord ratio the profile loss starts to increase rapidly. It is important to note that this optimum only takes profile loss into account. For the Traupel loss also the trailing edge loss is included, however no secondary losses are taken into account for none of them at this stage. The new design will be a re-design of the BC7M. The new profile should be as similar to the BC7M as possible, to avoid having problems with the strength of materials and to avoid being forced to do a structural analysis. Another main aspect was to keep the throat area constant to get the same mass flow through it. To keep the work done by the rotor at the same level as before, the turning of the flow will still be kept constant.

4.4.1 Import and adaption of BC7M.

To get a good profile to start with the BC7M coordinates for the tip-, mid- and hub-sections were exported and then imported back to Cato v.4.5.3.0, now with 50 blades. No rotations were made since the axial chord was desired to be constant.

When the coordinates are exported back, it gives a curve side by side with the default Bezier curve, as shown in Figure 31. The input design parameters that Cato offers has to be adjusted to get the Bezier curve to fit or match with the coordinate curve. This can be done in many different ways. However it can still be useful to follow a certain method to obtain suitable values of the design parameters and to get a smooth curvature. It is possible to get the curves to look the same with unsuitable values of the design parameters. To avoid this, the method described by (Flydalen & Sohaib, 2011) will be used and described below.

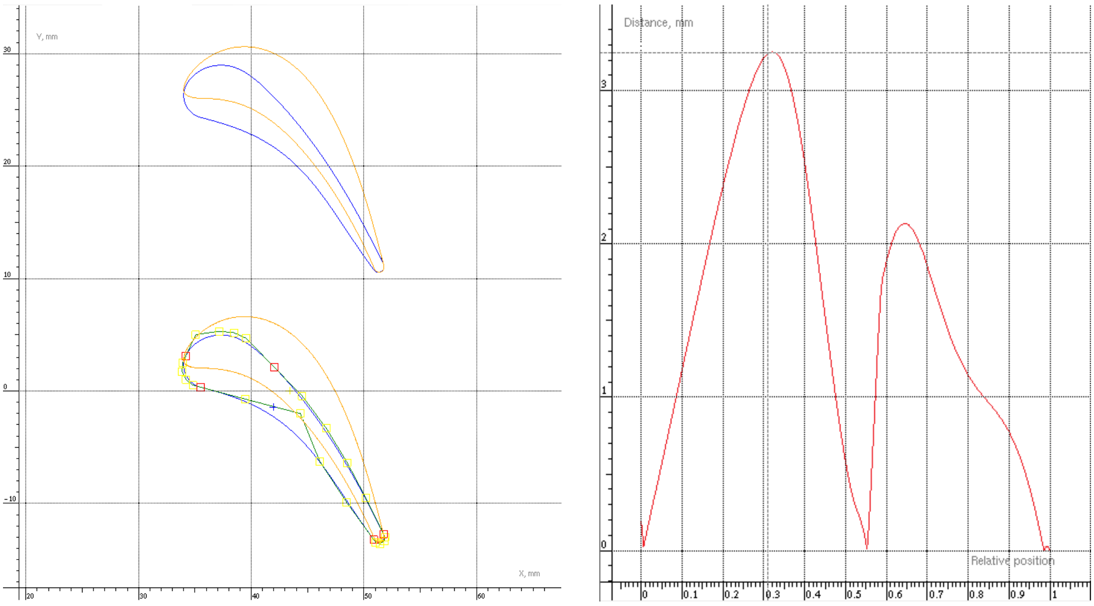

Figure 31: To the left, the imported coordinates for BC7M mid-section (orange) and default Bezier curves (blue) and to the right, the deviation in mm between the curves. (Cato v.4.5.3.0)

The first section of the profile that is adapted is the trailing edge and close to it. Then the distance between the trailing edge and the throat on the suction side is adapted. This is done by adjusting the parameters in the two upper boxes in Figure 32. These steps should be repeated until the distance between the coordinate curve and the Bezier curves is small enough.

Then the inlet angle was adjusted followed by the slope, pressure side camber and curve LE. Then all steps were repeated to make sure that the adaption was as good as possible close to the trailing edge.

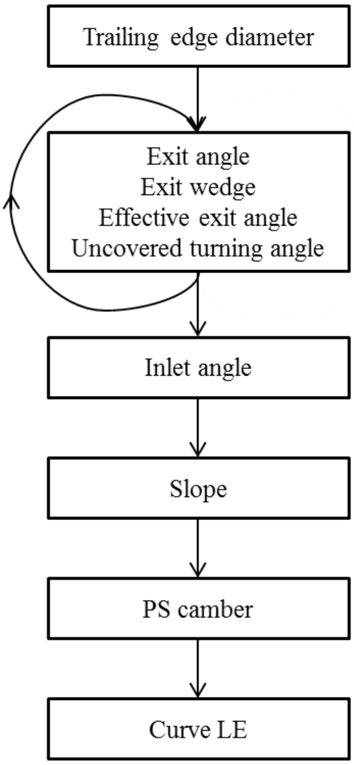

Figure 32: Trailing edge and suction side adaption method. Redesign of (Flydalen & Sohaib, 2011, p. 13)

When the deviation or error was small enough the next step that was done was to let Cato make a loop containing more fine adjustment parameters to fit the Bezier curves much closer to the coordinate curve. The parameters included in these loops have been listed by (Flydalen & Sohaib, 2011, p. 16) and are shown below.

- Inlet wedge
- Uncovered turning angle
- Leading edge diameter
- Slope
- Curve throat
- Curve trailing edge
- Curve leading edge
- Pressure side camber 3
- Pressure side camber 4

This loop was done until the deviation did not get any smaller. Then the whole process was restarted at the trailing edge diameter. This method progressed until the adaption was good enough. Since these coordinates were exported from Cato it was not that difficult to get the adaption to match the Bezier functions. In Figure 33, the deviation can be seen for the finished adaption of the mid-section. The largest deviation can be seen to be approximately 0.02 mm which is assumed to be good enough. Of course this adaption process had to be done for all three sections tip, mid and hub, however since these adaptations only will be used as starting values for the continued development of the new profile, the tip- and hub-section adaptions will not be presented in this report. It can though be mentioned that at this stage the uncovered turning angle is 30, 30 and 32 degrees at the hub-, mid- and tip-section. At the same sections the effective exit angle is approximately 22.5 degrees. At this stage the profile is named B50_v01_00, where B50 means 50 blades, and v01 is the overall version number, and 00 is a smaller update number.

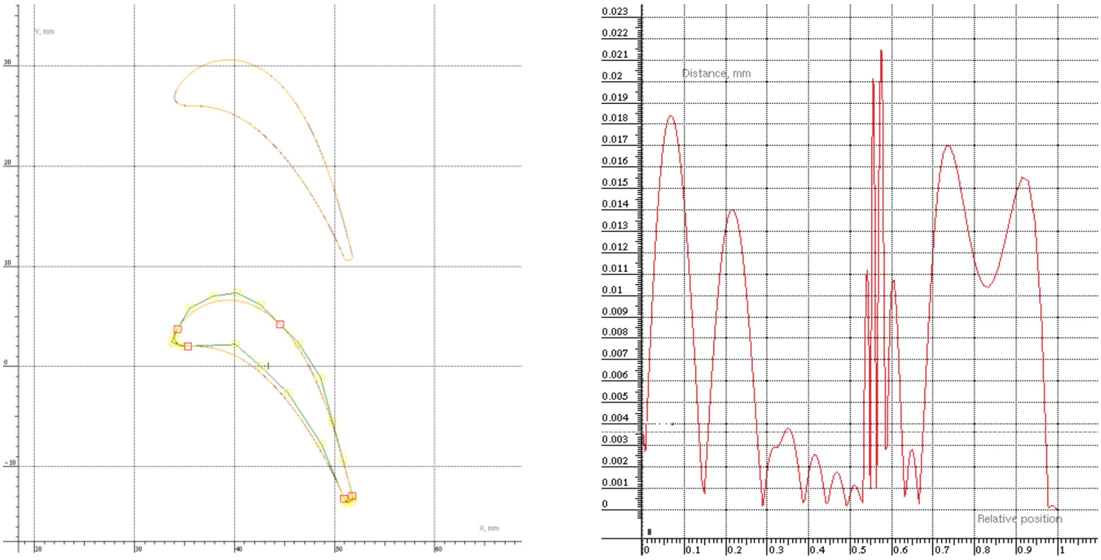

Figure 33: To the left the imported coordinates for BC7M mid-section (orange) and the adapted Bezier curves (blue) and to the right the deviation in mm between the curves. (Cato v.4.5.3.0)

4.4.2 Adapted profile B50_v01 run with Mises in Cato.

When the profile was adapted, it was used as a starting geometry for the continued designing process. The new profile could have been designed directly from the default Bezier curves however this would have been even more complicated, and since the geometry should be as close as possible to the old geometry, the option to adapt the profile first was the best alternative.

To get an idea of what adjustment that was needed to be made in addition to the obvious that the turning is not enough, the sections were run in the Mises solver in Cato v.4.5.3.0. To start with, the Mises solver parameters were kept at the same values as before and these are shown in Appendix A. The results of all three sections are presented in Table 5 and in Figure 34 to Figure 37. These results cannot be compared directly to the BC7M results, since the Reynolds number, throat distance and turning of the flow is different. This will be further investigated in the next section.

Table 5: Mises results for the adapted profile B50_v01. Note that the flow outlet angle is not adjusted at this stage. (Mises, Cato)

Aerodynamic results	**B50_v01_hub**	**B50_v01_mid**	**B50_v01_tip**
$M_{1,real}$ [-]	0.27	0.25	0.24
$M_{2,real}$ [-]	0.78	0.78	0.78
$M_{1,is}$ [-]	0.27	0.25	0.24
$M_{2,is}$ [-]	0.80	0.80	0.80
β_1 [°]	49.14	56.59	60.23
β_2 [°]	21.35	21.42	21.67
p_1 [Pa]	142000	146200	149300
p_2 [Pa]	98210	100100	102100
p^*_1 [Pa]	149600	152600	155400
p^*_2 [Pa]	147100	150200	153300
T^*_1 [K]	312.5	313.6	315
T^*_2 [K]	312.5	313.6	315
w_1 [m/s]	96.47	87.44	85.23
w_2 [m/s]	262.00	263.20	263.80
Re_1 (chord) [-]	149000	134600	125400
Re_2 (chord) [-]	323600	322400	309100
Forces and moments			
Force in x-direction/(mass V1)	3.64	4.15	4.22
Torque about y/(mass r1 V1)	3.19	3.36	3.38
Torque about z/(mass r1 V1)	-0.094	-0.089	-0.088
Losses			
Outlet ref. viscous [%]	4.81	4.43	3.98
Outlet ref, inviscid [%]	0.00	0.00	0.00
Outlet ref. total [%]	4.81	4.43	4.98
Energy viscous, [%]	3.74	3.44	3.09
Energy inviscid [%]	0.00	0.00	0.00
Energy total [%]	3.74	3.44	3.09
Traupel, TE [%]	4.26	4.08	3.93
Hart TE (unrealiable yet) [%]	3.82	3.45	3.34

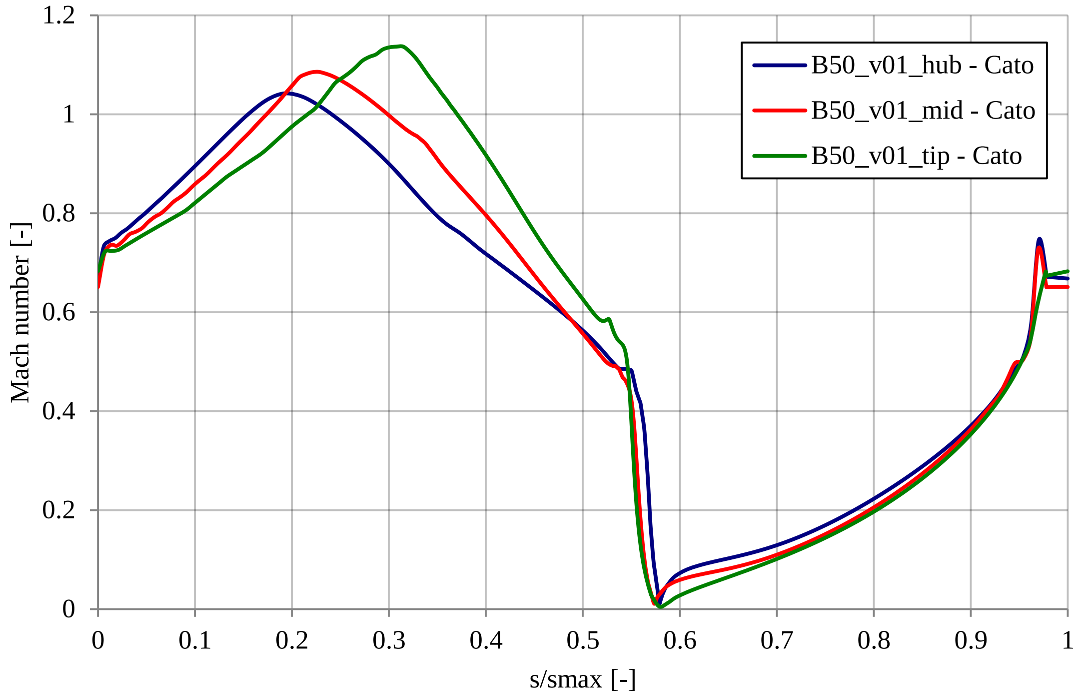

Figure 34: Mach number distribution as a function of s/s_{max} for B50_v01. Note that the flow outlet angle is not adjusted at this stage. (Mises, Cato v.4.5.3.0)

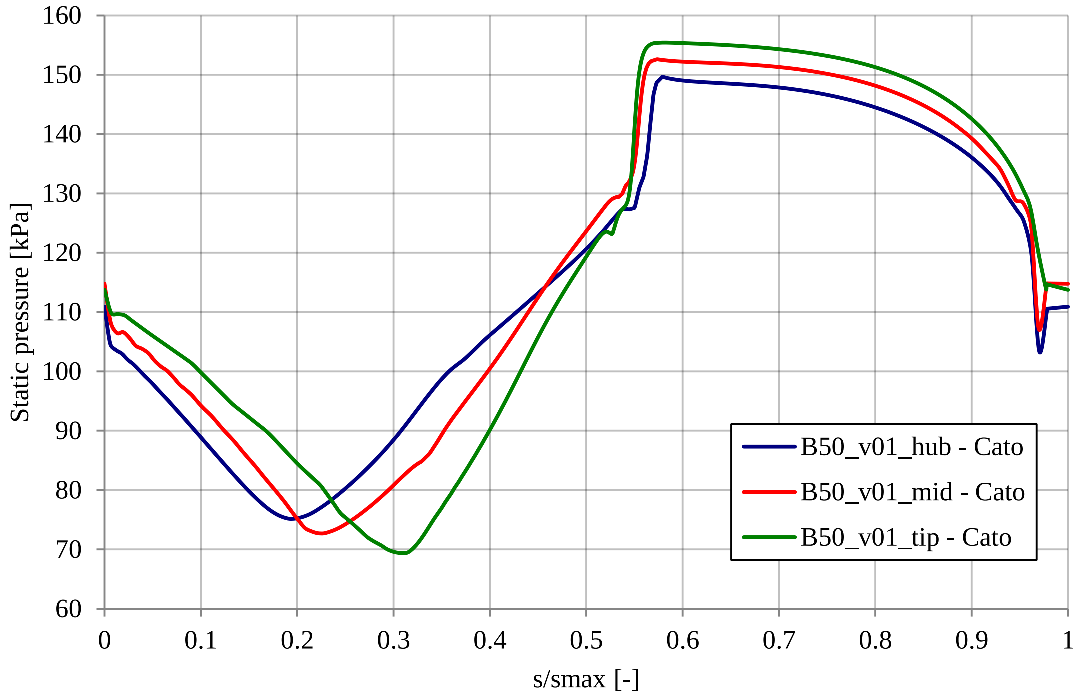

Figure 35: Static pressure distribution as a function of s/s_{max} for B50_v01. Note that the flow outlet angle is not adjusted at this stage. (Mises, Cato v.4.5.3.0)

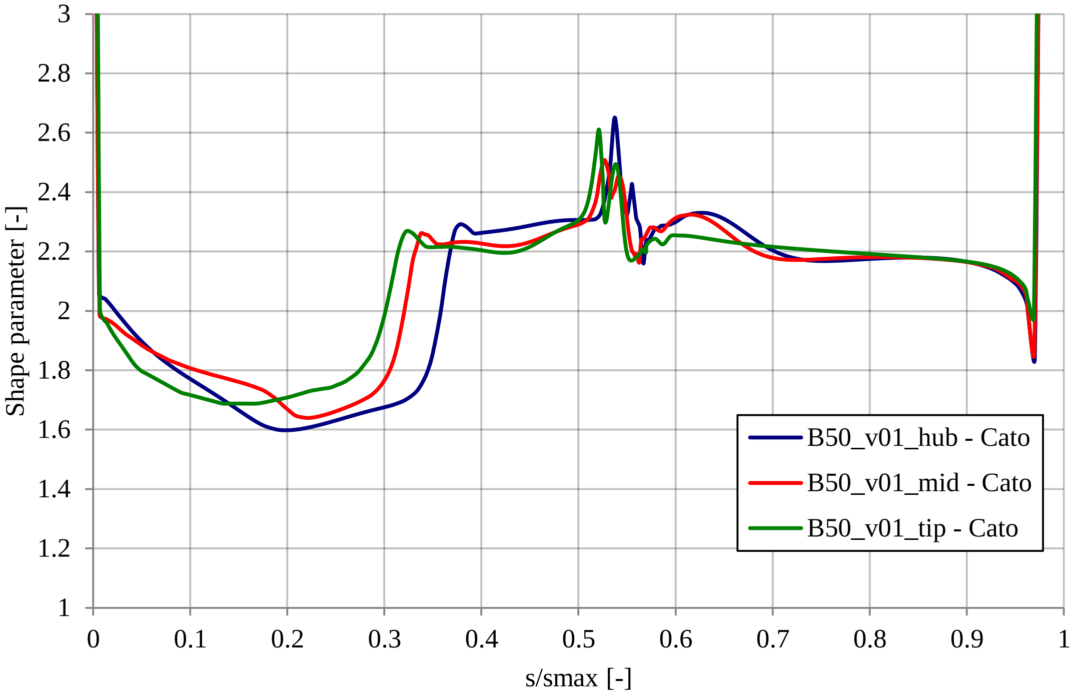

Figure 36: Shape parameter distribution as a function of s/s$_{max}$ for B50_v01. Note that the flow outlet angle is not adjusted at this stage. (Mises, Cato v.4.5.3.0)

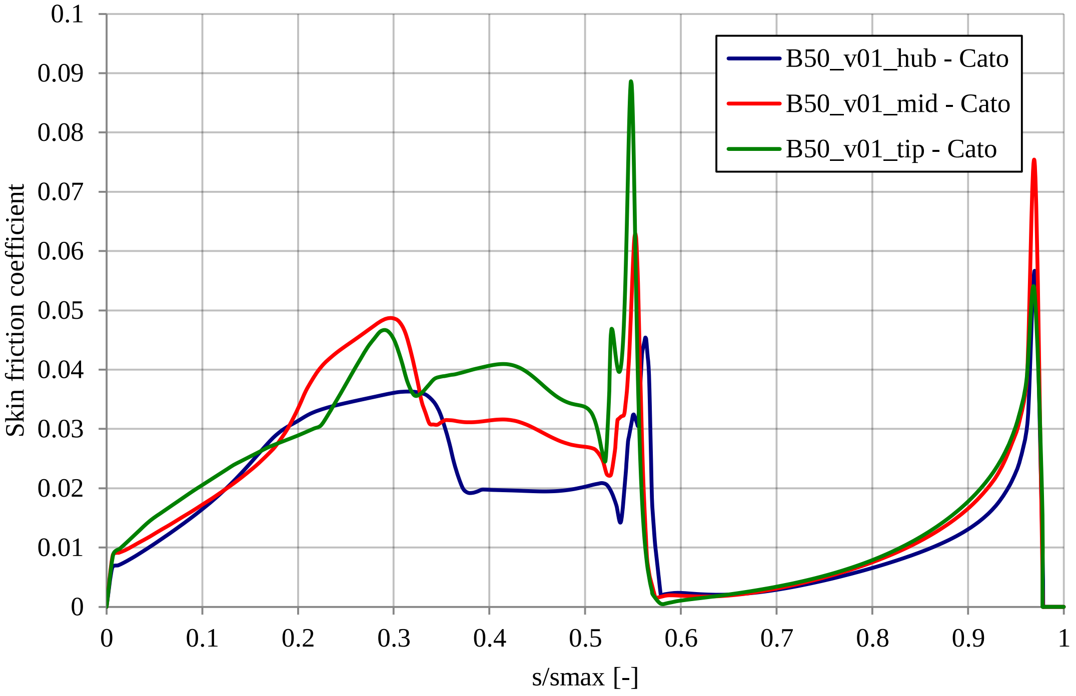

Figure 37: Skin friction coefficient distribution as a function of s/s$_{max}$ for B50_v01. Note that the flow outlet angle is not adjusted at this stage. (Mises, Cato v.4.5.3.0)

4.5 B50_v01_03

4.5.1 Design principles for B50_v01_03

The hub-, mid- and tip-section are now fully adapted. To go any further, some design requirements are listed below.

- Keep the trailing edge thickness at the same value as for the BC7M, to make sure that it will be possible to manufacture. Casting methods demands a certain thickness to be able to make space for two walls and a cooling slot in the middle. (TE diameter)
- The total throat distance should also be kept constant to avoid affecting the degree of reaction.
  (Throat distance)
- Axial chord should be constant to be able to fit the blade in the existing turbine.
  (Axial width)
- Keep constant profile area to ensure that the strength of material is not changed drastically. Actually there would probably not be any problem at the test turbine, however problems may occur at the full scale turbine.
  (Section area)
- The leading edge diameter should be kept as close to the BC7M as possible. (LE diameter)
- Keep the Mach number peak below one or even lower if possible, to avoid shock waves.
- The flow outlet angle should be kept at the same values as for the BC7M, due to the fact that the turning of the flow should be the same to keep the same total work done by the blades.
- Design the blade inlet angle according to Figure 4.2 in (Moustapha, Zelesky, Baines, & Japikse, 2003).

4.5.2 Further B50_v01_03 design development

As when adapting the profile, the mid-section will be described below and the hub- and tip-sections will not be fully described, however the results for the hub- and tip-sections will of course be stated.

The LE- and TE-diameters were directly set to the same values as for BC7M. The result from the Mises calculation showed that the flow outlet angle was 21.42 degrees. This is a much higher value than for the reference flow outlet angle which is 18.82 degrees. Hence the effective exit angle was decreased with approximately the size of the difference. Reducing the effective exit angle will decrease the throat distance.

To get the correct blade metal inlet angle, Figure 38 was used. The flow inlet angle was 56.59° at the mid-section, giving an induced incidence at approximately 0.5°. The flow inlet angle is 49.14° and 60.23° for hub- and tip-sections respectively. This gives an induced incidence at 2.0° and -0.5°. As described in the theory, positive incidence means that the metal angle is larger than the flow inlet angle. This gives a blade metal inlet angle rounded to 51°, 57° and 60° at the hub-, mid- and tip-section respectively.

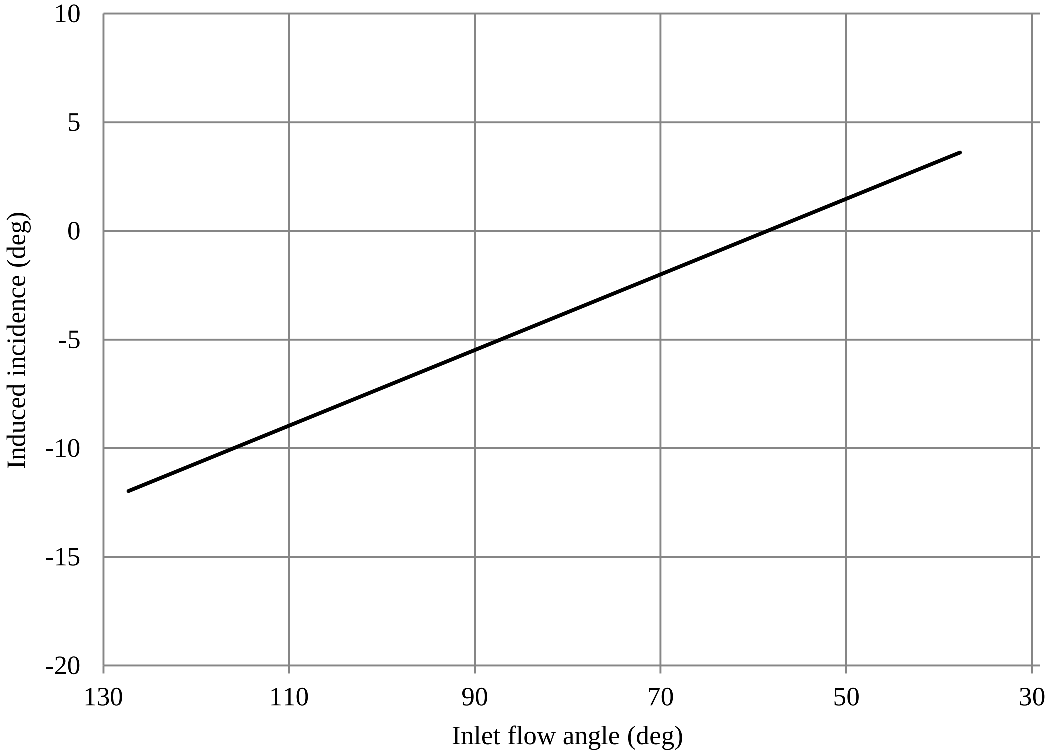

Figure 38: Induced incidence as a function of flow inlet angle. Redesign of Figure 4.2 (Moustapha, Zelesky, Baines, & Japikse, 2003, p. 99)

To get the same total throat it has to be taken into account that there will be fewer passages when having fewer blades. For each section the throat distance has to be calculated as:

$$Throat\ distance_{B50\_v01\_03} = \frac{60\ blades}{50\ blades} \cdot Throat\ distance_{BC7M} \tag{59}$$

Use of Equation (59) resulted in that the throat distance for the B50_v01_03 should be:

Table 6: Target values for B50_v01_03 throat distance

	Throat distance [mm]
B50_v01_03 - hub	7.308
B50_v01_03 - mid	7.887
B50_v01_03 - tip	8.474

The uncovered turning angle is a parameter that will adjust the throat distance, however not in the same range as the effective exit angle does. The uncovered turning does explain how much turning of the flow that appears after the throat. During the adaption, the uncovered turning angle was set to approximately 30 degrees. Since the total turning of the flow is given, a decrease of the uncovered turning angle leads to less turning of the flow after the throat and more before.

As can be seen in Figure 34 the velocity peaks are above Mach one at each section. The adjustment of the uncovered turning angle will be the best alternative to move and decrease these peaks. By decreasing the uncovered turning angle, more turning of the flow will occur before the throat. This will lead to that a part of the blade load will be moved upstream and hence a decreased velocity peak.

In turbine design in subsonic flows the velocity peak may occur optimally at the throat. In some cases when having supersonic flows the velocity peak will occur downstream the throat, since the flow is choked in the throat. The convergent-divergent nozzle will then act as a Laval nozzle creating supersonic flows (Hedlund, 2015). The choice of the value for the uncovered turning angle is also based on designer’s experience.

The Reynolds number was also changed as a Mises solver parameter to make sure that the outlet Reynolds number was kept constant, since when closing the profile the chord will be changed affecting the Reynolds number since it is based on chord.

A large part of this process was of course iterative. Small adjustment of the other blade parameters had to be made to get a good velocity distribution and a smooth curvature, especially on the suction side.

When all sections are considered to be complete, the sections were stacked at the centre of gravity for each section.

4.5.3 Final design B50_v01_03

The final design of the B50_v01_03 will be presented below.

In Table 7, section output parameters are presented for B50_v01_03 including a comparison to BC7M. These parameters are geometrical parameters that are automatically presented in Cato. The inlet wedge angle can be seen to be smaller for B50_v01_03 compared to BC7M. It can also be seen that even though the goal was to design a profile with the same size of the section area, the new profile was 2-6 % smaller. The total profile area has changed even more since there is a difference in number of blades. The total section area that will affect the cooling mostly is the area at the hub since if this decrease, this will give raise to an increased cooling need on the rotor platform.

$$A_{BC7M,hub,tot} = 60 * 104.08 = 6244.8mm^2 \tag{60}$$

$$A_{B50\_v01\_03,hub,tot} = 50 * 99.385 = 4969.3mm^2 \tag{61}$$

This means that the hub-section area will decrease by 20.4 % or 1276 mm^2, which is the extra area on the rotor platform that has to be cooled.

The B50_v01_03 blade also has an increased wetted area compared to BC7M by 8.3 %. However the total blade wetted area has decreased by 9.7 % or 9320 mm^2.

$$A_{BC7M,wetted,tot} = 60 * 1598.43 = 95906mm^2 \tag{62}$$

$$A_{B50\_v01\_03,wetted,tot} = 50 * 1731.71 = 86586mm^2 \tag{63}$$

In Figure 39 both the section geometry and curvature are shown for the hub-, mid- and tip-section. The new B50_v01_03 can be seen to have much longer chord compared to BC7M. The thickness is almost the same, however B50_v01_03 is more slender. The curvature is almost the same, however a tendency is that it is higher close to the leading edge compared to BC7M and almost zero on the other half of the profile

A Mises solver result comparison is shown in Table 8. Only small differences occur for the flow outlet angle and Reynolds number. The biggest difference can be seen for the losses where all losses are lower for the B50_v01_03.

At the end of this section a comparison for the Mach number, static pressure, shape parameter and skin friction coefficient is shown in Figure 40 to Figure 43, followed by a Mach number distribution at the hub-, mid- and tip-section for the BC7M and the B50_v01_03. The stagnation point can be seen to have been moved more to the pressure side than before.

Table 7: Section output parameters for B50_v01_03. The difference is compared to BC7M. (Mises, Cato)

Section Output Parameters	B50_v01_03 hub		B50_v01_03 mid		B50_v01_03 tip	
Section name	B50_v01_14_hub		B50_v01_05_mid		B50_v01_05_tip	
	Diff	Value	Diff	Value	Diff	Value
Section area [mm^2]	-4.5 %	99.39	-2.5 %	89.19	-5.7 %	79.93
Area 2D/Chord $2D^2$	-15.7 %	0.16	-17.7 %	0.14	-22.3 %	0.12
Axial width [mm]	0.0 %	18.86	0.0 %	17.78	0.0 %	16.70
CG X-coordinate [mm]	-0.2 %	43.32	-0.2 %	43.32	-0.5 %	43.32
CG Y-coordinate [mm]	62.1 %	-0.00	-267 %	-0.00	-95.4 %	-0.00
Chord 2D [mm]	6.4 %	24.88	8.9 %	25.70	10.2 %	26.29
Chord 3D [mm]	6.4 %	24.89	8.9 %	25.70	10.2 %	26.30
Effective exit angle [°]	-0.2 %	19.17	-0.3 %	19.15	-0.2 %	19.22
Exit angle [°]	6.5 %	19.84	1.6 %	18.90	5.0 %	19.50
Exit wedge [°]	-6.6 %	9.000	-11.9 %	8.400	-1.0 %	9.400
Flexural resistance w3	4.0 %	107.06	-0.6 %	81.97	-4.2 %	63.06
Flexural resistance w4	9.1 %	420.98	13.3 %	404.37	16.8 %	374.97
Flexural resistance w5	-6.6 %	72.60	-8.6 %	54.20	-14.9 %	40.18
Flexural resistance w6	3.4 %	260.55	10.1 %	251.53	11.2 %	239.10
Inlet angle [°]	-8.9 %	51.00	-6.6 %	57.00	-7.7 %	60.00
Inlet wedge [°]	-6.2 %	62.29	-3.7 %	56.94	1.5 %	55.16
Lean [°]	24.2 %	-3.09	15.3 %	-2.86	7.5 %	-2.66
LE diameter [mm]	0.0 %	2.32	0.0 %	2.32	0.0 %	2.31
LE row distance [mm]	-1.0 %	9.55	-0.5 %	9.29	-1.4 %	8.77
Main axis angle [°]	-11.5 %	0.74	-12.9 %	0.65	-13.5 %	0.58
Maximum thickness [mm]	-4.3 %	5.78	-7.3 %	4.92	-11.0 %	4.42
Max. thick. pos./Chord 2D	-31.4 %	0.13	-32.5 %	0.12	-39.3 %	0.11
Max. thick. / Chord 2D	-10.1 %	0.23	-14.9 %	0.19	-19.2 %	0.17
Moment of inertia u	15.6 %	4459.70	23.1 %	4320.20	25.9 %	4156.40
Moment of inertia v	1.2 %	428.26	-6.7 %	284.01	-14.0 %	189.28
Pitch / Chord 2D	12.8 %	0.89	10.2 %	0.93	8.9 %	0.98
Pitch / Chord 3D	12.8 %	0.89	10.2 %	0.93	8.9 %	0.98
Radius TE [mm]	0.0 %	176.91	0.0 %	190.97	0.0 %	204.54
Stagger angle [°]	-8.2 %	47.80	-10.5 %	42.54	-11.3 %	38.40
TE diameter [mm]	0.0 %	0.86	0.0 %	0.87	0.0 %	0.87
Throat distance [mm]	20.0 %	7.31	20.0 %	7.89	20.0 %	8.47
Uncovered turning [°]	-9.2 %	20.30	-2.8 %	22.00	-5.6 %	22.00
Blade wetted area [mm^2]	8.3 %			1731.71		

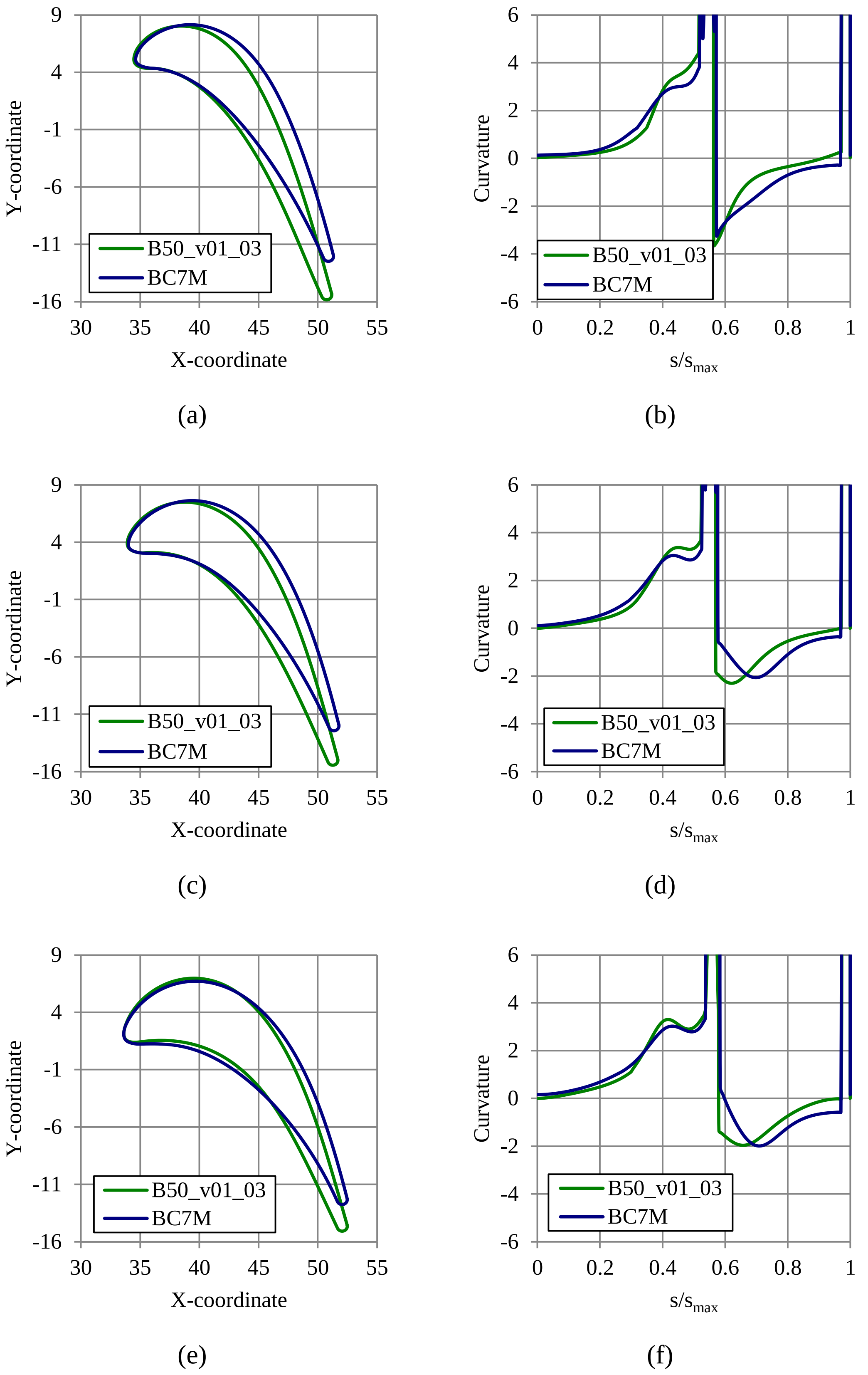

Figure 39: Geometry comparison between BC7M and B50_v01_03 at the sections: (a) tip, (c) mid and (e) hub. A comparison of the curvature for the same profiles at the sections: (b) tip, (d) mid and (f) hub. (Mises, Cato)

Table 8: Mises run results for B50_v01_03 in the right column for each section and difference compared to BC7M is the percent values in the left column for each section. (Mises, Cato)

Aerodynamic results	B50_v01_03 hub		B50_v01_03 mid		B50_v01_03 tip	
Section name	B50_v01_14_hub		B50_v01_05_mid		B50_v01_05_tip	
Mises solver parameters	B50_v01_14_hub		B50_v01_05_mid		B50_v02_01_tip	
	Diff	Value	Diff	Value	Diff	Value
$M_{1,real}$ [-]	0.6 %	0.24	-0.4 %	0.22	0.2 %	0.21
$M_{2,real}$ [-]	0.0 %	0.78	0.0 %	0.78	0.0 %	0.78
$M_{1,is}$ [-]	0.6 %	0.24	-0.4 %	0.22	0.2 %	0.21
$M_{2,is}$ [-]	-0.4 %	0.80	-0.4 %	0.80	-0.3 %	0.80
β_1 [°]	0.0 %	49.15	0.0 %	56.58	-0.1 %	60.20
β_2 [°]	0.2 %	18.89	-0.6 %	18.70	0.0 %	18.93
p_1 [Pa]	0.0 %	143700	0.0 %	147700	-0.1 %	150700
p_2 [Pa]	0.3 %	98100	0.3 %	99910	0.2 %	101900
p^*_1 [Pa]	0.0 %	149600	0.0 %	152600	0.0 %	155400
p^*_2 [Pa]	0.3 %	146900	0.3 %	150000	0.2 %	153000
T^*_1 [K]	0.0 %	312.5	0.0 %	313.6	0.0 %	315
T^*_2 [K]	0.0 %	312.5	0.0 %	313.6	0.0 %	315
w_1 [m/s]	0.6 %	84.99	-0.3 %	76.10	0.3 %	74.23
w_2 [m/s]	0.0 %	262.00	0.0 %	263.20	0.0 %	263.80
Re_1 (chord) [-]	0.3 %	149600	-0.6 %	133900	3.7 %	130200
Re_2 (chord) [-]	0.0 %	366000	0.0 %	366100	3.7 %	366000
Forces and moments						
Force in x-direction/(mass V1)	-1.8 %	4.93	0.2 %	5.72	-1.0 %	5.81
Torque about y/(mass r1 V1)	-0.5 %	3.58	0.3 %	3.84	-0.3 %	3.87
Torque about z/(mass r1 V1)	1.8 %	-0.081	4.2 %	-0.074	13.4 %	-0.081
Losses						
Outlet ref. viscous [%]	-14.1 %	5.15	-14.0 %	4.87	-11.6 %	4.52
Outlet ref, inviscid [%]	-100 %	0.00	-95.7 %	0.00	-	0.00
Outlet ref. total [%]	-14.1 %	5.15	-14.0 %	4.87	-11.6 %	4.52
Energy viscous [%]	-14.1 %	4.00	-14.0 %	3.78	-11.6 %	3.51
Energy inviscid [%]	-100 %	0.00	-96.5 %	0.00	-	0.00
Energy total [%]	-14.1 %	4.00	-14.0 %	3.78	-11.6 %	3.51
Traupel, TE [%]	-13.8 %	4.21	-11.8 %	4.04	-10.6 %	3.85
Hart TE(unrealiable yet) [%]	-18.0 %	3.69	-15.8 %	3.52	-14.0 %	3.32

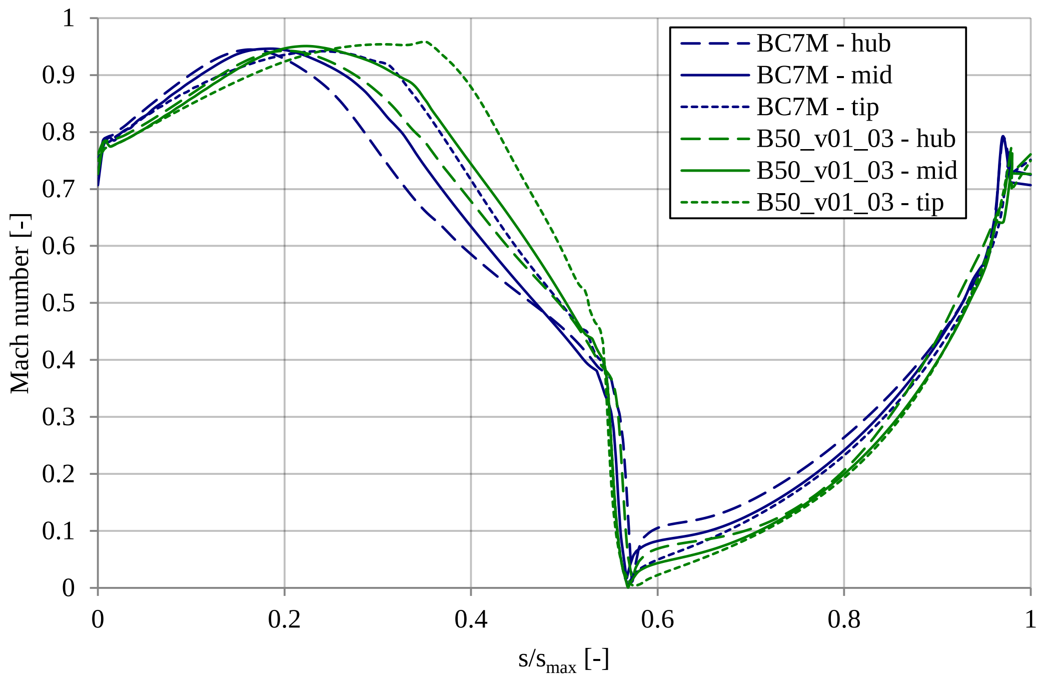

Figure 40: Velocity distribution difference between the BC7M and B50_v01_03 at the hub-, mid- and tip-section. (Mises, Cato)

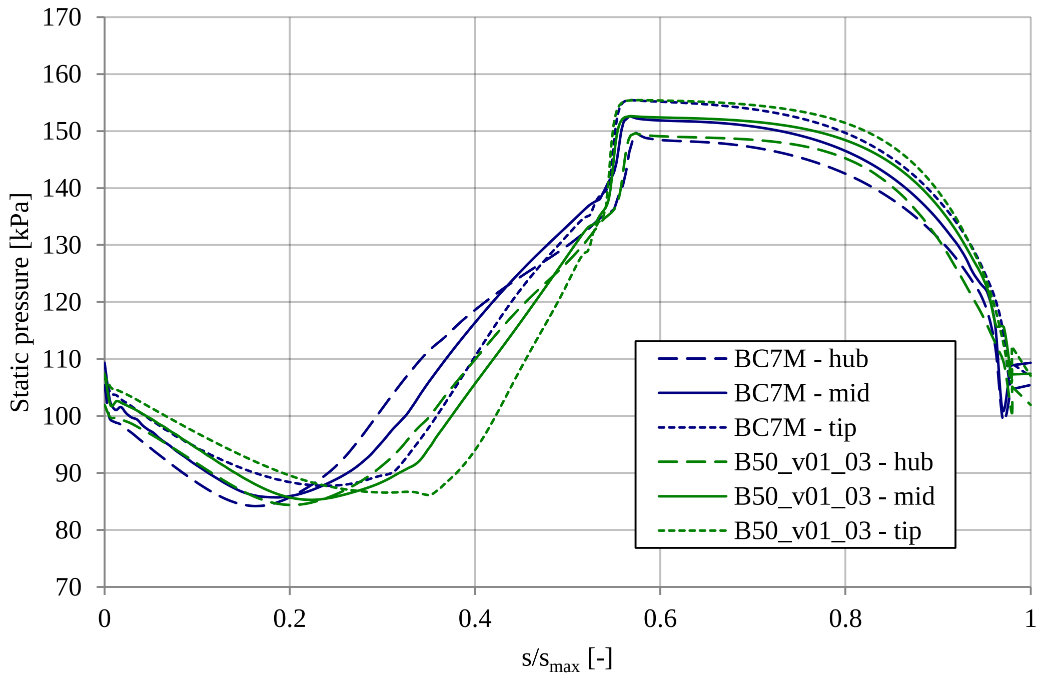

Figure 41: Static pressure distribution difference between the BC7M and B50_v01_03 at the hub-, mid- and tip-section. (Mises, Cato)

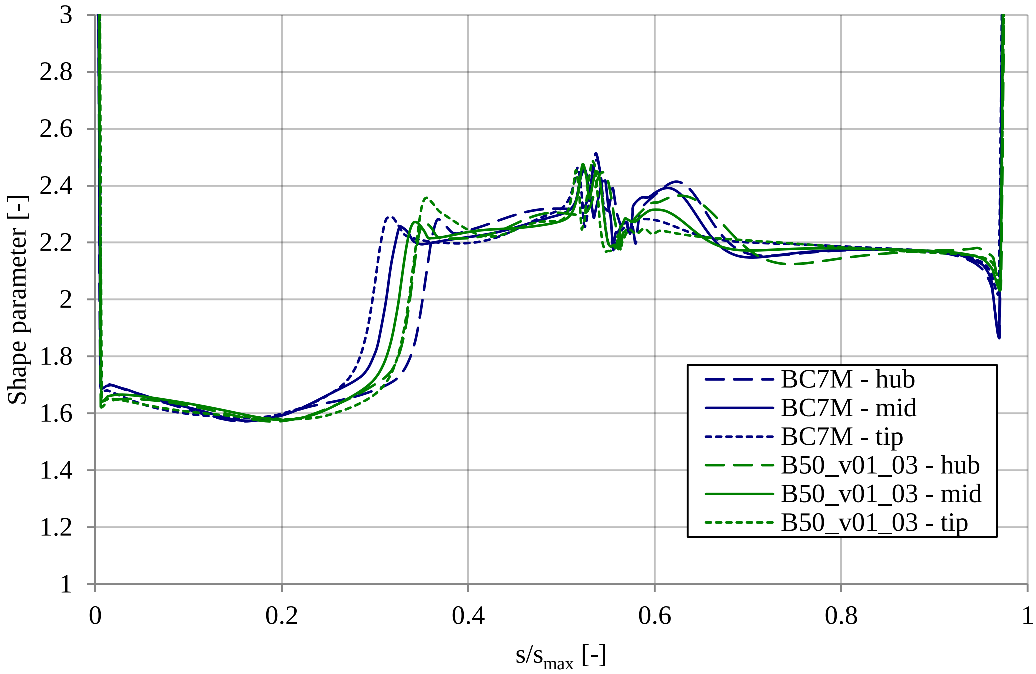

Figure 42: Shape parameter distribution difference between the BC7M and B50_v01_03 at the hub-, mid- and tip-section. (Cato)

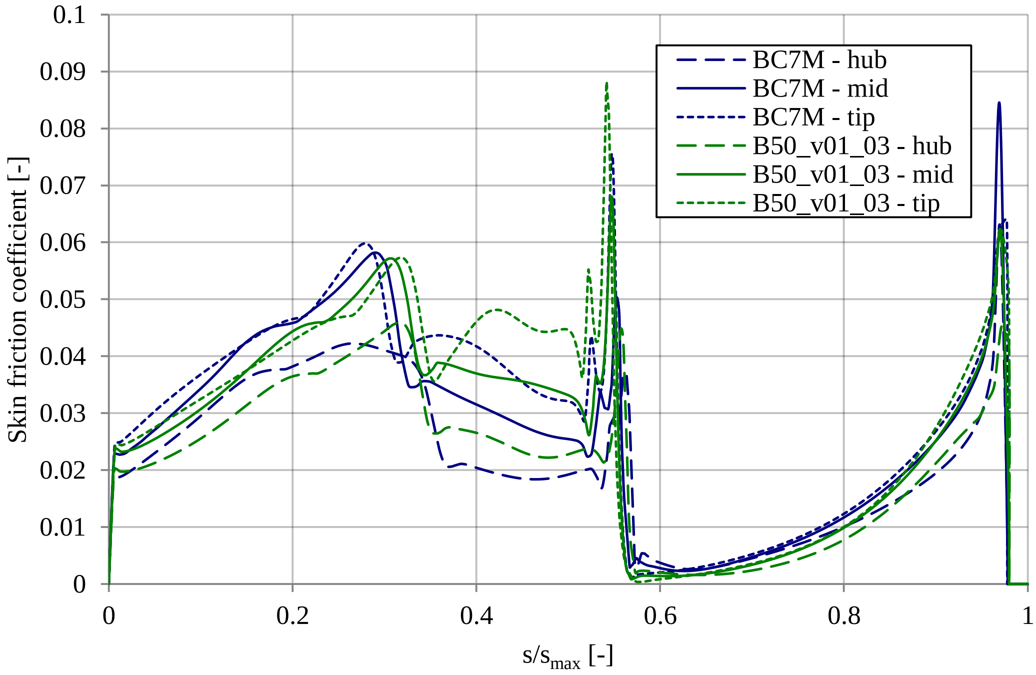

Figure 43: Skin friction coefficient distribution difference between the BC7M and B50_v01_03 at the hub-, mid- and tip-section. (Cato)

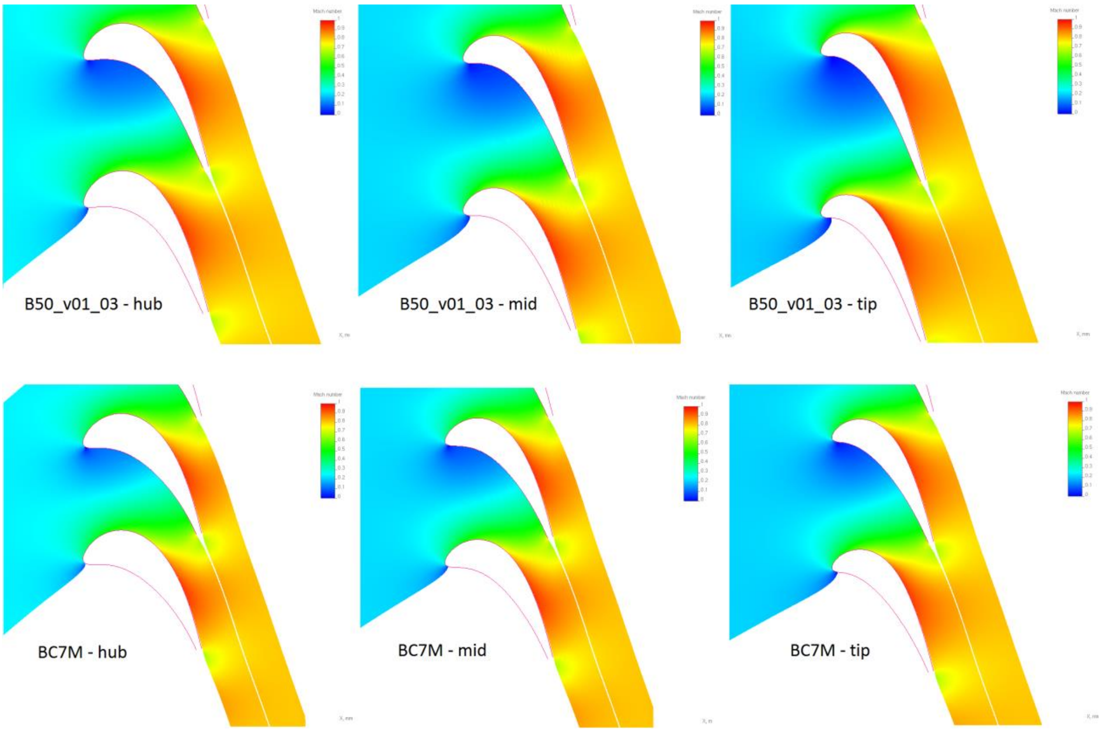

Figure 44: Mach number distribution at tip-, mid- and hub-section for BC7M and B50_v01_03. The scale is from Mach number equal to zero to Mach number equal to one. (Mises, Cato)

4.6 Incidence sensitivity

The flow inlet angle that the rotor feels is depending on its relative position to the stator. This since the rotor is rotating and will therefore alternate between feeling the wake from the stator and the freestream. To analyse how these effects will affect the velocity distribution, Mises calculations at plus and minus ten degrees incidence were performed at the mid-section for both BC7M and B50_v01_03. The velocity distribution is shown in Figure 45 and the shape parameter is shown in Figure 46. In Figure 45 it can be seen that both B50_v01_03 and BC7M are more sensitive for positive incidence than negative incidence since both gets a small velocity peak close to the leading edge due to over acceleration. However, in Figure 46 it can be seen that these over accelerations will not lead to any separation.

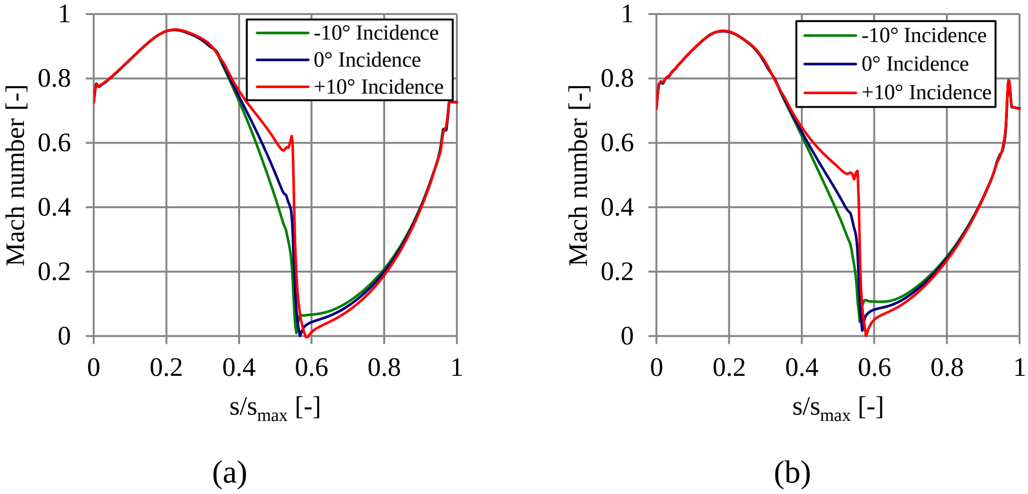

(a) (b)

Figure 45: Velocity distribution at plus and minus ten degrees incidence for (a) B50_v01_03 and (b) BC7M. (Mises, Cato)

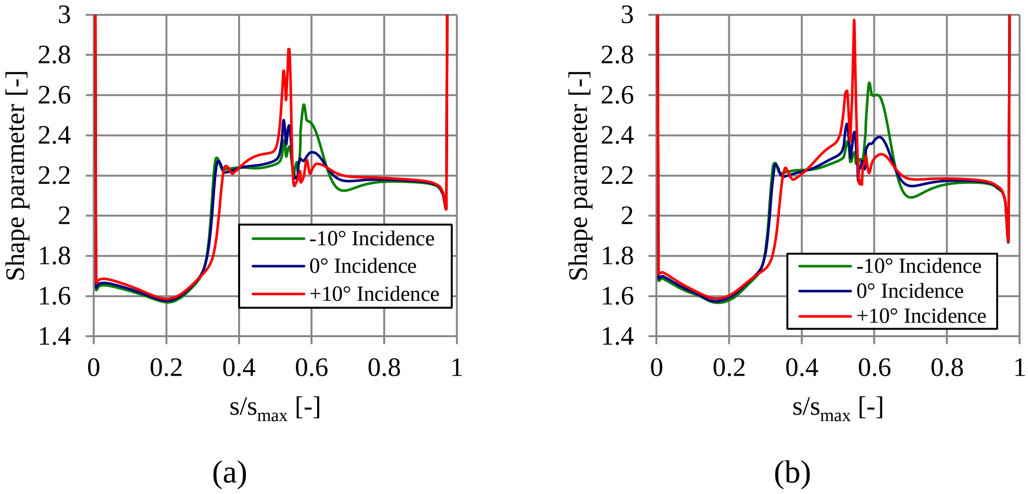

(a) (b)

Figure 46: Shape parameter at plus and minus ten degrees incidence for (a) B50_v01_03 and (b) BC7M. (Mises, Cato)

4.7 Comparisons

4.7.1 Calculations done

When a final design of B50_v01_03 was achieved it was time to make a full comparison to the BC7M. This was done by some calculations in Cato, beta2, MAC1 and Multall. The cases that were analysed in the different programs were:

Cato

- B50_v01_03
- BC7M

Beta2

- B50_v01_03 with tip recess and the boundary layer loss model
- BC7M with tip recess and the boundary layer loss model

MAC1

- B50_v01_03 with tip recess
- BC7M with tip recess

Multall

- B50_v01_03 with tip recess
- BC7M with tip recess

4.7.2 Comparison

The comparison will include the following parts:

- An overall comparison of the stage parameters
- Profile losses in Cato
- Losses in beta2
- Losses in MAC1
- Laval number and static pressure distribution
- Diffusion factor (Multall)
- Radial distribution of (relative) total pressure, static pressure, (relative) total temperature, (relative) Mach number and (relative) flow angles
- 3D results

5 Results

5.1 Overall stage parameters

In Table 9 below, one dimensional result are presented. Some values are directly taken from result files and some are calculated values. See footnotes for more information.

Table 9: Overall parameters for the BC7M and B50_v01_03 turbine

Profile	B50_v01_03	BC7M	B50_v01_03	BC7M
Program	Multall	Multall	Beta2	Beta2
Loss Model	-	-	BL	BL
Tip Recess	Yes	Yes	Yes	Yes
p_0^* [bar]	2.167	2.167	2.168	2.168
p_0 [bar]	2.152	2.152	-	-
p_2^* [bar]	1.066	1.065	1.070	1.070
p_2 [bar]	1.013	1.012	1.013	1.013
p_0^*/p_2^* [-]	2.034[2]	2.035[2]	2.026	2.026
p_0^*/p_2 [-]	2.140[2]	2.141[2]	2.139	2.139
in$_{\text{in}}$ [kg/s]	3.421	3.433[3]	3.48	3.48
in$_{\text{out}}$ [kg/s]	3.421	3.430[3]	3.48	3.48
Re$_{\text{vane}}$ [-]	684574	684848	670000	669000
Re$_{\text{blade}}$ [-]	378975	347564	395000	364000
$\eta_{tt,is}$ [%]	90.25[3]	90.26[3]	90.9[4]	90.75[4]
$\eta_{tt,is}$ [%]	91.90[5]	92.02[5]	92.19[6]	92.03[6]
ZW$_{\text{I}}$	1.043[7]	0.938[7]	-	-
ZW$_{\text{II}}$	0.800[7]	0.670[7]	-	-
N [MW]	0.195[3]	0.197[3]	0.201[4]	0.201[4]
Ψ	-	-	1.356[4]	1.354[4]
Φ	-	-	0.420[4]	0.420[4]
Λ_{p}	0.400	0.401	-	-

---

[2] Calculated value

[3] Value from Multall.out file

[4] Value from Output1.bta file

[5] Calculated value using Equation (15) with the mass averaged 1D results in Multall.out.file

[6] Calculated value using Equation (15) with the mass averaged 2D results from Output2.bta

[7] Calculated value using Equation (46) and (47) with the mass averaged values for the radial distribution of the Zweifel coefficient

5.2 Losses

5.2.1 Losses - Mises

As a result of the Mises solver in Cato, the profile loss is presented either as energy or Traupel loss. It can be seen in Figure 47 and Figure 48 that the profile loss is lower for the new profile in all studied sections.

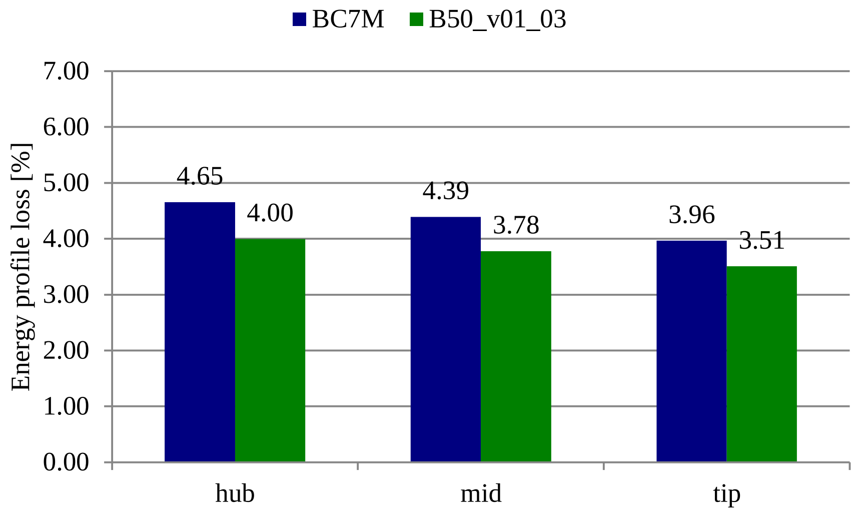

Figure 47: Energy profile loss at hub-, mid- and tip-section. (Mises, Cato)

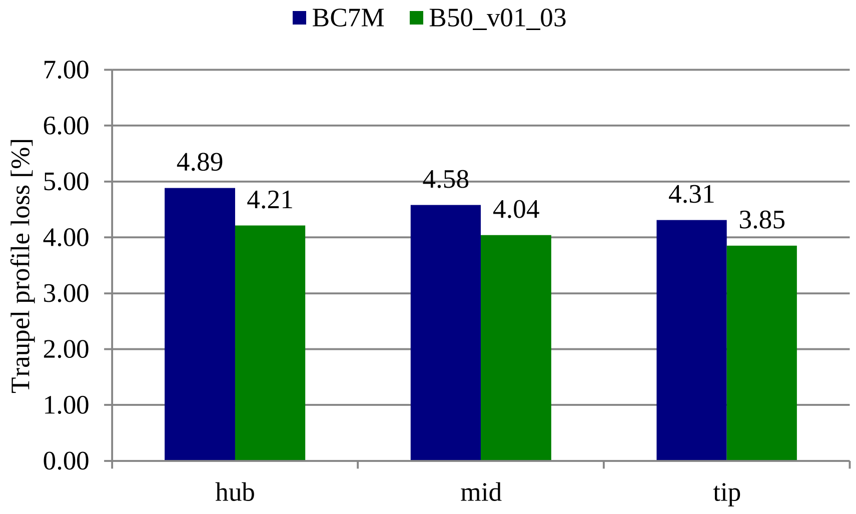

Figure 48: Traupel profile loss at hub-, mid- and tip-section. (Mises, Cato)

5.2.2 Losses - beta2

From beta2 the losses are presented in eleven different groups. These are presented in Table 10 and in Figure 49. It is worth mentioning that the friction loss is higher for the case with fewer blades which is not consistent with the previously described theory. In beta2 the transition point is let to the code to decide by itself. For the BC7M the transition point on the blade appears at the s/s_{max} equal to 0.53. For the B50_v01_03 this is instead 0.39. In other words the boundary layer is laminar for a longer distance on the BC7M suction side surface, giving lower profile loss. The secondary loss is larger for the row with larger pitch as expected. The total loss is also surprisingly seen to be lower for B50_v01_03.

Table 10: Loss comparison between the blades BC7M and B50_v01_03. (beta2)

Blade Losses [%]	BC7M	B50_v01_03
Friction	2.59	2.69
Roughness	0.00	0.00
Edge	1.95	1.64
Angle of attack (incidence)	0.51	0.31
Turbulence	0.00	0.00
Reynolds number	0.00	0.00
Shock	0.00	0.00
Secondary	3.47	3.78
Cooling	0.00	0.00
Radial clearance	2.38	2.19
Extra	0.00	0.00
Total	10.90	10.62

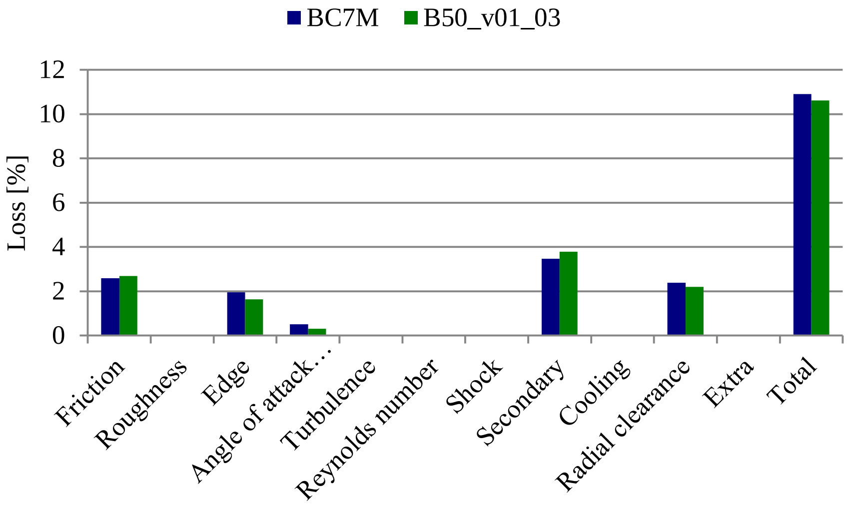

Figure 49: Loss comparison between the blades BC7M and B50_v01_03. (beta2)

From beta2 calculations the radial distribution of the losses is also obtained and can be seen in Figure 50 and Figure 51. Here it can be seen that the friction loss is larger for BC7M. Some parameters are zero since they are included in the friction loss in the boundary layer loss model.

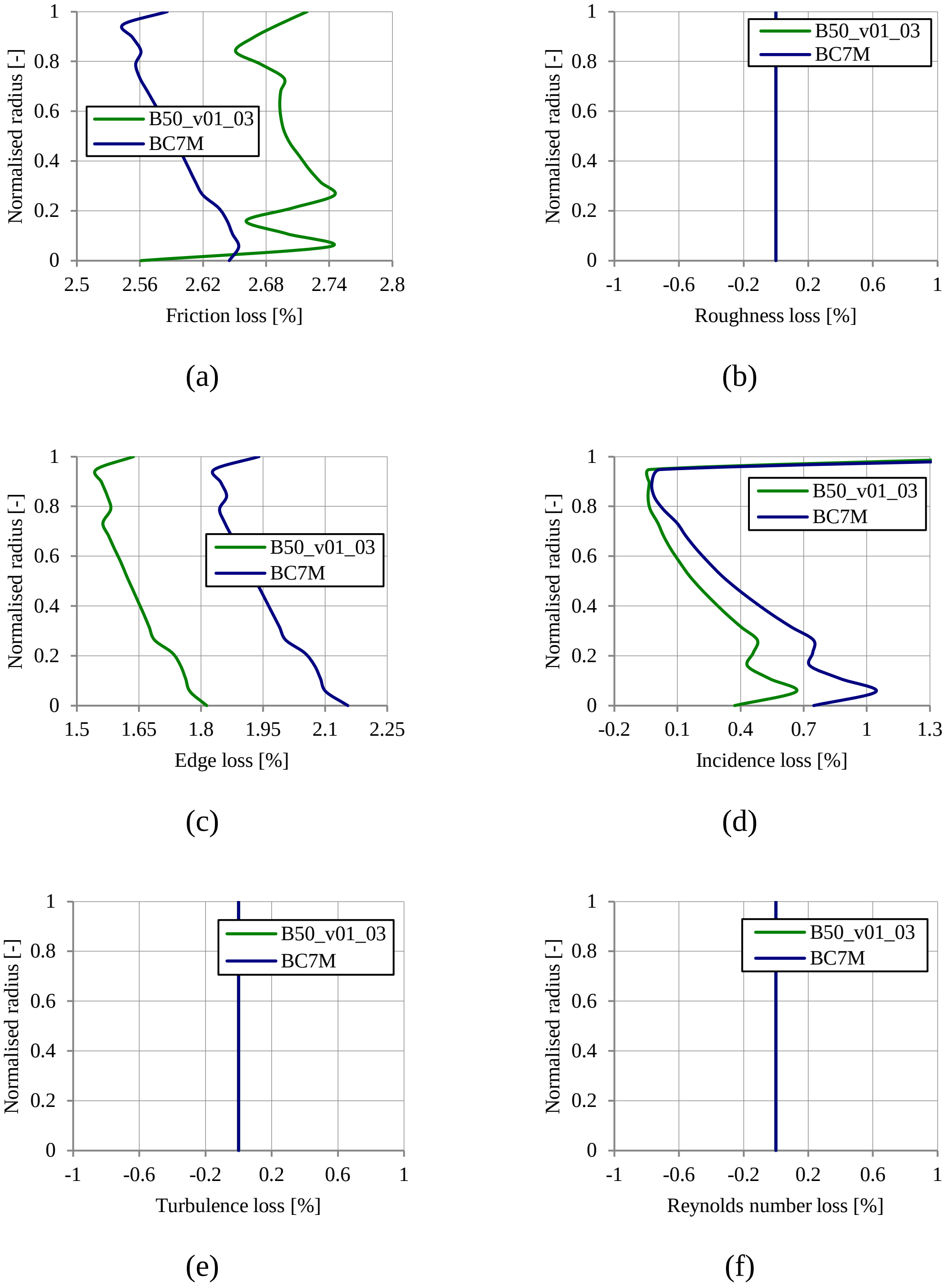

(a) (b)

(c) (d)

(e) (f)

Figure 50: Radial distribution comparison between the blades BC7M and B50_v01_03 for (a) friction loss, (b) roughness loss, (c) edge loss, (d) incidence loss, (e) turbulence loss, (f) Reynolds number loss. (beta2)

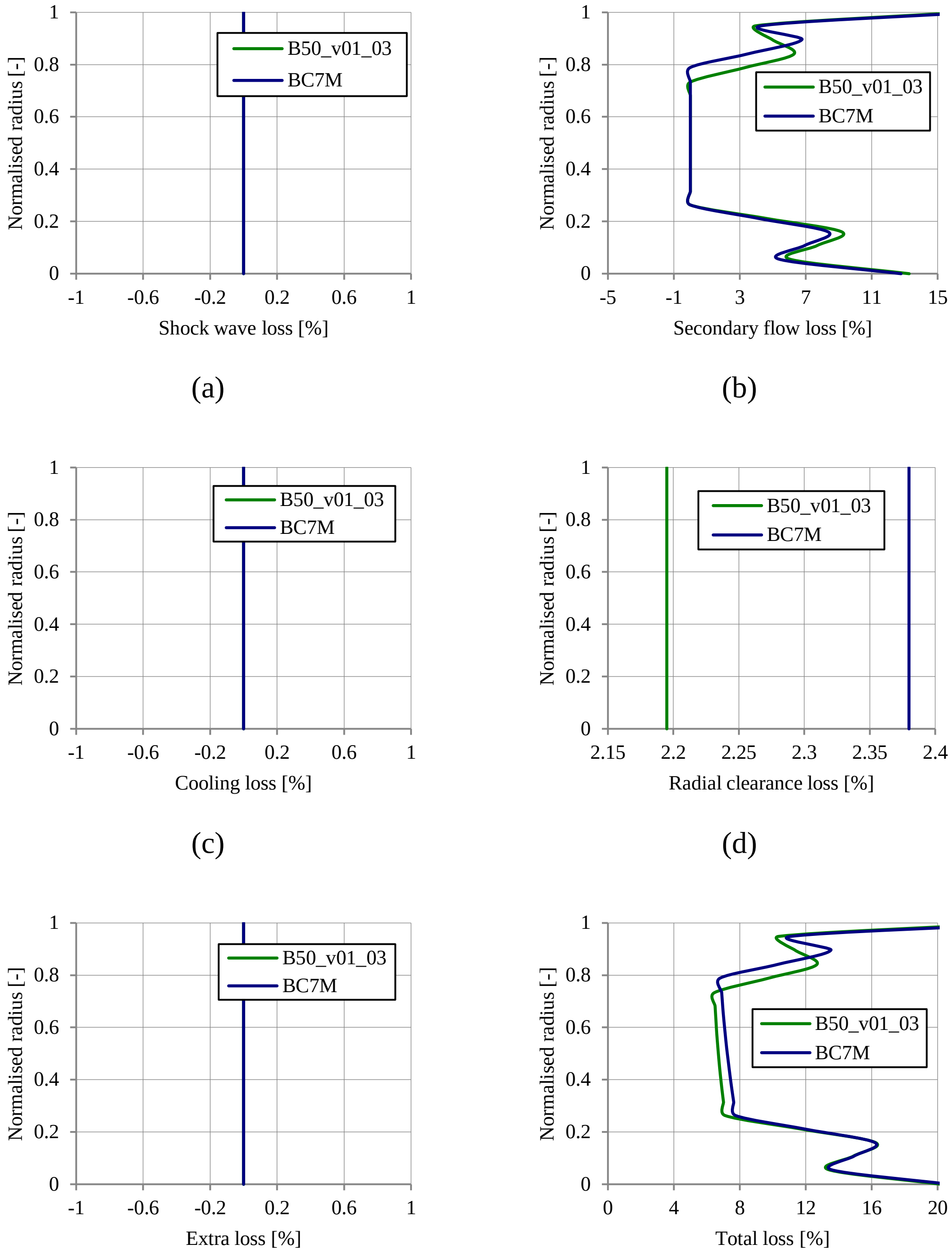

(a) (b)

(c) (d)

(e) (f)

Figure 51: Radial distribution comparison between the blades BC7M and B50_v01_03 for (a) shock wave loss, (b) secondary flow loss, (c) cooling loss, (d) radial clearance loss, (e) extra loss, (f) total loss. (beta2)

5.2.3 Losses - MAC1

For the MAC1 code the losses are presented in Table 11 and Figure 52 in the same manner as for beta2. Since MAC1 is a 1D solver, there is no radial distribution. The friction loss is almost the same for BC7M and B50_v01_03. The biggest difference is for the trailing edge, secondary and radial clearance loss.

Table 11: Loss comparison between the blades BC7M and B50_v01_03. (MAC1)

Blade Losses [%]	BC7M	B50_v01_03
Friction	2.61	2.64
Roughness	0.00	0.00
Edge	1.96	1.65
Angle of attack (incidence)	0.23	0.09
Turbulence	0.00	0.00
Reynolds number	0.00	0.00
Shock	0.00	0.00
Secondary	2.95	3.25
Cooling	0.00	0.00
Radial clearance	2.57	2.34
Extra	0.00	0.00
Total	10.32	9.97

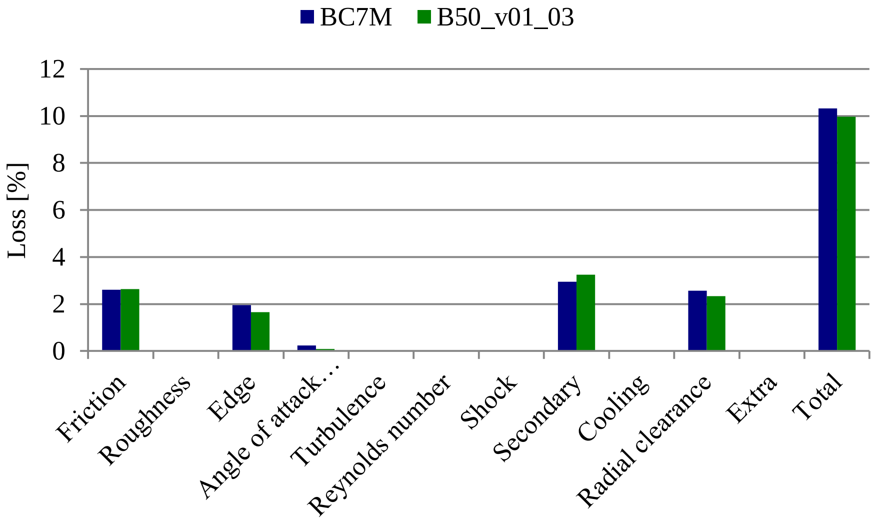

Figure 52: Loss comparison between the blades BC7M and B50_v01_03. (MAC1)

5.3 Laval number and static pressure distribution

5.3.1 Laval number distribution – Multall

The Laval number distribution at the blade pressure and suction side surface for B50_v01_03 and BC7M at blade span 10, 25, 50, 75 and 90 % are shown in Figure 55 and Figure 56 respectively. The largest difference can be seen at blade span 90 %. In Figure 57 it can be shown that the profile with larger pitch is more front-loaded. The peak values are quite constant. However at the 75 % span for B50_v01_03 the peak is higher.

5.3.2 Diffusion coefficient - Multall

Due to the fact that the velocity peak is higher for the B50_v01_03 at 75 % span the diffusion coefficient was much larger at this section, which can be seen in Figure 53. Comparing this to the diffusion coefficient for BC7M in Figure 54, it can be seen that at all spans the diffusion coefficient is higher for B50_v01_03. All spans for both profiles except the 75 % span for the B50_01_03 have a diffusion coefficient lower than the maximum diffusion coefficient recommended by Mamaev.

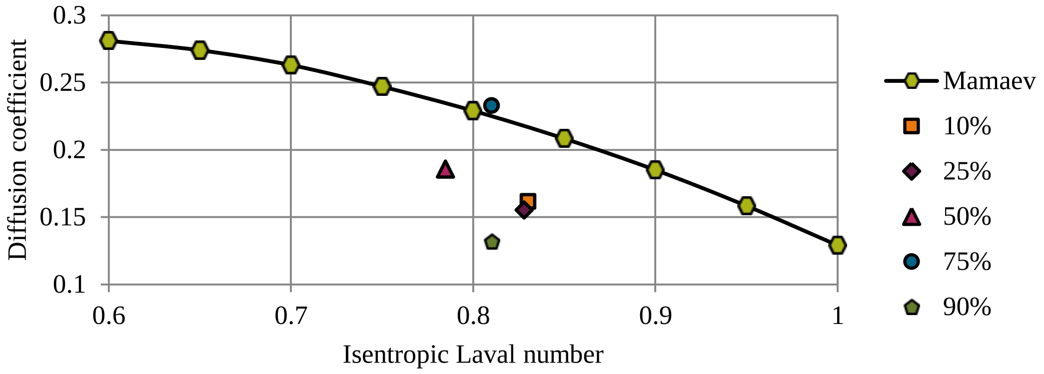

Figure 53: Diffusion coefficient for the blade in B50_v01_03. (Multall)

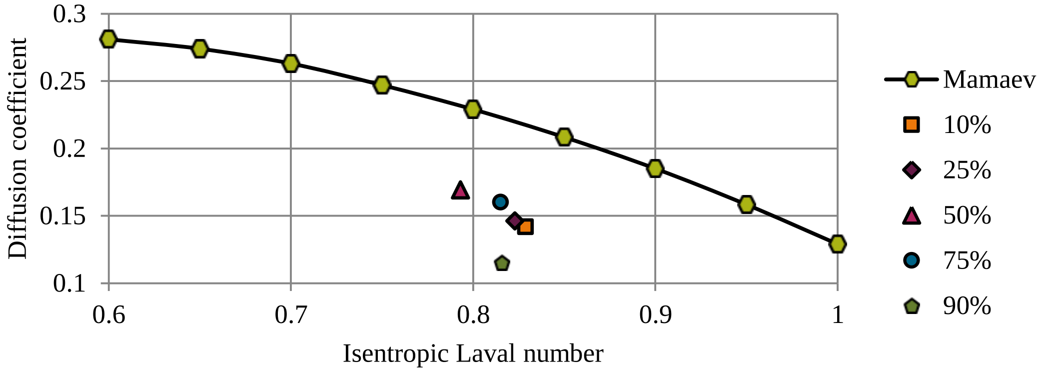

Figure 54: Diffusion coefficient for the blade in BC7M. (Multall)

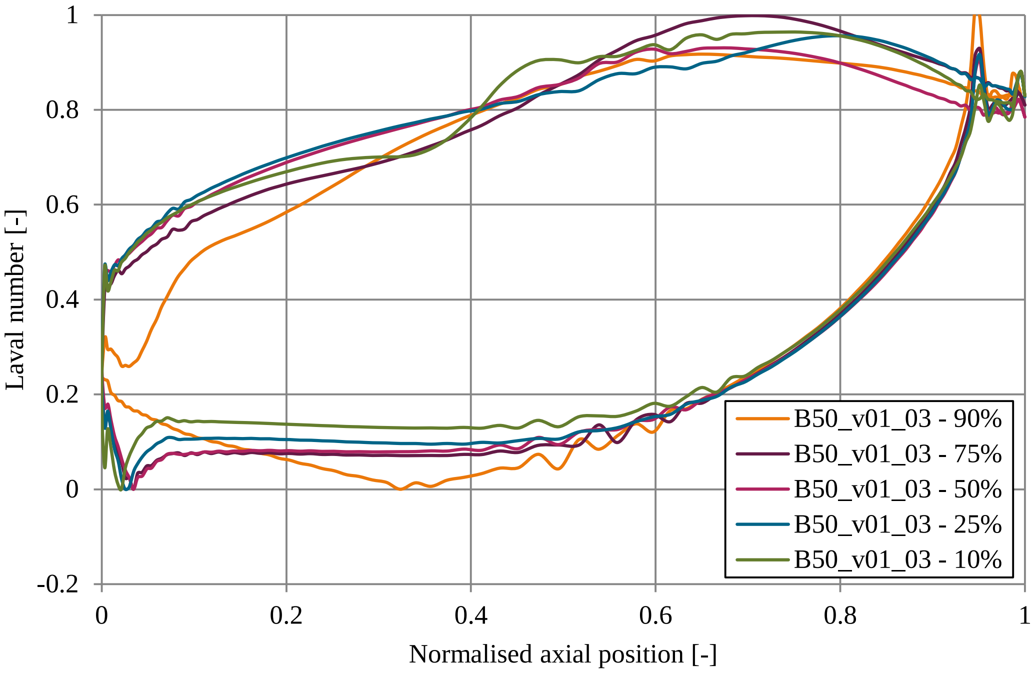

Figure 55: Laval number at the five different blade spans 10, 25, 50, 75 and 90 % for B50_v01_03. (Multall)

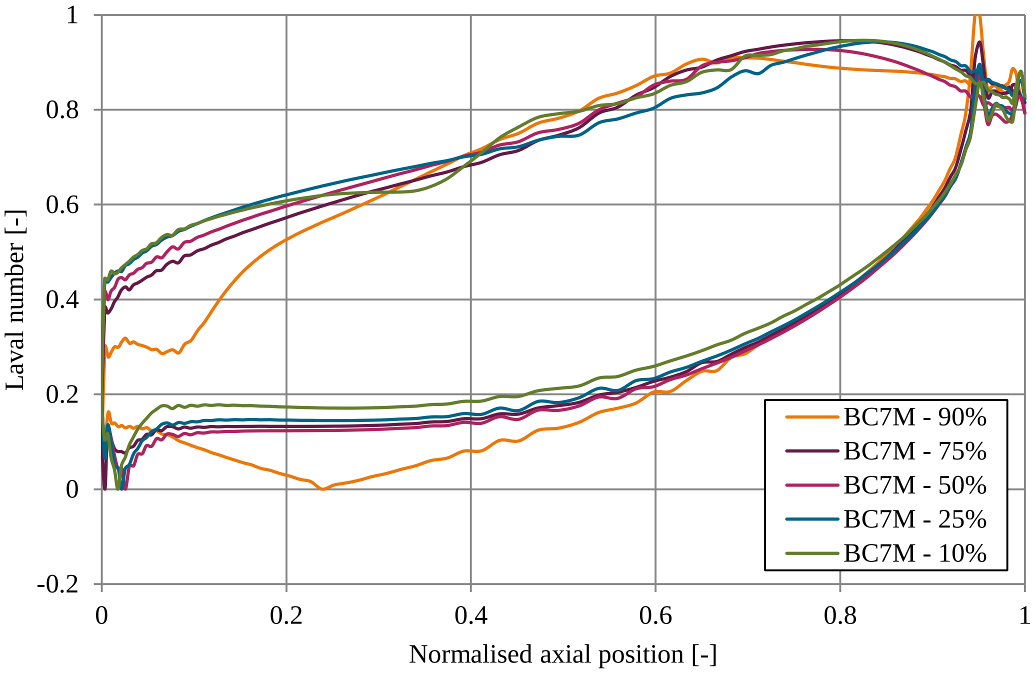

Figure 56: Laval number at the five different blade spans 10, 25, 50, 75 and 90 % for BC7M. (Multall)

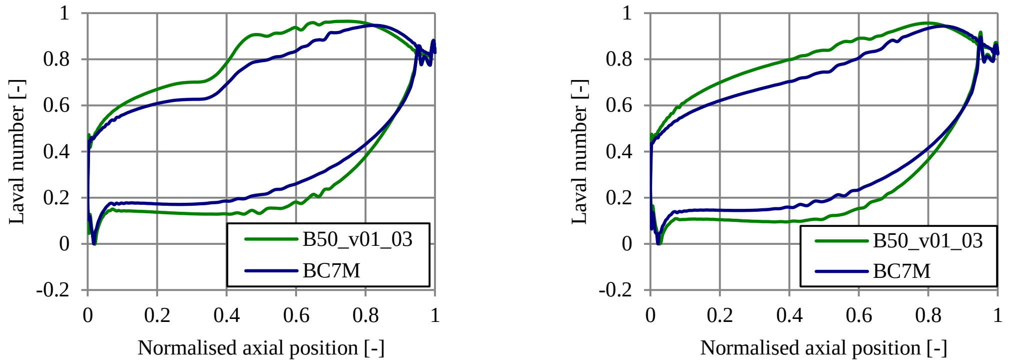

(a) 10 % span

(b) 25 % span

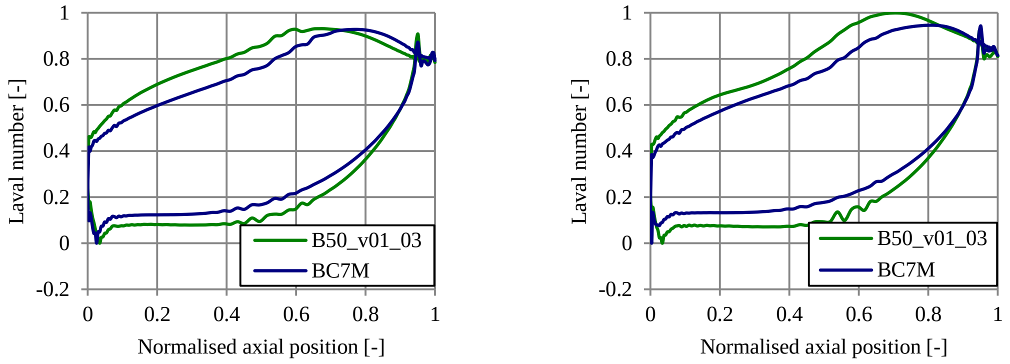

(c) 50 % span

(d) 75 % span

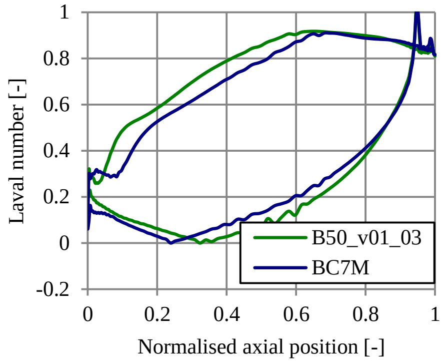

(e) 90 % span

Figure 57: Laval number distribution for B50_v01_03 and BC7M at span: (a) 10 %, (b) 25 %, (c) 50 %, (d) 75 % and (e) 90 %. (Multall)

5.3.3 Static pressure – Multall

As for the Laval number the static pressure is shown at five different spans for B50_v01_03 and BC7M in Figure 58 to Figure 60.

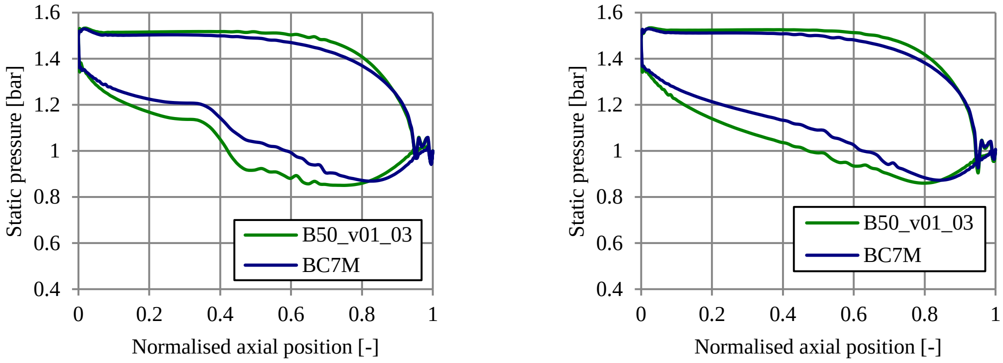

(a) 10 % span

(b) 25 % span

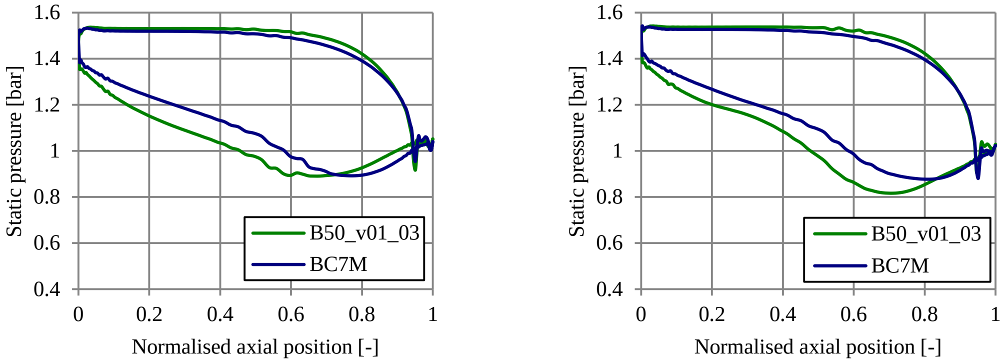

(c) 50 % span

(d) 75 % span

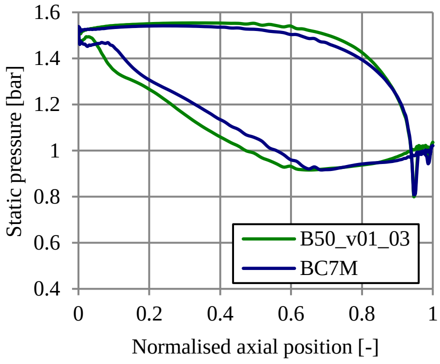

(e) 90 % span

Figure 58: Static pressure for B50_v01_03 and BC7M at span: (a) 10 %, (b) 25 %, (c) 50 %, (d) 75 % and (e) 90 %. (Multall)

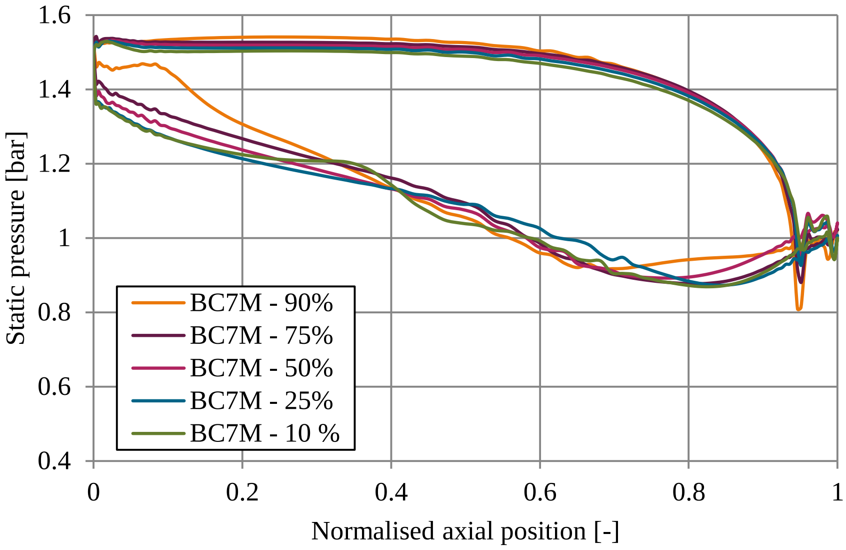

Figure 59: Static pressure at five different blade spans 10, 25, 50, 75 and 90 % for BC7M. (Multall)

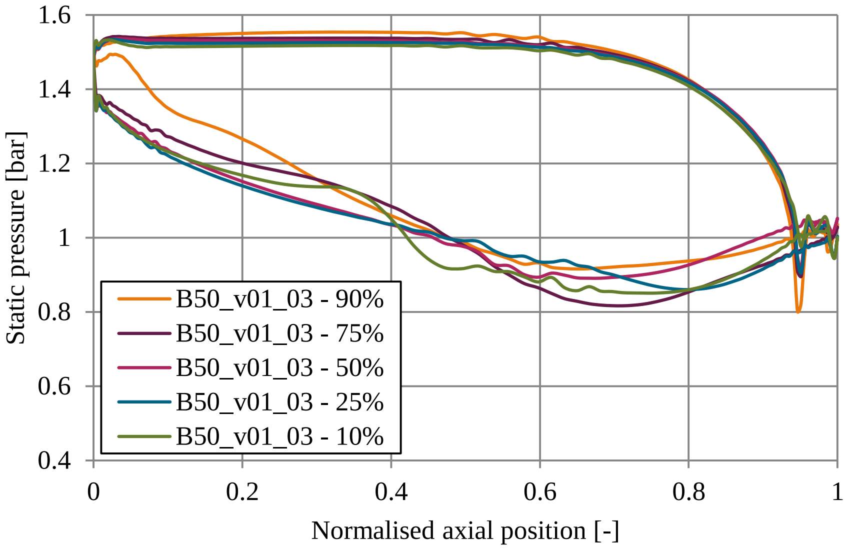

Figure 60: Static pressure at five different blade spans 10, 25, 50, 75 and 90 % for B50_v01_03. (Multall)

5.4 Radial distribution

A few important parameters are presented as radial distributions in Figure 61 to Figure 65.

In Figure 61 and Figure 62 the radial distribution for the vane leading and trailing edge are presented. At the leading edge there is no significant difference. At the trailing edge the differences are very small, however a little difference in static pressure and Mach number exist.

The radial distribution for the blade leading and trailing edge is presented in Figure 63 and Figure 64. At the blade leading edge the difference is small; at the trailing edge the difference is larger. However the B50_v01_03 results follow the same pattern that the BC7M results have. Note that the relative pressures and temperatures are calculated by using Equation (25).

In Figure 65 the total-to-total isentropic efficiency, degree of reaction and Zweifel coefficient is presented. These values are manually calculated using Equation (15), (30), (46) and (47). At the 47 % to 69 % span BC7M has better efficiency and from span 69 % to 88 % the B50_v01_03 is better. At other spans there is no major difference in efficiency between the two blade profiles.

For the degree of reaction the target was to keep the degree of reaction constant. In the radial distribution it became some minor differences between the profiles, however the pattern is the same.

For both definitions of the Zweifel coefficient it can be seen that the increase in Zweifel coefficient is greatest in the middle of the blade span. Closer to the tip, the tip clearance affects the possibility for the blade to be highly loaded.

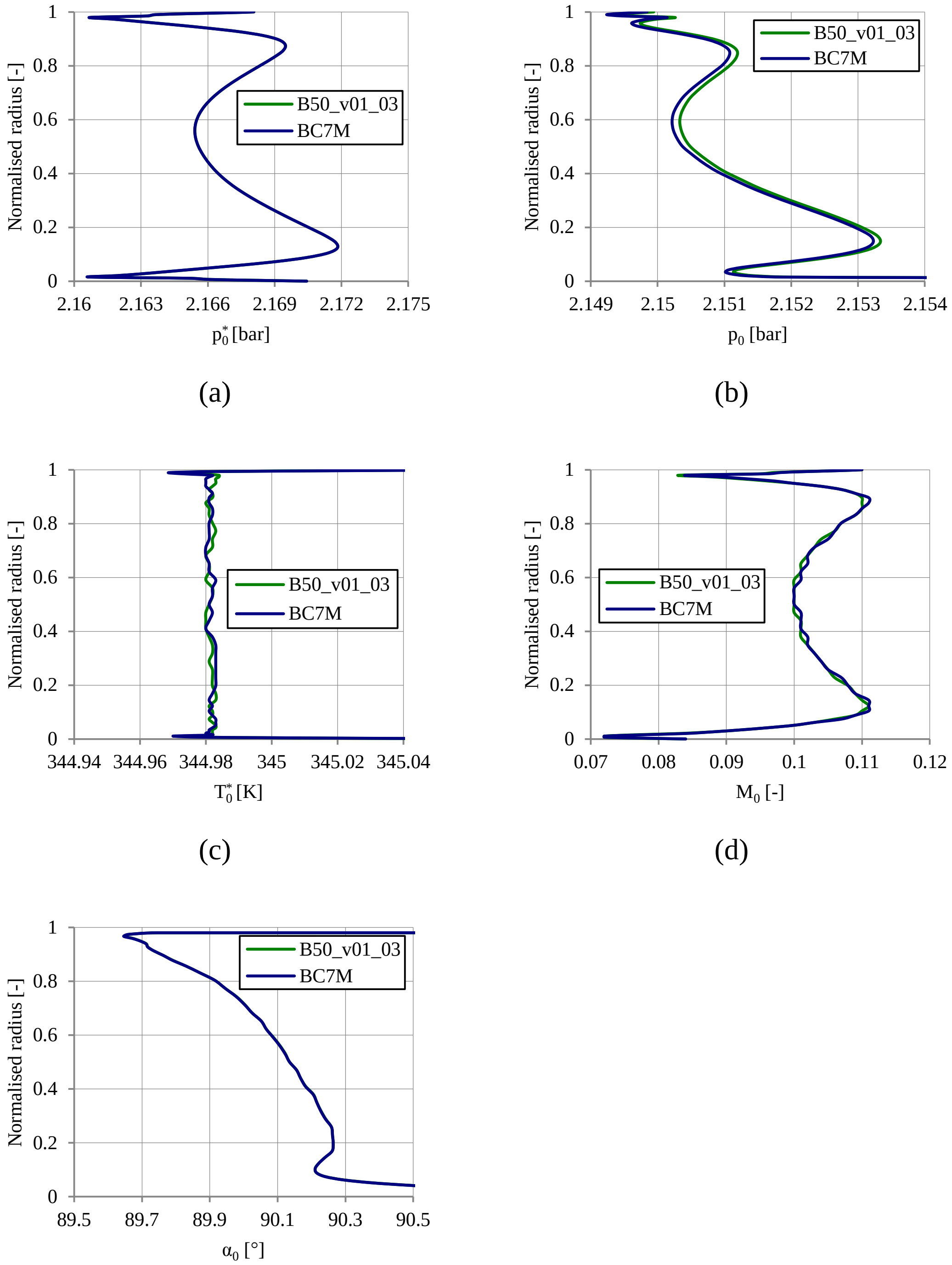

(a) (b) (c) (d) (e)

Figure 61: Radial distribution comparison between B50_v01_03 and BC7M at vane leading edge for (a) total pressure, (b) static pressure, (c) total temperature, (d) Mach number, (e) tangential flow angle. (Multall)

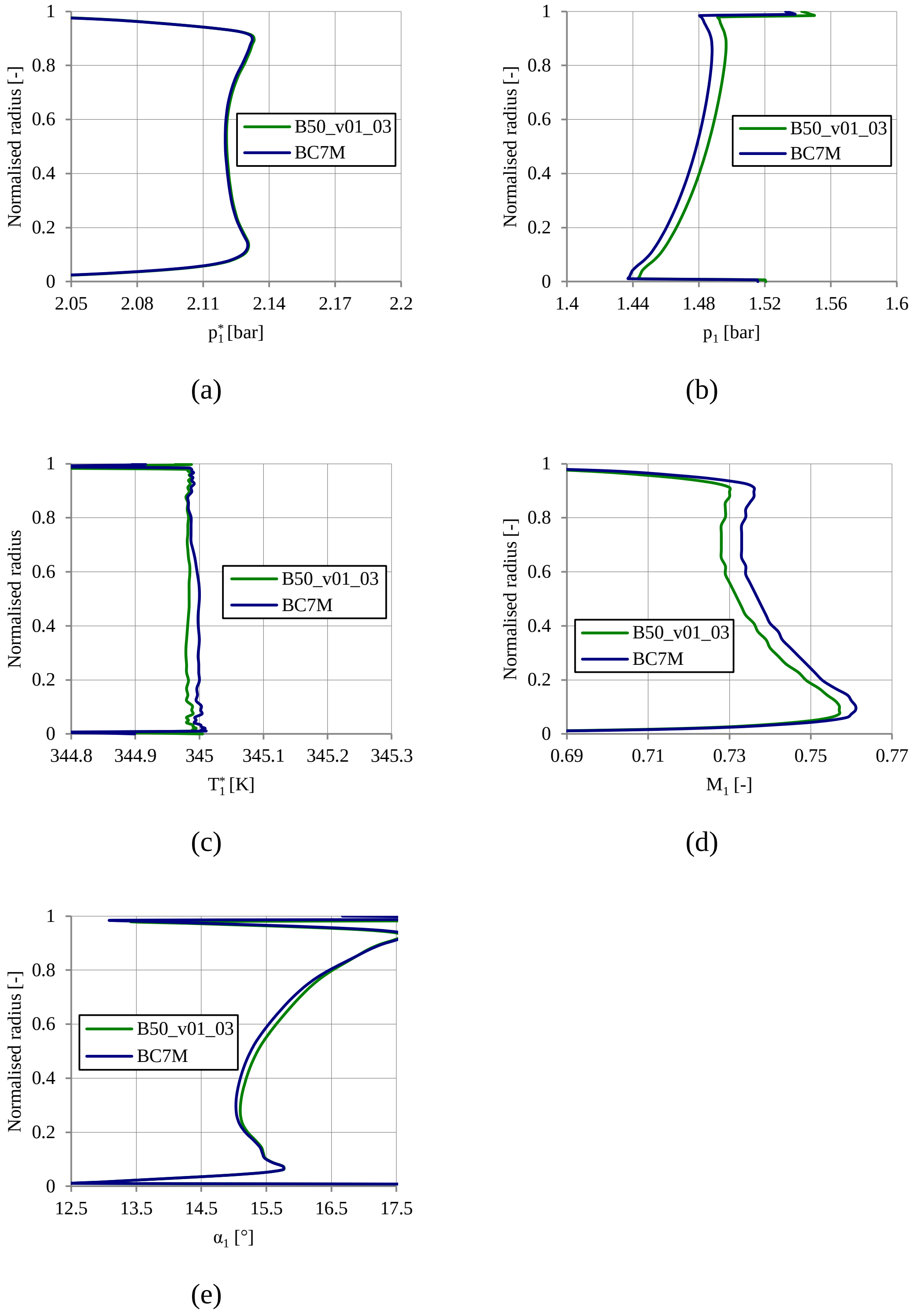

Figure 62: Radial distribution comparison between B50_v01_03 and BC7M at vane trailing edge for (a) total pressure, (b) static pressure, (c) total temperature, (d) Mach number, (e) tangential flow angle. (Multall)

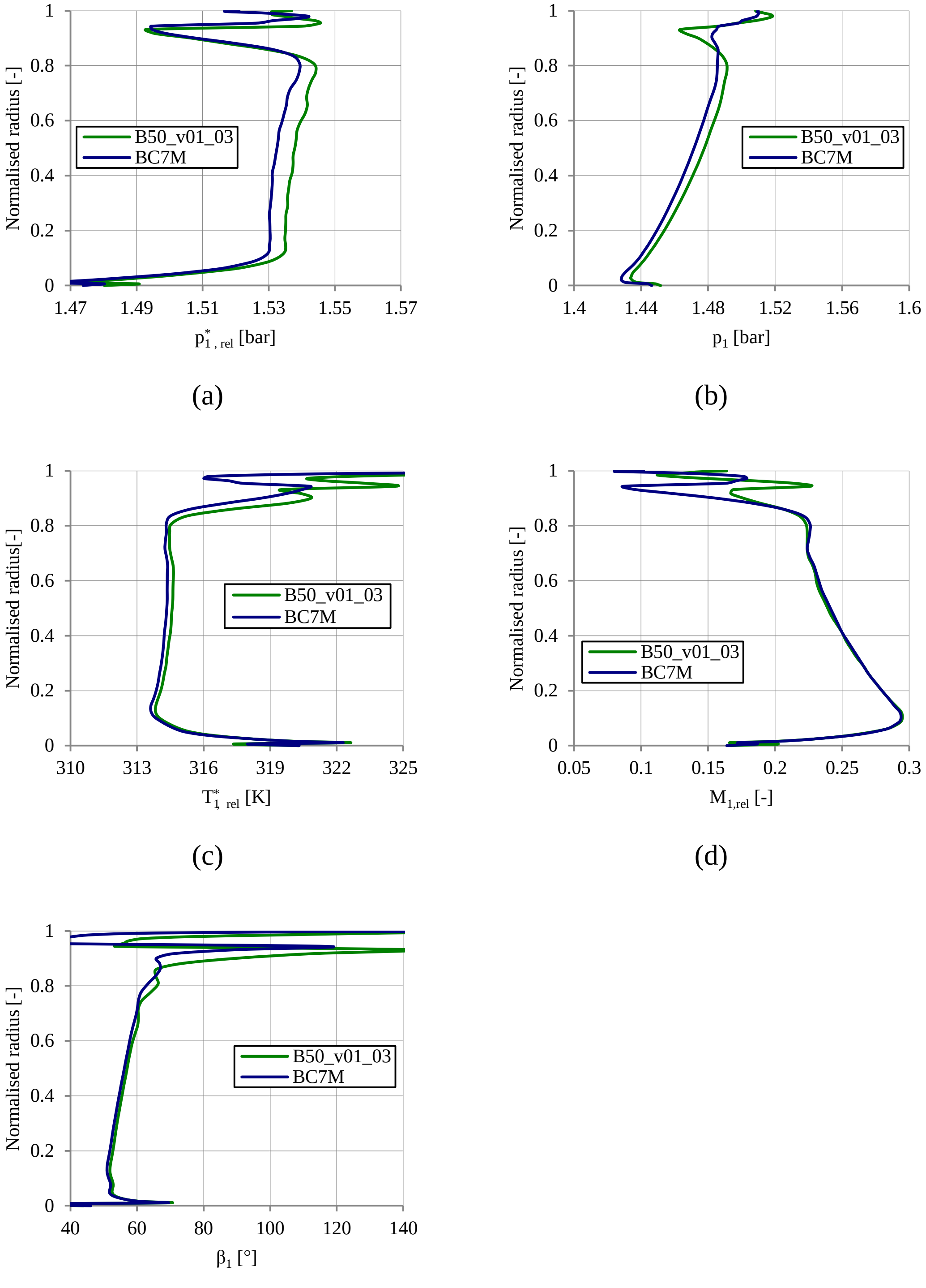

(a)

(b)

(c)

(d)

(e)

Figure 63: Radial distribution comparison between B50_v01_03 and BC7M at blade leading edge for (a) relative total pressure, (b) static pressure, (c) relative total temperature, (d) relative Mach number, (e) relative tangential flow angle. (Multall)

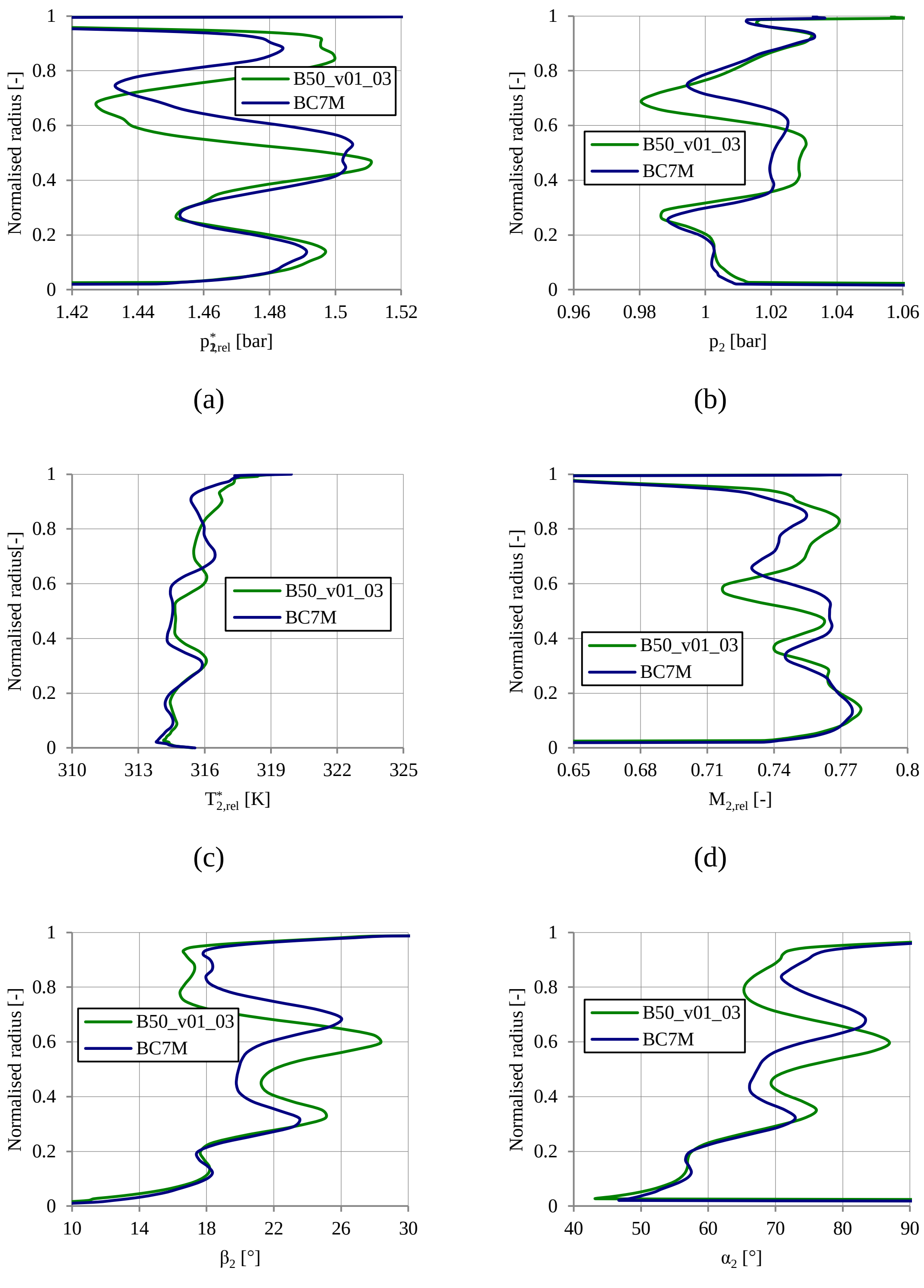

(a) (b)

(c) (d)

(e) (f)

Figure 64: Radial distribution comparison between B50_v01_03 and BC7M at blade trailing edge for (a) relative total pressure, (b) static pressure, (c) relative total temperature, (d) relative Mach number, (e) relative tangential flow angle, (f) absolute tangential flow angle. (Multall)

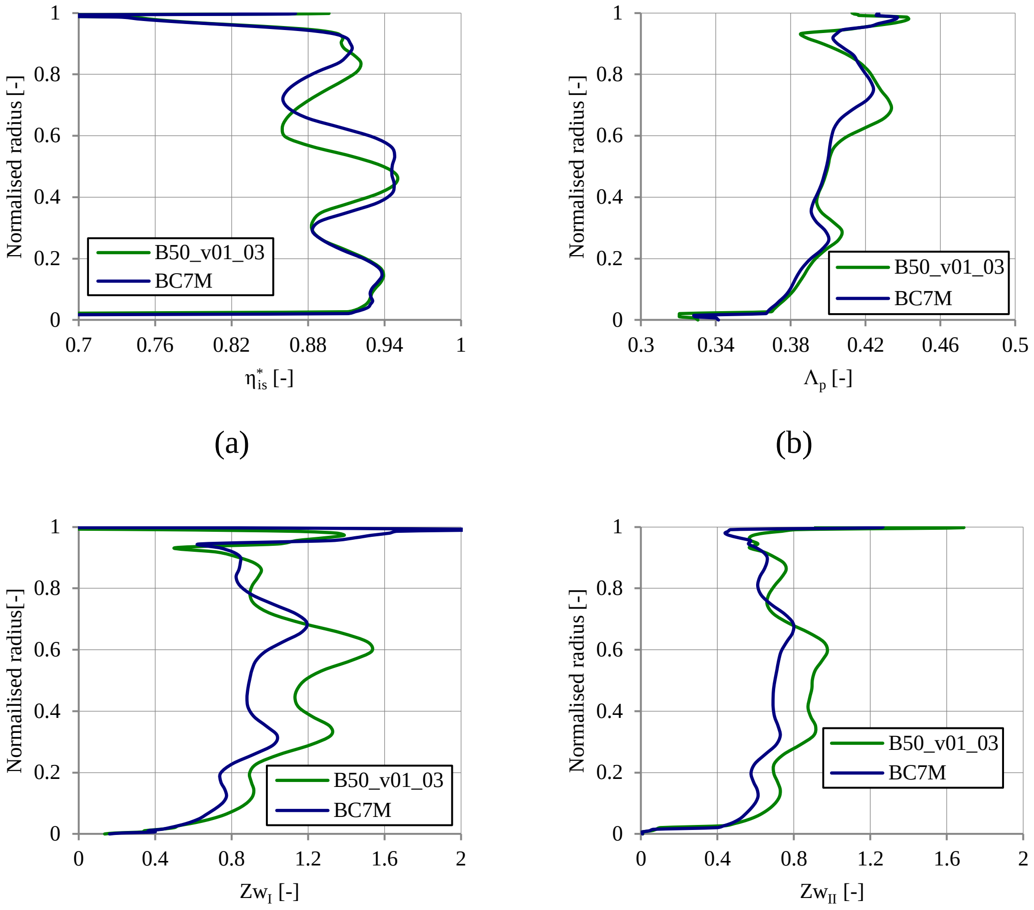

(a) (b)

(c) (d)

Figure 65: Radial distribution for B50_v01_03 and BC7M for (a) total-to-total isentropic efficiency, (b) pressure based degree of reaction, (c) Zweifel coefficient based on Equation (46) and (d) Zweifel coefficient based on Equation (47). (Multall)

5.5 3D results - BC7M and B50_v01_03

In Figure 66 to Figure 69 the velocity is shown on the suction side surface on the blades BC7M and B50_v01_03. Here it can be seen where the secondary flows exist, close to the tip and hub. At the mid-span the flow is not disturbed by the secondary flows. The vortex that is created in front of the blade is another secondary flow. This does actually affect the mixing plane. A test was done to try to move the mixing plane to get rid of that problem. Unfortunately the problem was not solved, since the secondary flows from the vane trailing edge also started to affect the mixing plane. The cylindrical vortex in front of the blade that can be seen in Figure 67, Figure 69 and Figure 70 is a result of many different factors, e.g. the blade loading and the relative velocity difference between the blade and casing. Also the blade leading edge relative position to the vane trailing edge might affect the size of this vortex. In Figure 71 the losses close to the suction side surface for B50_v01_03 blade are shown. The top vortex is the tip clearance vortex shown earlier in the theory chapter. The other two are the suction side horseshoe vortices. The last two pictures are just shown to give the reader a clearer picture of what happens.

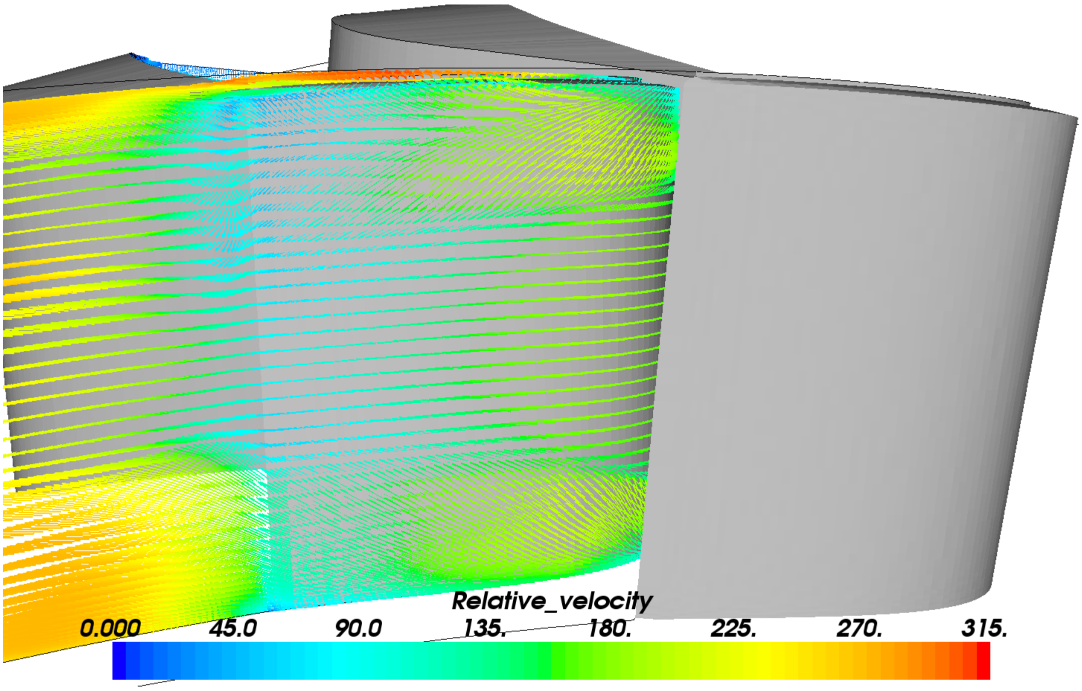

Figure 66: Relative velocity distribution at BC7M blade suction side surface. (Multall, MayaVi)

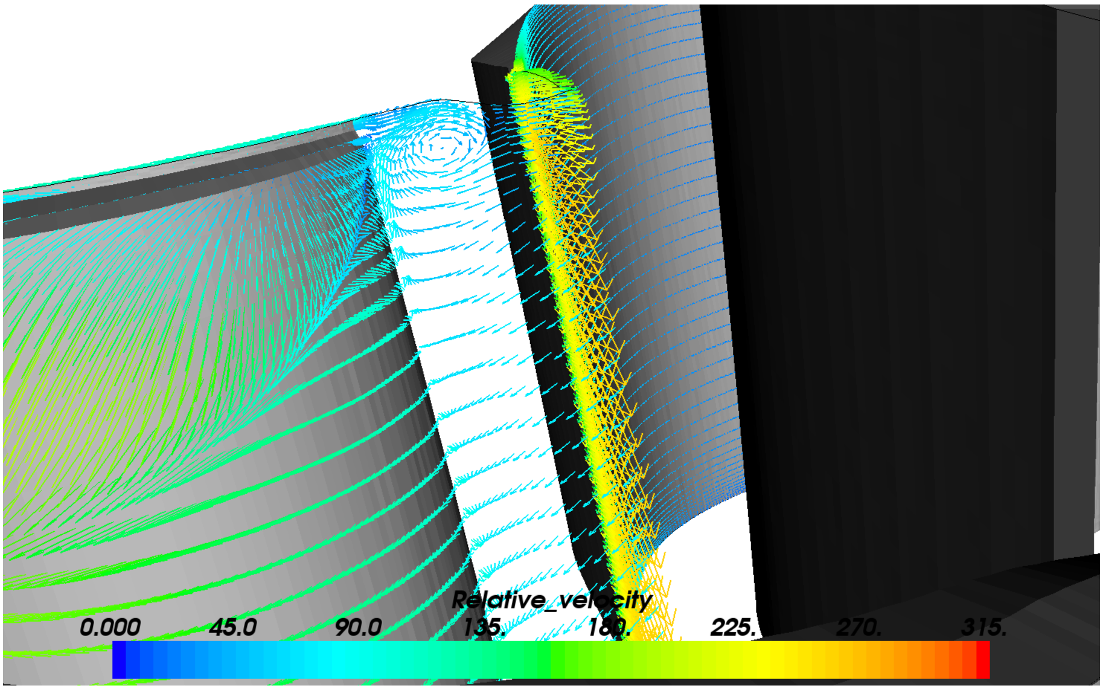

Figure 67: Relative velocity distribution at BC7M blade suction side surface close to leading edge. (Multall, MayaVi)

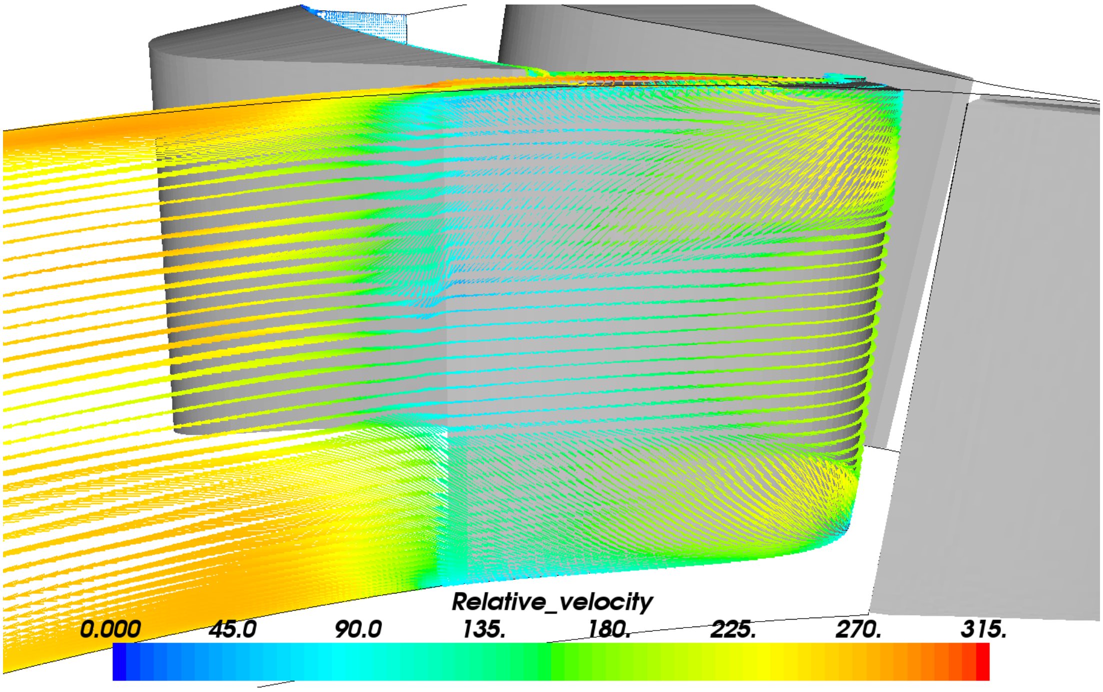

Figure 68: Relative velocity distribution at B50_v01_03 blade suction side surface. (Multall, MayaVi)

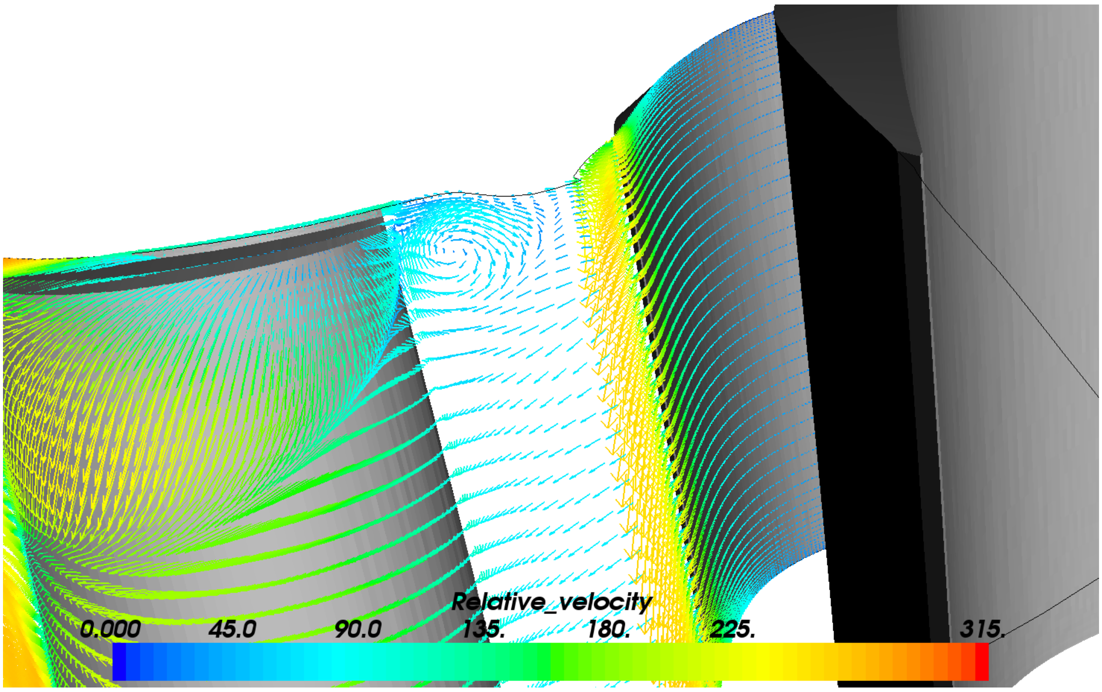

Figure 69: Relative velocity distribution at B50_v01_03 blade suction side surface close to leading edge. (Multall, MayaVi)

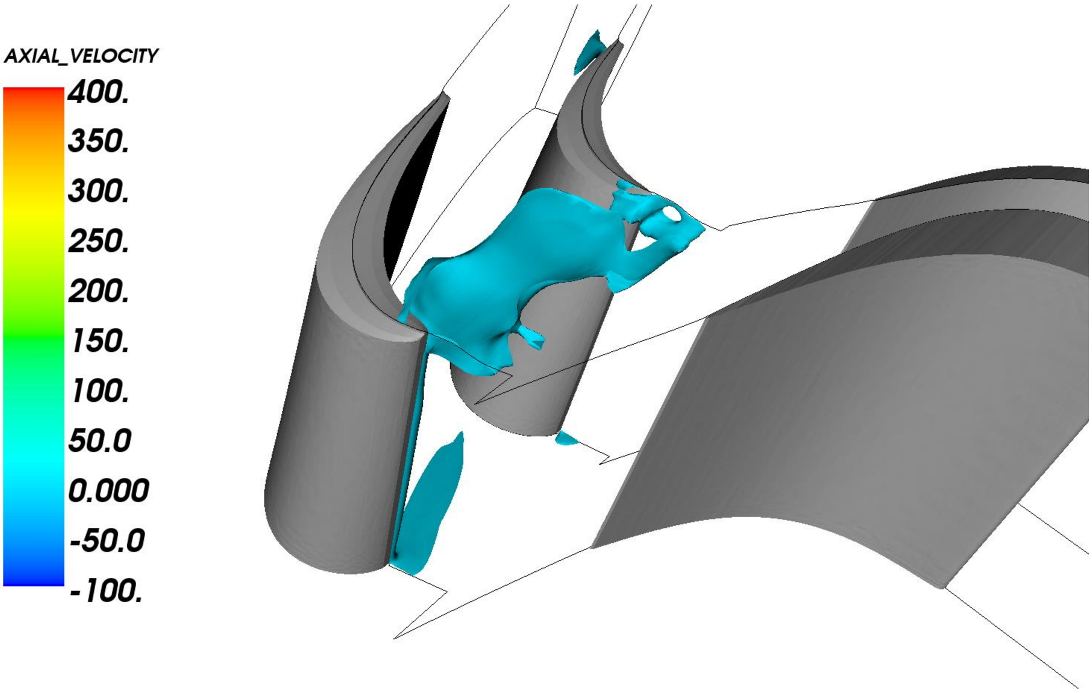

Figure 70: B50_v01_03, -1 m/s axial velocity ISO-surface. (Multall, MayaVi)

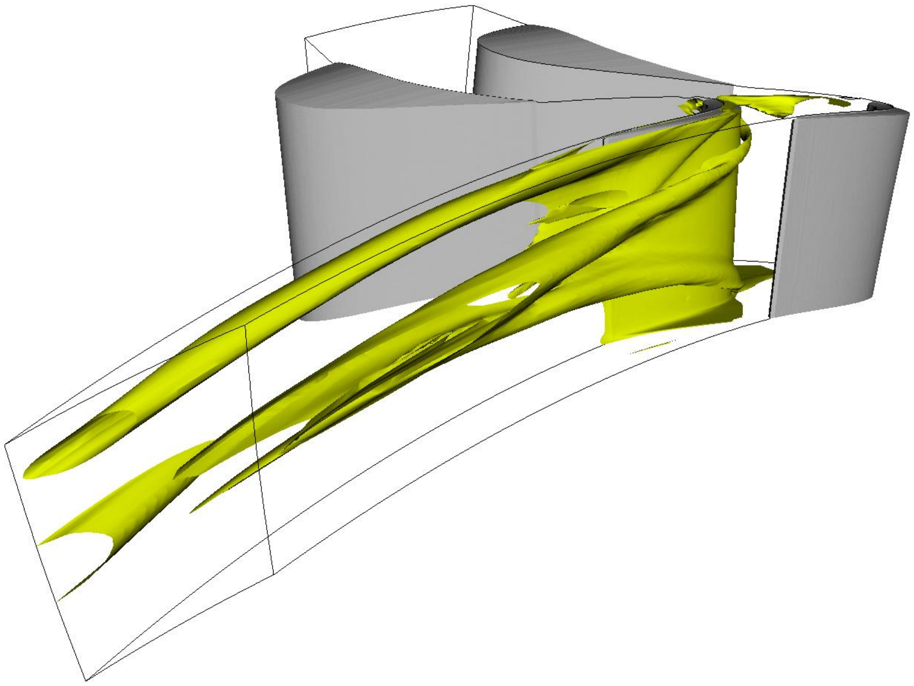

Figure 71: Losses at B50_v01_03 blade suction side surface. (Multall, MayaVi)

6 Conclusion and discussion

A new blade row B50_v01_03 was designed with 50 blades instead of 60 blades which was the case for the BC7M. The pitch-to-chord ratio has increased from 0.85 to 0.93 at the mid-section for the new blade. The new blade has an increased blade loading to make sure that the new blade row produces the same work output as the BC7M blade row.

By examining the results, it was a positive surprise that the total-to-total isentropic efficiency for the new blade row B50_v01_03 with 20 % fewer blades was almost unaffected compared to the BC7M. In Multall the efficiency decreased from 92.02 % to 91.90 % but in beta2 it has increased from 92.03 % to 92.19 %.

Another interesting result was that the rotor platform wetted area has increased by 1276 mm^2. This actually provides an increased cooling demand on the rotor platform. However since the blade profile wetted area has decreased with 9.7 % or 9320 mm^2 there will be a significant cooling air need net profit. How much cooling air that can be saved depends on other things as well.

One problem that can be seen in the results is that the stagnation point is located on the pressure side, downstream the geometric leading edge. The effects of this will not have a great significance for this uncooled blade. However, this study should preferably be applicable to a full-scale blade where cooling air is needed. For this it would not be optimal to have the stagnation point at the pressure side, because then the flow will bring all the showerhead film cooling to the suction side, leaving the pressure side undercooled. There is not only one solution to this rather serious problem. The stagnation point can be moved towards the suction side by designing the blade with negative incidence. Another idea might be to use a much larger inlet wedge angle, since a quite small one has been used. This will reduce the tendency of over acceleration since there will be less curvature at the leading edge. Unfortunately a larger inlet wedge angle leads to increased section area and hence increased mass in the blade. Since the number of blades has decreased, the mass has been reduced by having almost the same section area, so maybe it would be acceptable to have a small increase of mass at each section. However the tensile stresses will then increase. With increased section area it could have been possible to remove some material inside the blade. This would though affect the cooling system. The cooling air velocity would decrease due to an increased area giving a less effective cooling system. Increasing the axial chord could also be a solution to the stagnation point problem however this will lead to a smaller pitch-to-chord ratio. There are pros and cons with every solution, hence which one that is preferable is hard to decide.

As expected the secondary flow losses increased for the B50_v01_03. The diffusion looks reasonable at almost every section for the B50_v01_03 except at the 75 % span. The reason for that is not determined. Even though it is assumed not to be a problem, this will be fixed before manufacturing the blisc. The Mach number distribution curves at different spans have a tendency not to be smooth. This problem is more likely a numerical problem than a physical problem. It was shortly investigated by a test with a finer mesh in that region, unfortunately without any improvements. This is assumed to be more of an esthetical problem. However it could be of interest to look further into this problem.

Early in this thesis, a decision was made to design a blade with a pitch-to-ratio of approximately one. Unfortunately this was not fully completed in the presented version since the chord became longer when the profile was closed.

During the profile loss study with changed pitch-to-chord ratio not much work was done with the mesh. It could have been possible to get the solution to converge at even higher pitch-to-chord-ratio, however it has been seen that a change in mesh would have a large influence of the result.

7 Further work

If decision will be taken to continue to develop the B50_v01_03, more analysis should be done, e.g. a part load and incidence analysis should be of interest to implement. No cavity flows have been analysed so far, however it should be of interest for further work.

There are also some adjustments that can be made especially on the tip. As have been seen, it looks like there is a lot of tip leakage. One alternative to decrease the tip leakage loss can be to move a small part of the loading from close to the tip downwards to the mid-section, and simultaneously fix the problem with to high diffusion at the 75 % span.

Since the B50_v01_03 blade became very slender, it must be studied very carefully to make sure that it is possible to design the internal cooling system in a full scale version of this blade. It might actually be appropriate to develop a new concept with a new thicker blade with shorter chord to make room for more cooling. By designing a new shorter and thicker blade, maybe it will be possible to decrease the wetted area as well.

Further investigations should be carried out in order to improve where the stagnation point is located. One approach might be to abandon the old design philosophies regarding the incidence. A solution might be to have a few degrees negative incidence. Another solution might be to increase the inlet wedge angle. However this will affect the cross-sectional area.

No matter what decision that will be taken, further structural analysis or mechanical integrity parameter check should be performed since the blade is so slender.

Finally, calculations should be made on a full-scale version of the designed blade profile to make sure that it will fulfil its requirements. In the full-scale blade, cooling air should be included in the calculations.

Bibliography

Anton, N., & Wiberg, W. (2013). *Aerodynamic design of a gas turbine rotor blade for the KTH test turbine.* Finspång.

Cebeci, T., & Bradshaw, P. (1977). *Momentum Transfer in Boundary Layers.* (B. Davis, & M. A. Phillips, Eds.) Washington, United States of America: Hemisphere Publishing Corporation.

Cengel, Y. A., & Boles, M. A. (2011). *Thermodynamics: An engineering approach* (Seveneth edition in SI units ed.). New York, NY, United States of America: McGraw-Hill.

Dahlquist, A. N. (2008). *Investigation of Losses Prediction Methods in 1D for Axial Gas Turbines.* Lund.

Denton, J. D. (2012, June 25-29). Introductory Review of Basic Principles. *Cambridge Turbomachinery Course 2012, VOL. 1*, pages 1-31.

Dixon, S. L., & Hall, C. A. (2010). *Fluid Mechanics and Thermodynamics of Turbomachinery* (sixth ed.). Burlington, Massachusetts, United States of America: Elsevier Inc.

Flydalen, K. (2013). *Modifications and analysis of rotor design BC6M for test turbine.* Finspång.

Flydalen, K. (2015, March 5). Multall discussion. (M. Persson, Interviewer)

Flydalen, K., & Sohaib, M. (2011). *Power turbine geometry import to profiling tool CATO.* Finspång.

General Electric. *Jet Engines and Propulsion Systems for Engineers.*

Genrup, M. (2014, March 22). Lecture: Axial turbines, Steam and Gas Turbine Engineering. Lund, Sweden.

Hedlund, L. (2015, March 26). Horseshoe vortex. (M. Persson, Interviewer) Finspång.

Hedlund, L. (2015, March 20). Uncovered turning discussion. (M. Persson, Interviewer)

Hodson, H. P. (2012, June 25-29). Blade to Blade Flowfields in Axial Flow Turbomachines. *Cambridge Turbomachinery Course 2012, VOL. 1*, pages 35-75.

Klebanov, A. G., & Mamaev, B. I. (1969). Optimal pitch for a turbine blade cascade. *Teploenergetika, VOL 16*, 59-59.

Korpela, S. A. (2011). *Principles of Turbomachinery.*

Lampart, P. (2009). Investigation of endwall flows and losses in axial turbines. Part I. Formation of endwall flows and losses. *Journal of theoretical and applied mechanics*, 321-342.

Longley, J. P. (2012, June 25-29). Introduction to 3-D Flows in Turbomachinery. *Cambridge Turbomachinery Course 2012, VOL.1*, 79-116.

Mamaev, B. I., & Sandymirova, T. A. (1995). Refinement of recommendations on a relative pitch choice for turbine cascades. *Transactions of the Aviation Institute*, 37-43.

Mikaillian, N. (2012). *Test turbine measurements and comparison with mean-line and throughflow calculations.* Finspång.

Miller, R. J., & Denton, J. D. (2012, June 25-29). Loss mechanisms in turbomachines. *Cambridge Turbomachinery Course 2012*, *VOL.1*, 149-179.

Moustapha, H., Zelesky, M. F., Baines, N. C., & Japikse, D. (2003). *Axial and Radial Turbines.* White River Junction, Vermont, USA: Concepts NREC.

Saravanamuttoo, H., Rogers, G., Cohen, H., & Straznicky, P. (2009). *Gas Turbine Theory* (6 ed.). Harlow, England: Prentice Hall.

Sieverding, C. H. (1985, April). Recent Progress in the Understanding of Basic Aspects of Secondary Flows in Turbine Blade Passages. *Journal of Engineering for Gas Turbines and Power, Vol. 107*, pages 248-257.

Appendix A - Mises solver parameters

The solver parameters that were used for the Mises solver in Cato for the BC7M and the new profile with 50 blades are shown in Table 12. Note that these values are not equal to the boundary conditions for the whole turbine stage since the Mises calculations are only done on the blade profiles at the rotor. The Reynolds number was adjusted until the outlet Reynolds number based on chord was equal to 366 000. Another parameter that is decided iteratively is the inlet Mach number. It is assumed to be equal to the result inlet Mach number. This inlet Mach number is not a strict boundary condition.

Table 12: Solver parameters for BC7M and the new profile with 50 blades (Mises, Cato)

	hub	mid	tip
Drive inlet slope	True	True	True
Drive inlet total pressure	True	True	True
Drive outlet Mach	True	True	True
Set LE Kutta	True	True	True
Set TE Kutta	True	True	True
Specific gas constant[8]	287.9	287.9	287.9
Specific Heat Ratio[8]	1.4	1.4	1.4
Pitch/Chord 3D[9]	0.79	0.85	0.90
Flow inlet angle[10]	49.14	56.59	60.24
Inlet Mach number	0.24	0.22	0.20
Inlet pressure ratio	0.96	0.97	0.97
Inlet relative tangential velocity	0	0	0

---

[8] Values are taken from a beta2 calculation for the BC6M, (Anton & Wiberg, 2013, p. 130)

[9] Geometry specified parameter for the case with 60 blades. (For the rotor row with 50 blades, the values will be different.)

[10] Values are taken from own beta2 BC7M calculation at stream tube 2 and 19 and the mean value of stream tube 10 and 11.

Inlet total pressure[10]	149580	152575	155410
Inlet total temperature[10]	312.5	313.6	315.0
Inlet-condition location	24.31	25.18	26.31
Artificial dissipation coeff.	1	1	1
Critical Mach number	0.98	0.98	0.98
Flow outlet angle	18.6	18.6	18.6
Outlet Mach number[11]	0.78	0.78	0.78
Outlet pressure ratio	0.68	0.67	0.65
Outlet relative tangential velocity ratio	0	0	0
Outlet static pressure	101500	101500	101500
Outlet-condition location	61.62	60.38	59.38
Number of iterations	50	50	50
Thickness mode 1 amplitude	1	1	1
Thickness mode 2 amplitude	1	1	1
Calculate Reynolds Nr	False	False	False
Crit. Amplifications number[12]	-5	-5	-5
Reynolds number	6382000	5707000	5261000
Side 1 surface transition trip location	1	1	1
Side 2 surface transition trip location	1	1	1

---

[11] Values are taken from own beta2 BC7M calculation at stream tube 2, 19 and the mean value of stream tube 10 and 11.

[12] Crit. amplification number equal to minus five means that the turbulence intensity is five percent.

Appendix B - beta2 input parameters

To be able to use the beta2 software, some input parameters have to be stated. The boundary conditions that are needed are presented in the boundary condition section. Also the gas composition needs to be decided. The KTH test turbine uses standard air as working fluid. The absolute humidity is obtained from laboratory measures at KTH, where the relative humidity was measured and then the absolute humidity was calculated. They had 0.3 % absolute humidity in January and 1 % in June. From this the absolute humidity was decided to be 0.5 %.

There is an option to choose which gas table beta2 uses. Both the Rumer-Ryvkin and the NASA SP-273 were tested. Due to problems with the Rumer-Ryvkin gas table, the NASA SP-273 gas table was considered to be more accurate. The problem with the Rumer-Ryvkin gas table was probably that negative enthalpies were calculated due to the fact that smaller pressures than for a normal gas turbine were studied. However, this statement is not confirmed and should be taken with caution.

The program GasTable v1.9 was used to get the gas composition values. These values can be seen in Table 13.

Table 13: Mass fractions for the working fluid in the KTH test turbine.

Gas	Chemical formula	Mass fraction
Oxygen	O_2	0.23028
Nitrogen	N_2	0.75147
Water	H_2O	0.00500
Carbon Dioxide	CO_2	0.00045
Sulphur Dioxide	SO_2	0.00000
Argon	Ar	0.01280
Helium	He	0.00000

Further it was stated that the clearance, the gap between the casing and the tip of the blade should be 0.3 mm. This clearance will be 1.1 % of the blade height. This gap will then be measured during the tests for the BC7M with some carbon pins in the casing. The disadvantage with this method is that it will only measure the smallest gap during all operating modes. The smallest gap will not necessary be in the design operation, it can also happen during start up and cool down. When the blade is heated up the blade will be longer due to thermal expansion. This expansion will take longer time for the casing, since this is a bigger object to be heated. Also the centrifugal effect comes into account since the rotor is rotating, which give some extension. The gap should never be too large since this will give huge secondary losses, and not too small to avoid that the rotor will get stuck in the casing.

The roughness was assumed to be 0.8µm for the rotor blade surface and 1.6µm for the stator vane surface. As long as the roughness peaks appears in the laminar boundary layer, it will not have any major effect, however if some small peaks of the surface enters the turbulent boundary layer it will affect the losses. The roughness is of most importance at high Reynolds number (Denton, 2012, p. 10).

Since the vane is placed in a cut in the rotor, the fillet radius (the radius between the blade and the casing) will be zero. At the tip of the rotor, the fillets radius will of course be zero, and at the hub there will be a 1.5 mm fillet.

Since the throats are calculated differently in Cato compared beta2, there is an option to adjust the throat in beta2 to get the same value as in Cato.